5/N6
L
36
L25
.96
2021

UNIVERSITY OF LAGOS, NIGERIA
Inaugural Lecture Series 2021

TOPIC:

THE NATURAL MIRROR: A GIFT OF NATURE FOR HUMANITY

By

PROFESSOR ELIJAH OYEDOLA OYEYEMI

5/N6
L
36
.L25
.96
2021

Complimentary Copy
Not for Sale

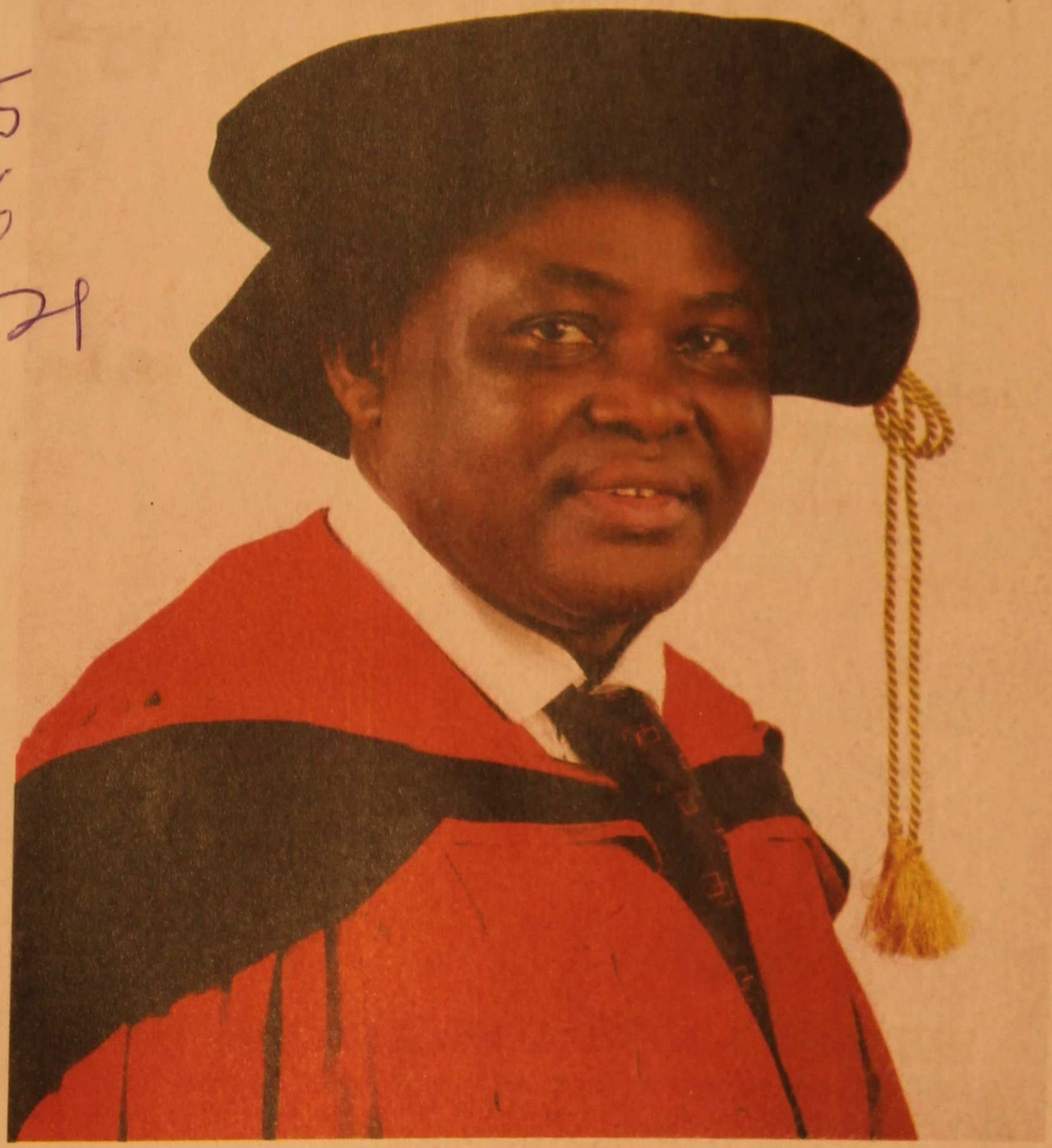

PROFESSOR ELIJAH OYEDOLA OYEYEMI

B.Sc. (Ed) (Unilorin), PGD. Comp Science, M.Sc. (Lagos), Ph.D. (Rhodes)

DONATED BOOK

DONATED BOOK

THE NATURAL MIRROR: A GIFT OF NATURE FOR HUMANITY

An Inaugural Lecture of the University of Lagos Delivered on 4th August 2021 at the JF Ade-Ajayi Auditorium

By

PROFESSOR ELIJAH OYEDOLA OYEYEMI

B.Sc. (Ed) (Unilorin), PGD. Comp Science, M.Sc. (Lagos), Ph.D. (Rhodes)

Simons Associate, Abdus Salam International Center for Theoretical Physics (ICTP) Trieste, Italy

Professor of Physics

(Ionospheric Physics and Radio Wave Propagation)`

Department of Physics

Faculty of Science

University of Lagos

Copyright © 2021, Elijah Oyedola Oyeyemi

All rights reserved. No part of this publication may be reproduced, stored in a retrieval system or transmitted in any form or by any means electronic, mechanical, photocopying, recording, or otherwise without the permission of the author.

ISSN: 1119-4456

Published by

University of Lagos Press and Bookshop Ltd
Works and Physical Planning Complex
P.O. Box 132
University of Lagos
Akoka, Yaba
Lagos, Nigeria
E-mail: press@unilag.edu.ng

DEDICATION

I dedicate this Inaugural Lecture to my late parents Mr. Moses Oyeyemi and Mrs. Ruth Oyeyemi.

I am also dedicating this Inaugural Lecture to the memory of my first academic child, Dr. Adekola Olajide Adewale (Senior Lecturer, Department of Physics, University of Lagos), who slept in the Lord on the 10th of June 2021. May his soul rest in perfect peace.

PROTOCOL

The Vice Chancellor
Deputy Vice Chancellor (Academic and Research)
Deputy Vice Chancellor (Development Services)
Deputy Vice Chancellor (Management Services)
The Registrar
The Bursar
The Librarian
The Provost, College of Medicine
Dean of Faculty of Science
Deans of Other Faculties
Members of the University Senate
Heads of Departments
Distinguished Academic and Professional Colleagues
Distinguished Non-Academic Colleagues (Administrative and Technical)
Your Lordship, Spiritual and Temporal
Dear Students (Past and Present)
Members of the Mass Media (Press, Broadcast & Virtual)
Invited Guests
Ladies and Gentlemen

PREAMBLE

I give glory to God Almighty for keeping my life, and making this inaugural lecture a reality. It is indeed a great thing of joy to be here this evening and present to you my journey so far since I joined this great University of first choice and nation's pride, the University of Lagos in 1996. I started my educational career from Maami Primary School and later The Apostolic Church Grammar School, Ogbomosho, for my secondary education, which I completed in 1984. I thereafter proceeded to St. Andrews College of Education, Oyo, Oyo State to study Physics and Mathematics, and finished with a grade point of 14 out of 15 points in 1988. I obtained my Honours degree in Physics and Education from the University of Ilorin in 1991, followed by a Master's Degree in Physics, and a Postgraduate Diploma in Computer Science from the University of Lagos in 1994 and 1997 respectively. I was appointed an Assistant Lecturer in July 1996 when Professor C.O. Oluwafemi was the Dean of the Faculty of Science. In January 2003, when there was no

headway with the Ph.D. programme in Geophysics, which I started in 1997, because of lack of equipment, I proceeded to Rhodes University in Grahamstown, South Africa, on Study Leave, for a Ph.D. in Ionospheric Physics and Radio Wave Propagation, which I completed in 2005. This decision could not have been possible without the advice of Professor Oluwatoyin Ogundipe (the current Vice Chancellor) who was then, the Sub Dean of the Faculty of Science and always on the neck of every young lecturer to obtain a Ph.D. I thank you Sir. I must say at this point that this inaugural lecture is the fourth to be delivered in the history of the Department of Physics, University of Lagos. The first was delivered by Professor E.O. Olatunji when I was not yet a member of staff in the Department. The second was delivered by Prof. C.O. Oluwafemi when I was an Assistant Lecturer and the third was delivered by Prof. M.A.C. Chendo in 2018, by then I was already a Professor. It is also worth mentioning that I am the fifth Professor to be appointed in this Department. I rose through the rank as an Assistant Lecturer in 1996, under the stead of Professor Jelili Omotola to a Professor in 2015 when Professor Bello Rahman was the Vice Chancellor. To God be the glory! I am privileged to have travelled to many countries (USA, Italy, Japan, Poland, India, Argentina, Brazil, South Africa, Zambia, Ethiopia, Congo Brazzaville, etc.) through the span of my career so far to present my work during conferences, workshops and as visiting scholar.

Why Physics?

Mr. Vice Chancellor, Sir, as a way of digression, I believe that even up till date majority of parents do not want their children/wards to study Physics as a course in the University. This is probably because of a lack of understanding of what Physics is all about and also because they believe that Physics is an abstract subject that cannot be understood by ordinary human beings. It may also be a consequence of improper teaching of this subject in our Secondary Schools. No wonder there used to be low applicants for Physics as a course in the University. But things have started changing gradually in the last few years when the Department of Physics no longer begs to get students. I must say that my case is different because I did

not find myself in Physics by chance. I decided to do Physics not because my parents knew anything about Physics but because I love it.

Physics is the greatest gift of knowledge without which it will be difficult, if not impossible, to understand the universe and everything therein. Physics is applicable wherever life (plants and animals) and all matter are found. The bedrock of Engineering and Technology is Physics as it generates fundamental knowledge needed for future technological advances that will continue to drive the economic engines of the world. In Summary:

- Physics extends and enhances our understanding of other disciplines, such as earth, agricultural, chemical, biological, and environmental sciences, plus astrophysics and cosmology – which are subjects of substantial importance to all the people of the world.
- Physics improves our quality of life by providing the basic understanding necessary for developing new instrumentation and techniques for medical applications, such as computer tomography, magnetic resonance imaging, positron emission tomography, ultrasonic imaging, and laser surgery.

INTRODUCTION

Motivation

Mr. Vice Chancellor, Sir, my choice of the title, "**The Natural Mirror: A gift of Nature for Humanity**", has been motivated by the important roles that the ionosphere plays on high frequency (HF) radio communication and navigation systems. Progress in HF radio communication depends on the capability to understand and predict ionospheric conditions. The radio waves propagating in the Earth's ionosphere are strongly affected by the maximum electron density of the F2 layer (NmF2), which is associated with the critical frequency (foF2) of the ionosphere. The critical frequency, foF2, is defined as the highest cutoff frequency at which the F2 region of the ionosphere reflects electromagnetic waves.

The Earth's ionosphere is subject to great temporal and spatial variations because its existence is directly related to the changes resulting from the interaction of solar radiations and geomagnetic field. As a result, there are systematic changes in the behaviour of ionospheric parameters with the ***season, time-of-day, solar ionospheric related disturbances and magnetic variations***. Radio waves propagating through the Earth's ionosphere are greatly influenced by these temporal and spatial variations. The F2 region ionospheric parameters [**maximum electron density (NmF2), critical frequency (foF2), peak height (hmF2) and propagation factor (M3000F2)**], as well as **Total Electron Content (TEC),** are important for HF planning for radio communication applications and navigations. It is, therefore, important to study the climatological behaviour of these ionospheric parameters as they affect communications and also predict and forecast them.

The applications of Artificial Neural Networks (ANNs), thereafter refers to as Neural Networks (NNs), is generally motivated by their principal ability to describe non-linear phenomena (***both in space and time***), a principal characteristic of the F2 region of the ionosphere due to its non-linear dynamic processes arising from global thermospheric circulation. Also, NN has the ability to generalise from a set of training patterns when presented with input patterns that are similar, but not identical to that with which the NN was trained. Various groups (Altinay et al., 1997; McKinnell, 1996, 2002; Williscroft and Poole, 1996; Lamming and Cander, 1999; Tulunay et. al., 2000; Wintoft, 2000, Oyeyemi et al., 2004, 2005, 2006) have shown the methods of NNs to be successful when employed to model the non-linear behaviour of the ionosphere.

A brief description of the discovery, structure and variability of the ionosphere is summarised in the following sections. Details can also be found in Rishbeth and Garriott, 1969; McNamara, 1994 and various articles (e.g. Forbes et al., 2000; Rishbeth and Mendillo, 2001).

Discovery of Ionosphere

A Scottish Physicist, Balfour Stewart, discovered the ionosphere in 1882. He suggested that the continuous but minor variations in Earth's magnetic field might be caused by the presence of a layer of air capable of conducting electricity in the upper atmosphere. Also, the movement of this layer in the terrestrial field could produce electric currents by dynamo effect; these currents could, in turn, generate magnetic fields, which would be superimposed upon the normal magnetic field observed at the Earth's surface. Stewart's suggestion attracted little interest until after December 1901. In 1901 an Italian radio pioneer G. Marconi succeeded in transmitting wireless signals over a distance of about 2000 miles (~3220 Km) across the Atlantic Ocean. In 1902 Oliver Heaviside (England) and Arthur E. Kennelly (United States), proposed independently from Marconi's unexpected achievement that there exists an electrically conducting layer in the atmosphere at a height of about 80 km. In 1924 and after, Edward Appleton and M. A. F Barnett in England, G Breit and M. A. Tuve in the United States used directional antennas and devised techniques for determining the height of the reflecting region and its different layers of the ionosphere.

The Earth's Ionosphere

The ionosphere is that region of the Earth's upper atmosphere extending from a height of about 50 km up to about 1000 km. This region is the ionized part of the upper atmosphere that is formed by photoionization due to solar extreme ultraviolet (EUV) and X-radiation (Rishbeth and Garriott, 1969; Hargreaves, 1979; McNamara, 1994). This process may also be caused by solar wind particles and cosmic rays but their effect is small in comparison with the EUV radiation. Within the ionosphere free ions and electrons exist in sufficient abundance to influence the propagation of radio frequency electromagnetic waves that are propagated within and through it, giving the ionosphere much of its practical importance. This region is an important region of the atmosphere because these charged particles and free electrons are responsible for the **reflection or bending** of **radio waves** occurring between certain critical

frequencies, which vary with the degree of ionization. Due to the changes in the sources of ionization (i.e. the sun activity), and also because the ionosphere responds to the changes in the neutral part of the upper atmosphere (i.e. the thermosphere), the structure and peak densities of the ionosphere vary with time (i.e. 11-year solar cycle, diurnally, and seasonally), with geographical location (i.e. geographic latitude and longitude), and with solar-related ionospheric disturbances (i.e. sporadic E, sudden ionospheric disturbances (SID), and ionospheric storms) (McNamara, 1994). This variability is known to cause distortion effects on satellite and HF communications, navigation and altimetry.

The ionosphere is vertically divided into three main regions, namely, D, E and F regions. These regions are classified according to their chemical composition, sources of ionization, level of variability and dynamic nature. An example of the daytime electron density variation of the ionospheric layers and their predominant ion populations as a function of height above the ground is illustrated in Figure 1. Table 1 shows layers of the lower and bottom-side ionosphere with maximum electron density and their major ions.

Table 1: Layers of the Lower and Bottom Side Ionosphere

Region	Height	Ne Maximum (cm^{-3})	Ion
D		1.5×10^4 (noon) absent at night	
E	90 – 150	1.5×10^5 (noon) $< 1 \times 10^4$ (night)	O_2+
F1	150 - 210	2.5×10^5 (noon) absent at night	NO+
F2	**210 - 400**	**10^6 (noon)** **10^5 (midnight)**	O+

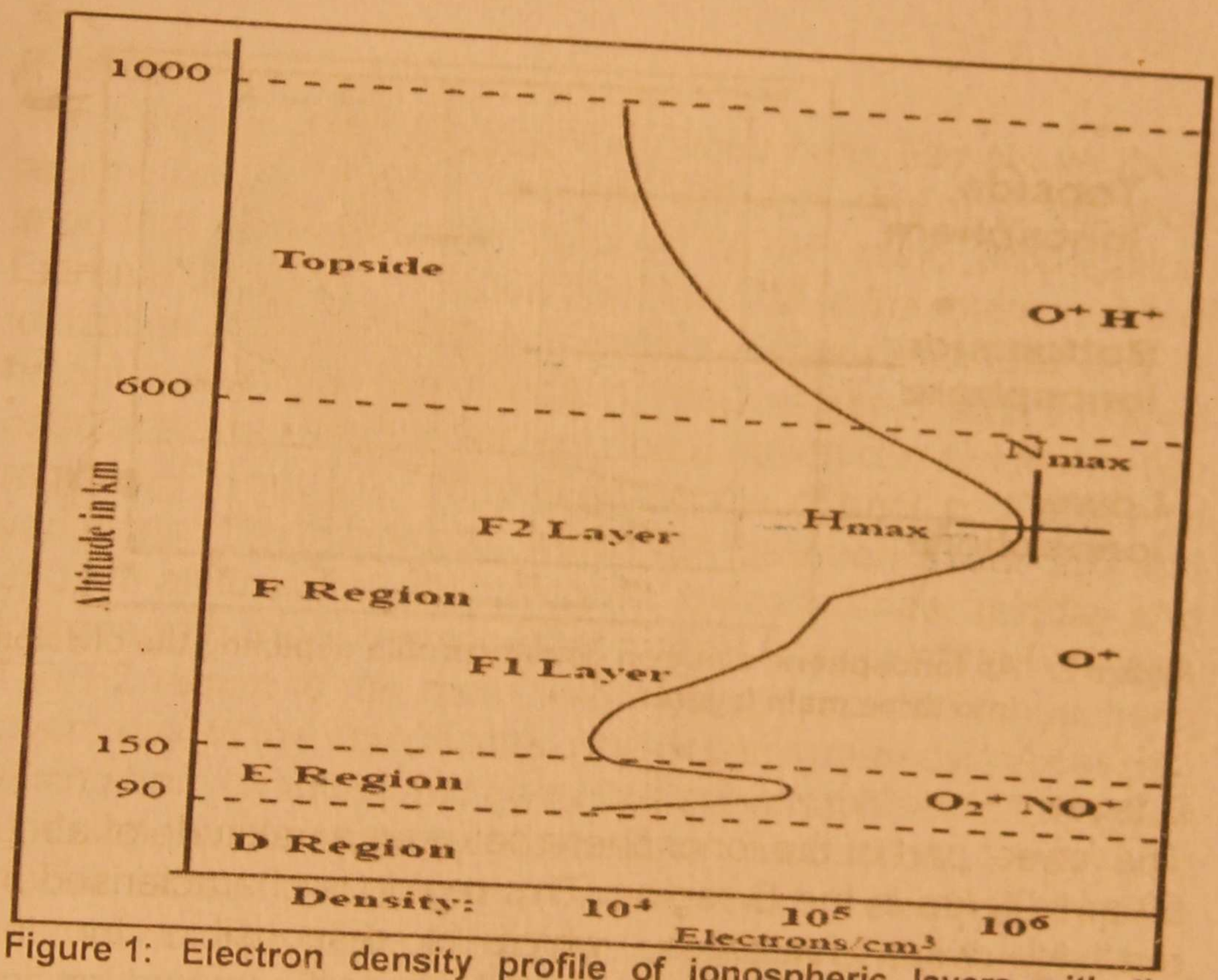

Figure 1: **Electron density profile of ionospheric layers with their predominant ion populations as a function of height**

Source: *Space Environment Center (SEC) and Space Oceanic and Atmospheric Administration (NOAA) by Anderson and Fuller-Rowell, 1999*

The ionosphere is multi-layered, with the different regions arising due to the complexity of the plasma at each altitude. The layers are referred to as "***lower ionosphere***' (between about 50 km and about 90 km), "***bottom-side ionosphere***" (between about 90 km and about 350 km), and the "***topside ionosphere***" (above about 350 km). Each of these 3 layers requires different measuring equipment for establishing the behaviour at these altitudes. These regions are represented using Figure 2.

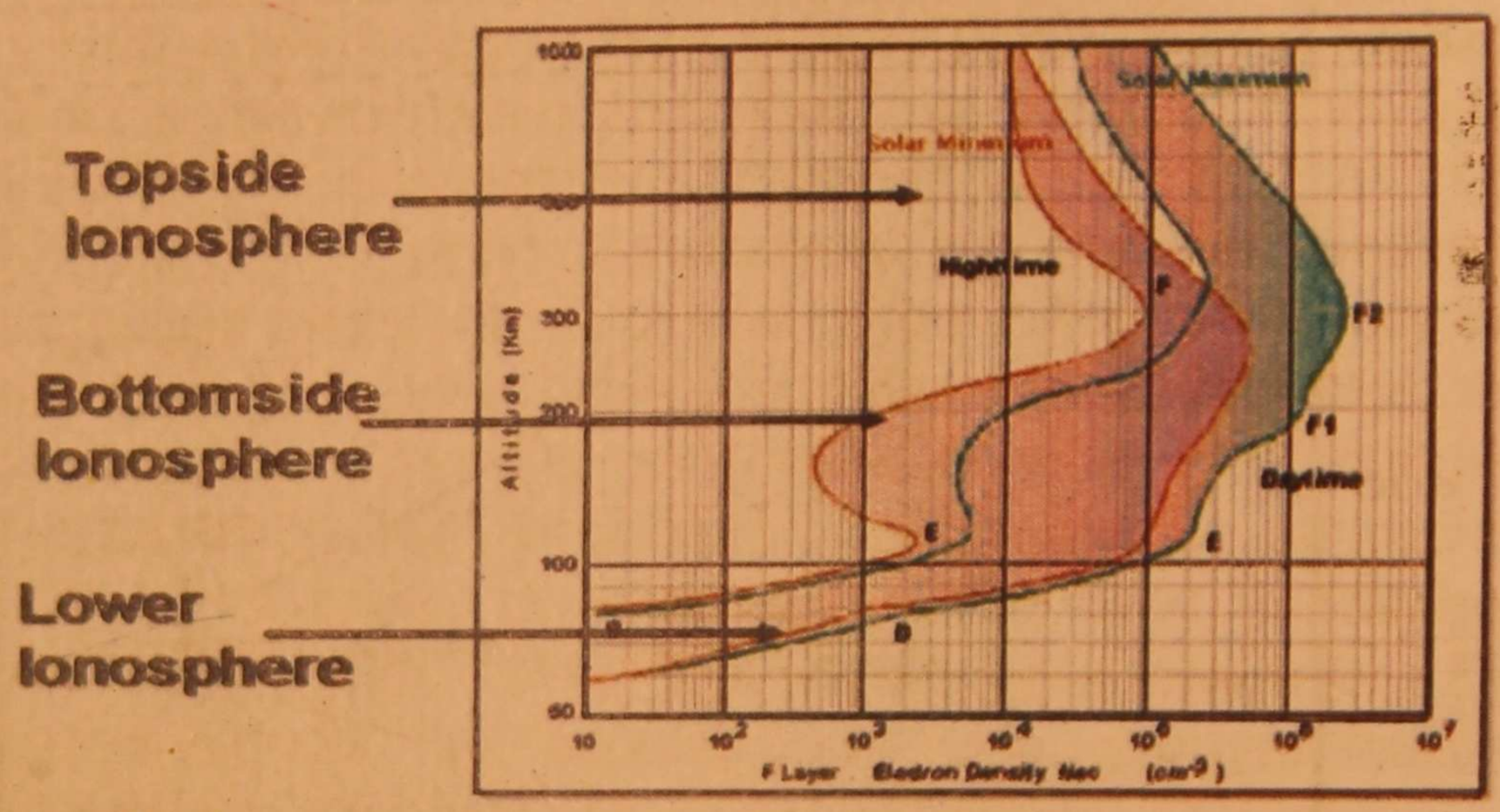

Figure 2: An ionospheric electron density profile depicting the division into three main layers

D layer

The lowest part of the ionosphere between an altitude of about 50 and 90 km is the D region. This region is characterised by relatively weak ionization, which is responsible for the absorption of HF radio waves, particularly those frequencies below 7MHz. Hard X-rays are the major source of ionization in this region (Rishbeth and Garriott, 1969).

E layer

The region just above the D region from about 90 to 150 km is the E region. Ionisation in this region is due to soft X-rays (1-10 nm) and far ultraviolet (UV) solar radiation of molecular oxygen (O_2). The E layer can only reflect radio waves with frequencies less than 10 MHz and has a negative effect on higher frequencies due to its partial absorption of these higher frequency radio waves. The E-layer is a daytime phenomenon because it develops shortly after sunrise and disappears a few hours after sunset, with maximum ionization around midday. Within the E region, a very thin region of extremely dense ionization that is different from the normal E layer ionization can form. This region is called the sporadic E region (E_s) and is capable of reflecting radio frequencies from about 30 to 300MHz. Sporadic E appears mostly during the summer months, and less during winter, with the peak during early summer.

F layer

The F region, which is the main focus here, lies above the E region, between about 150 and 350 km, and it is the most important region for the purpose of HF radio propagation. Extreme ultraviolet radiation from the Sun is the main source of ionization in this region. This region is heavily ionized and its height is a function of the season, latitude, time of day, and level of solar activity. During the day, the F region can divide into two regions, F1 and F2, depending on the diurnal and seasonal variations. The F1 region, which lies between about 150 and 210 km altitude, has its maximum ionization near midday and merges with the F2 region after sunset to reform the F region. The F2 region is the most variable region of the ionospheric layers due to the complicated non-linear dynamical processes, arising from temporal and geographical variabilities in the upper atmospheric chemistry, ionization production and loss mechanisms, particle diffusion and electrodynamical phenomena. In spite of the fact that much of the ionospheric variability can be explained from the basic principles of Physics, the F2 layer is so complex that its critical frequency does not behave in the manner of a simple Chapman layer (Rishbeth and Garriott, 1969, McNamara, 1994). The complex nature of the F2 region is a limiting factor for terrestrial and Earth-space communications (Tulunay et al., 2000; Richard et al., 2004). However, this upper part of the F region is the most important region for HF communications (Bent et al., 1978; Rush et al., 1984) because its altitude allows the longest communication paths, it is always present (24 hours of the day), and it can refract the highest frequencies in the HF range. The maximum electron density of this region is quantified by the critical frequency, foF2, and determines the maximum usable frequency (MUF). The critical frequency, foF2, which is defined as the highest cutoff frequency at which the F2 region reflects electromagnetic waves, is related to the maximum ionospheric electron density, N_e, according to

$$N_e/m^{-3} = 1.24 \times 10^{10} (f/MHz)^2 \ (el/m^3) \qquad (1)$$

The maximum usable frequency, MUF(3000), defined as the highest frequency at which radio waves can propagate from a given point over a distance of 3000 km, is expressed as:

$$M(3000)F2 = \frac{MUF(3000)}{f_oF2} \qquad (2)$$

where M(3000)F2 is the propagation factor closely related to the height of the F2-peak (hmF2) (Bilitza et al., 1979), and also, proportional to the secant of the ray zenith angle. Both ionospheric parameters, foF2 and M(3000)F2, are essential for HF planning for radio communication applications (Xenos, 2002).

Based on the significance of the F2 region to HF communications and its high-level of variability due to solar activity and magnetic activity, the subject of this lecture is, therefore, centred on the study of climatological behaviour of F2 region ionosphere and development of ionospheric empirical models for its peak density.

Variations in the F2 region

The F2 region of the ionosphere is subject to a number of influences because its existence is directly related to the changes resulting from the interaction of solar radiations, solar wind and the geomagnetic field. The structure of the F2 region at any geographical location and time is complex and depends on the amount of solar radiation from the sun and the electron density arising from the processes of photoionization and recombination. Due to the Earth's tilt and rotation around the sun, the path of the atmosphere through which the solar radiation passes varies with the time of the day and month of the year. As a result, the F2 region electron density varies with time of the day (diurnally) and with season (seasonally) due to the change in solar zenith angle, and over the ~11-year cycle (Rishbeth and Garriott, 1969; Hargreaves, 1979; Forbes et al., 2000). Because of these variations, a frequency which may provide successful propagation at one geographical location may not do so at another, and even from one hour to the next

hour within the same location. These variations are the result of the non-linear dynamical processes in the ionosphere, and can be grouped into two categories: those which are more or less regular and occur in cycles, and those which are irregular in their behaviour (irregular disturbances) due to disturbances in the atmosphere arising from solar-related ionospheric disturbances. These two classes of variations are briefly discussed in the next section.

Regular variations

Regular variations occur as a result of the rotation of the Sun and the Earth about their own axes. There are four types of regular variations: diurnal, seasonal, 27-day and solar cycle variations. An analysis of such variations has been performed on foF2 values measured at the Grahamstown (33.3°S, 26.5°E) ionospheric station over a period of 27 years (1973-2000) using Fourier transform (FT) techniques, see Figure 3 (Oyeyemi, 2005).

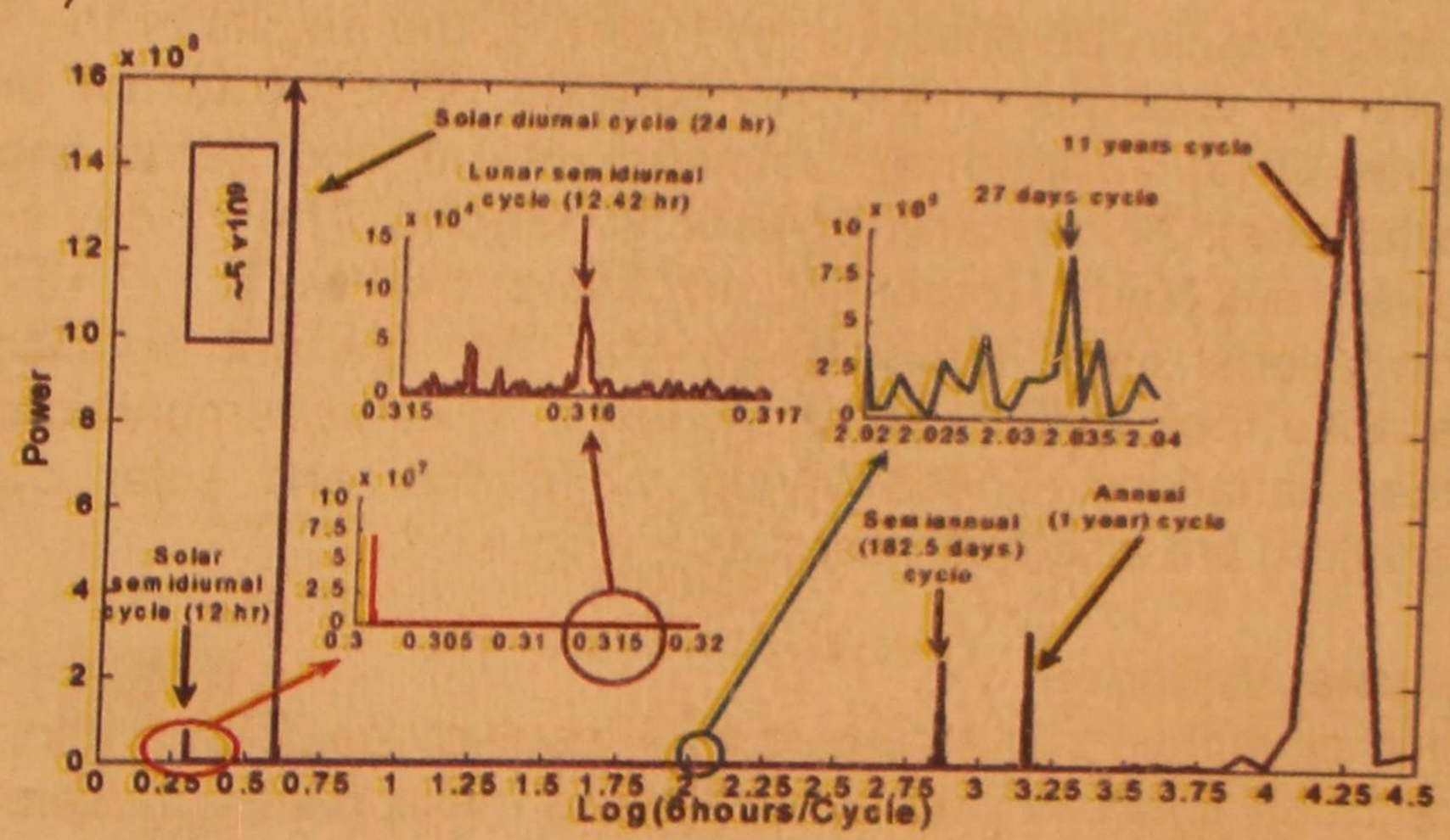

Figure 3: The result of Fourier transform (FT) of Grahamstown foF2 values for the interval January 1973 through December 2000 (a total of 27 years). The sampling period is an average of 6 hours per cycle

Source: *Oyeyemi, 2005*

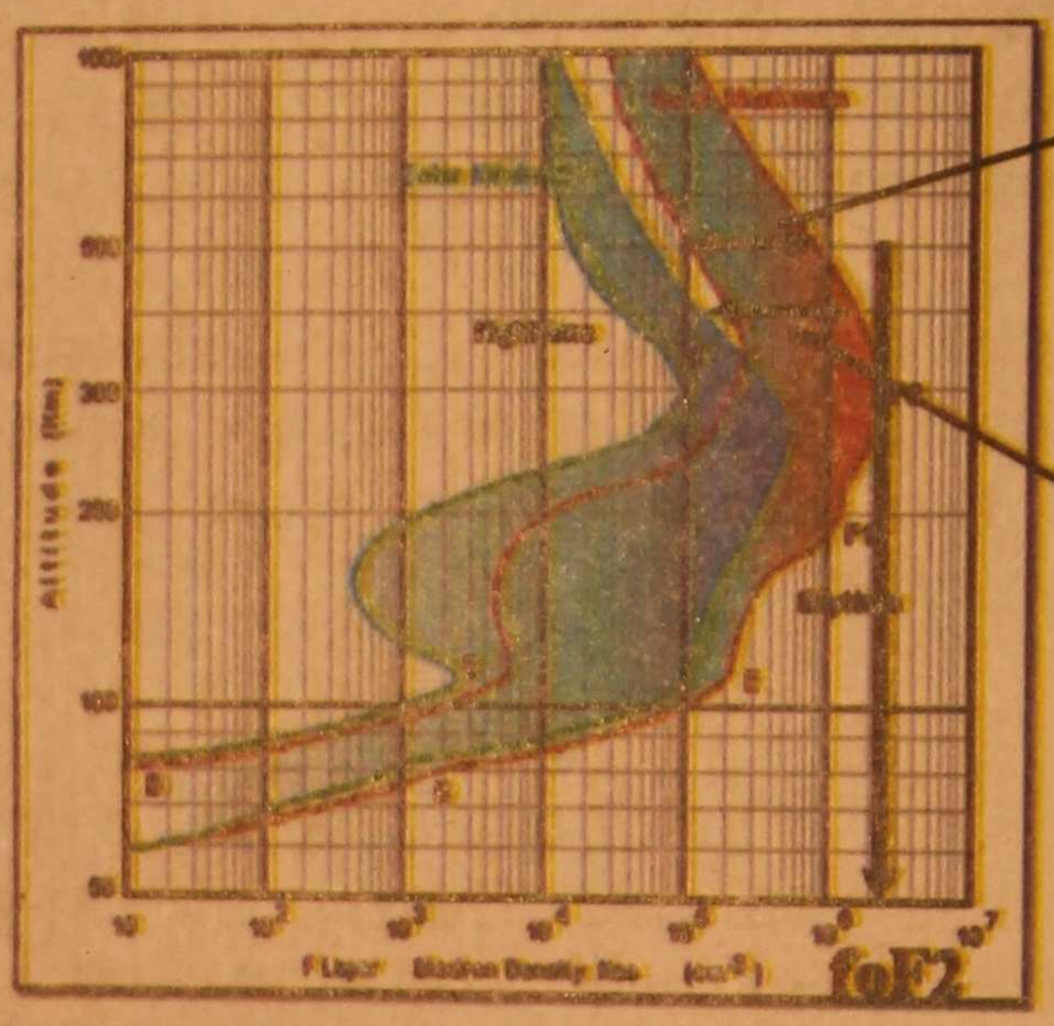

Figure 4: Ionospheric electron density profile showing diurnal and solar activity variations in the ionospheric

The FT technique makes it possible to show the extent to which periodicities in the secular variation of foF2 follow the solar activity. As can be observed in Figure 3, the results of the FT show the changes of foF2 in duration of day (**diurnal and semidiurnal variations**), season (**annual and semiannual variations**), **27-day and 11-year variations**. The 27-day with power amplitude (order of 10^5) and the weak 12.42 hr gravitational lunar periodicity (order 10^4) are not significant because their amplitudes are much smaller in comparison to other variations. These variations (diurnal and solar cycle variation) are also buttressed using Figure 4.

Diurnal Variation

Diurnal variations are caused as a result of the daily rotation of the Earth about its own axis following the apparent movement of the sun. The rotation of the Earth around the sun causes sunrise and sunset on a daily basis, which can be described by the solar zenith angle. As a result, the atmosphere undergoes a regular variation of the solar day (24 solar hours) due to the combined gravitational and thermal effects of the sun on the Earth. Figure 5 shows a typical example of diurnal variation of ionospheric critical frequency, foF2.

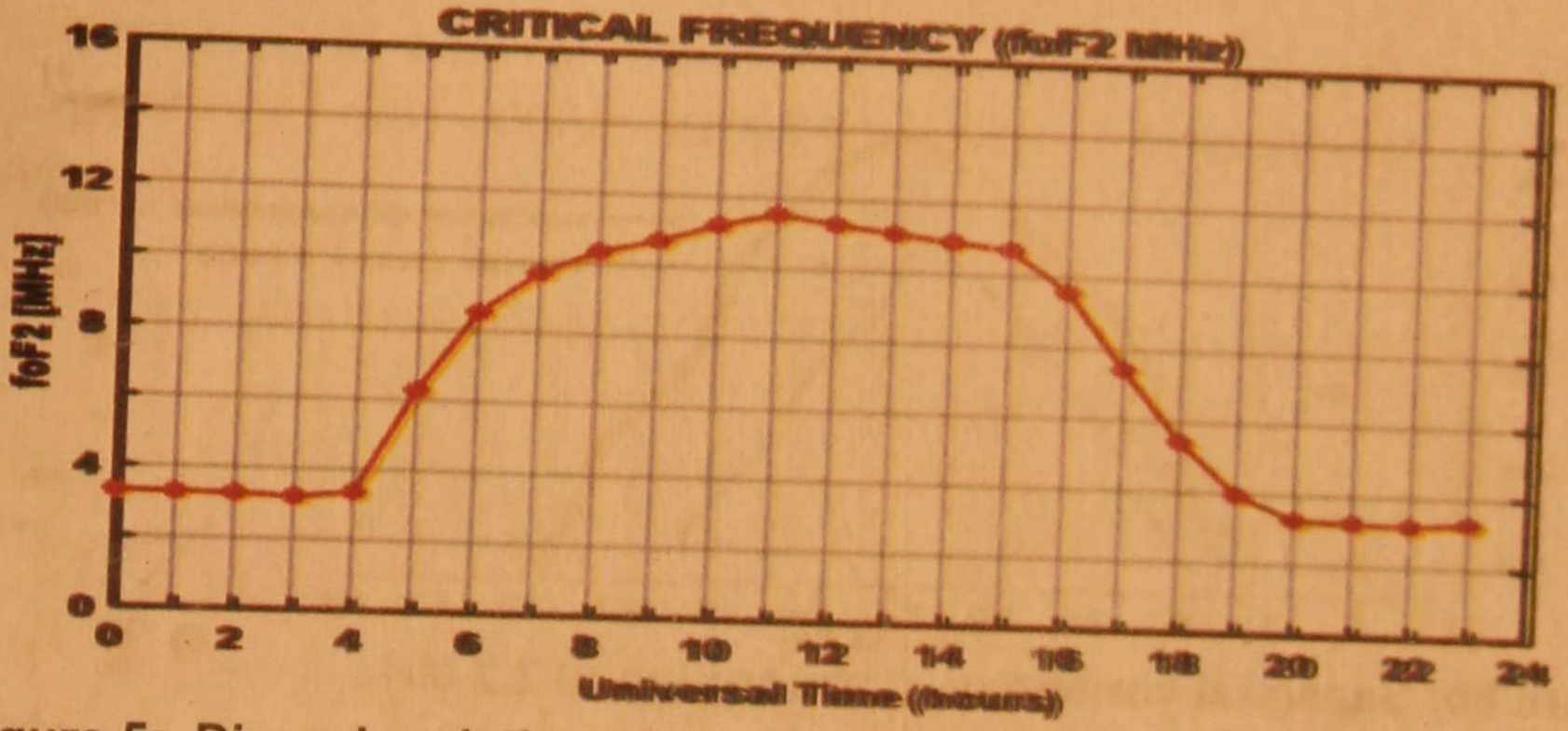

Figure 5: Diurnal variation of maximum frequency (foF2)

Seasonal Variation

Seasonal variations are caused by the tilt and rotation of the Earth on its axis. In this case, the Earth revolves around the sun such that the relative position of the sun moves from one hemisphere to the other with changes in seasons. During the year, the seasons change depending on the amount of sunlight reaching the Earth as it revolves around the Sun. This brings about seasonal variations in the angle of the sun (solar zenith angle) and its intensity at any geographical location on the surface of the Earth (Figure 6a). Figure 6b shows a typical example of seasonal variations in absorption at 2.2 MHz.

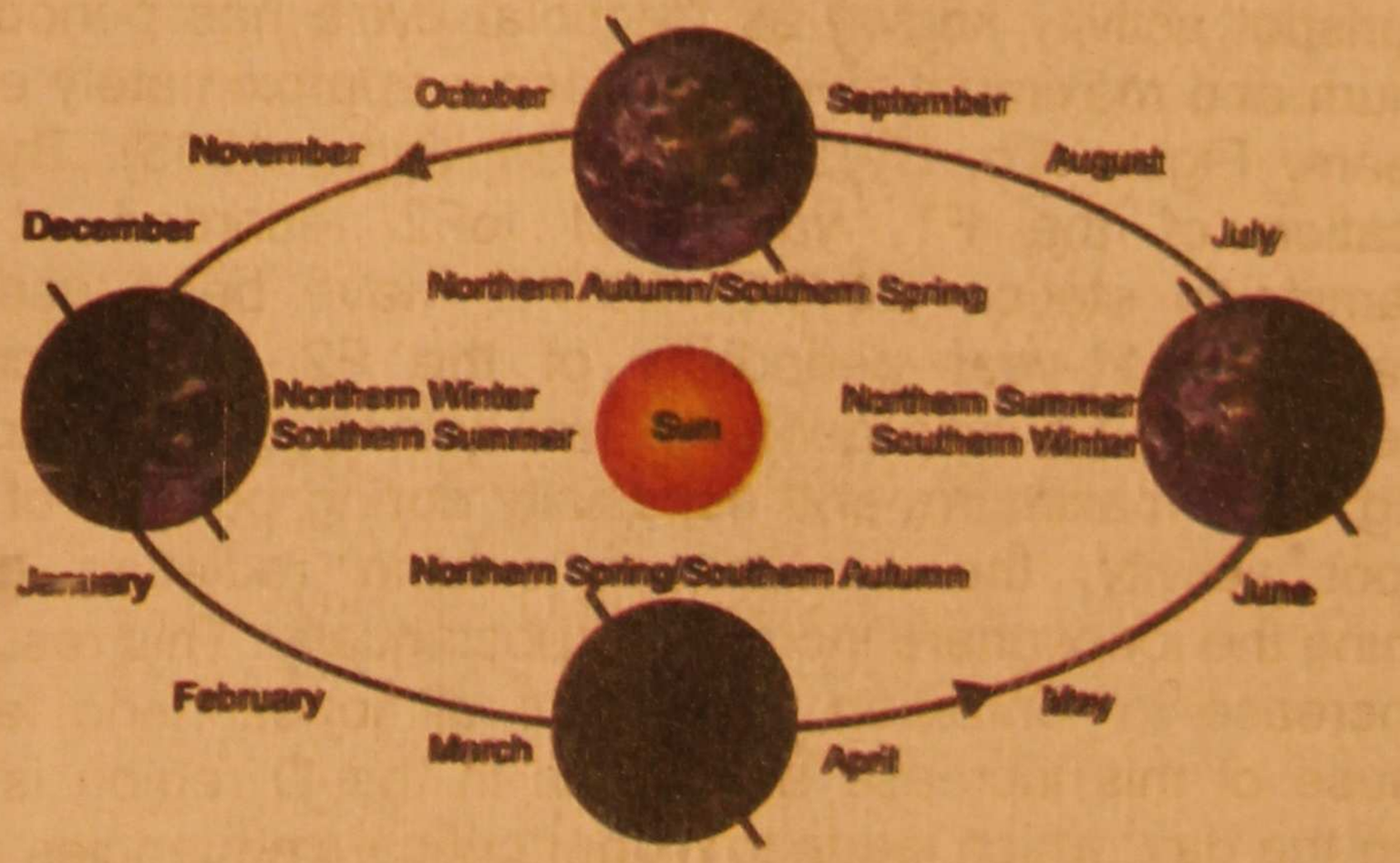

Figure 6a: The positions of the earth's axis relative to the sun at various times of the year
(https://www.google.com/search?q=seasonal+rotation+of+the+earth&tbm)

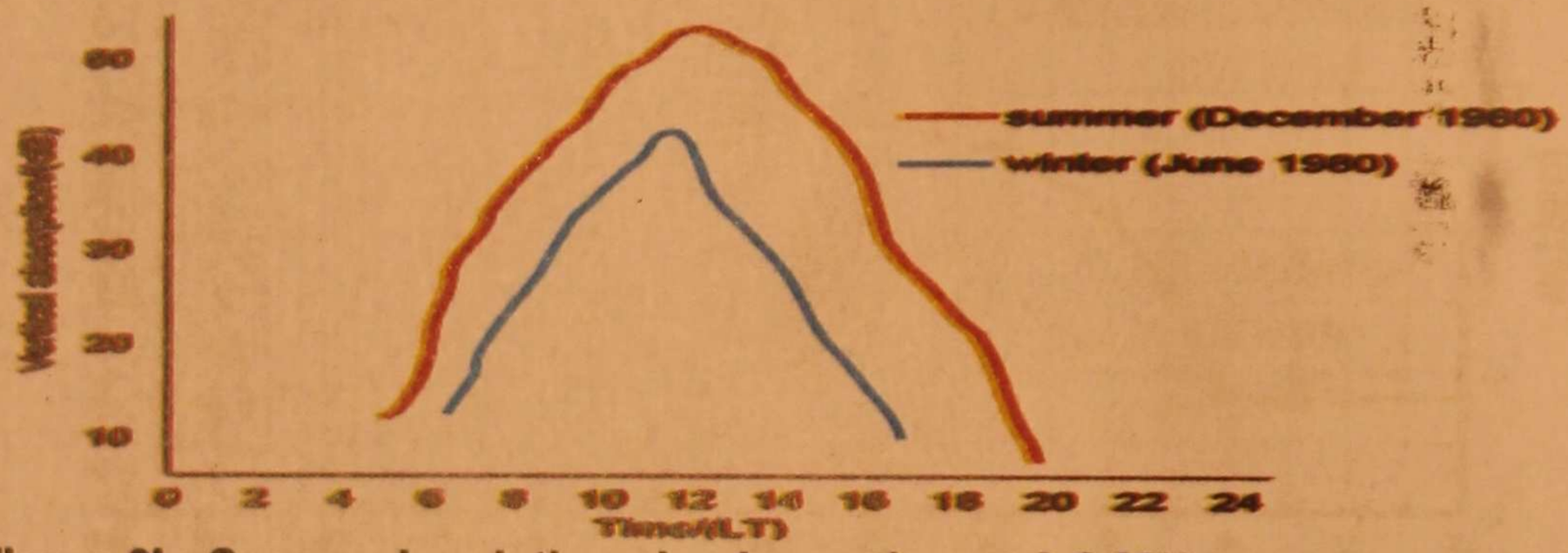

Figure 6b: Seasonal variations in absorption at 2.2 MHz

Solar Cycle Variation

Various groups (Forbes et al., 2000; Rishbeth and Mendillo, 2001; Sethi et al., 2002; Liu et al., 2003) have shown the dependence of the F2 region peak electron density on solar cycle activity. This is illustrated in Figure 7a which shows the relationship between solar cycles and maximum frequencies. The electron density concentration in the F2 region of the ionosphere is primarily due to the ionization of atmospheric constituents O, O_2 and N_2 by the solar extreme ultraviolet (EUV) radiations (Gupta and Lakha, 2001). Solar cycle activity is associated with the appearance and disappearance of dark spots (sunspots) on the surface of the sun. A regular cycle of the sunspot activity known as the solar cycle has periods of minimum and maximum levels that occur approximately every 11 years, Figure 7b, (Russell and Mulligan, 1995). By the application of the FT, values of foF2 recorded at the Grahamstown station (33.3°S, 26.5°E) have been used to illustrate the 11-year periodicity of the F2 region critical frequency (foF2) over a period of two solar cycles (Figure 3). During solar maximum, and especially during periods of high sunspot activity, the amount of ionizing radiation (EUV) reaching the ionosphere increases substantially. This results in an increase in ionization density of all ionospheric layers. Because of this increase absorption in the D region is high during the day, which leads to higher critical frequencies in the E, F1 and F2 regions. This is one of the geophysical conditions leading to the successful propagation of only higher operating

frequencies of the HF band during solar maximum, while the ionosphere can only support lower frequencies at solar minimum.

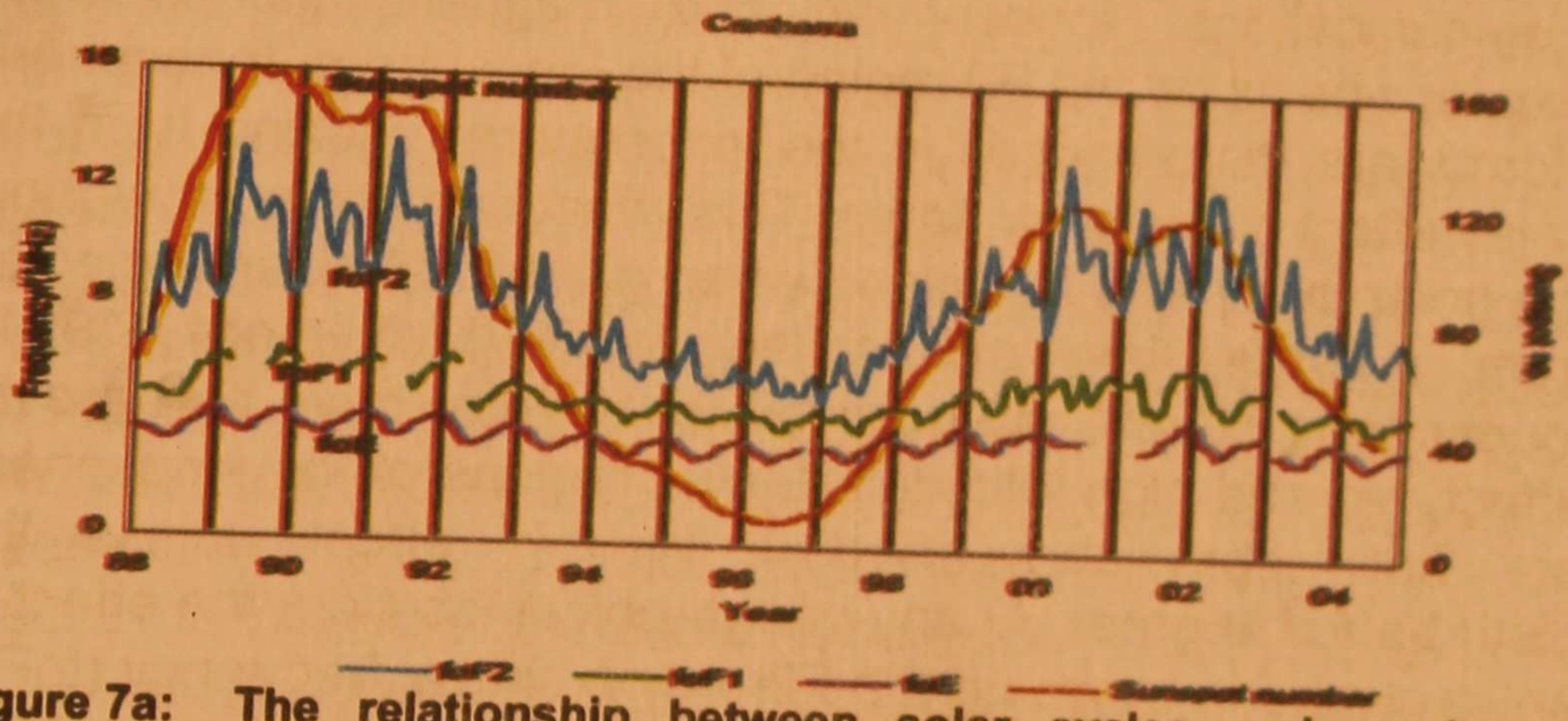

Figure 7a: The relationship between solar cycles and maximum frequencies. Vertical lines indicate the start of each year. Note also the seasonal variations

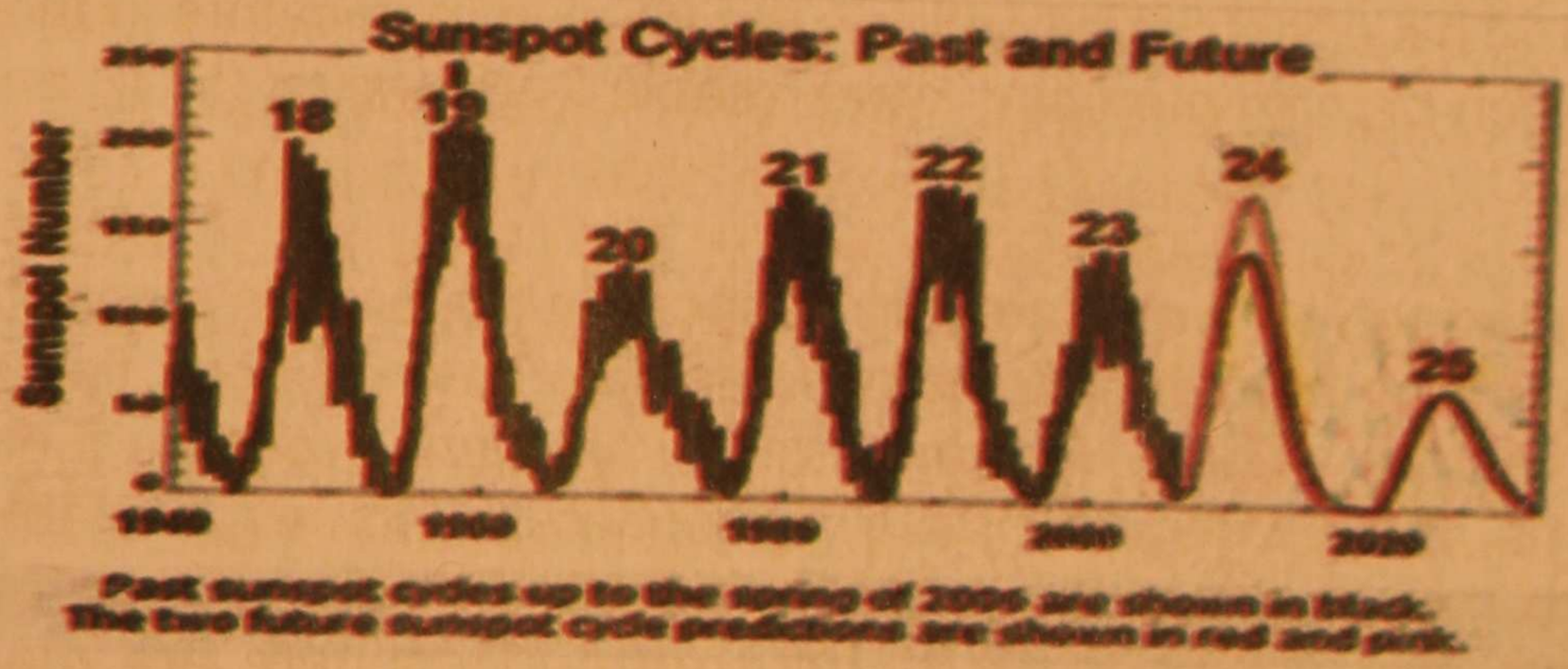

Figure 7b: Solar cycle variation (Russell, 1974)

Irregular disturbances

As the name implies, these variations occur randomly in such a way that make them difficult to model. The major source of these irregular disturbances is **solar flares**, which affect radio communication at all latitudes. Solar flares are huge explosions on the surface of the sun suddenly released from magnetic energy that has built up over time in the active sunspot region of the solar atmosphere (Rishbeth and Garriott, 1969; Hargreaves, 1979; McNamara, 1994). Ionospheric disturbances associated with **solar flares** include **sudden**

ionospheric disturbance (SID), polar cap absorption (PCA) and ionospheric and magnetic storms. They are classified according to the kind of emissions and effects they have on HF communications. Ionospheric and magnetic storms have greater effects on the F2 region of the ionosphere. Ionospheric storms are disturbances in the ionosphere resulting from the delay effect of the solar flares. This effect can occur throughout the solar cycle and is caused when a cloud of plasma ejected from a large flare strikes the earth (McNamara, 1994). Ionospheric storms may prevail for several days and mostly affect mid and high latitudes. Lower regions of the ionosphere are not appreciably affected by this effect unless the disturbance is great. At any geographical location, the effect of an ionospheric storm on the F2 region critical frequency (foF2) (either high or low) depends on the time of occurrence of the storm such as the time of the day and season, and the geographic latitude and duration of occurrence (McNamara, 1994). This effect usually affects the HF communicators in their selection of maximum and lower usable frequencies (MUF and LUF).

Geomagnetic storms are disturbances in the Earth's magnetic field, arising from the effects of solar disturbances (solar flares) (McNamara, 1994, Hargreaves, 1979). During geomagnetic storms, the F2 region of the ionosphere becomes unstable, which may result in the rapid fading of HF radio waves. The effects of a geomagnetic storm on the ionosphere are more severe over the aurora zone than in the lower latitudes (Rishbeth and Garriott, 1969). These effects usually lead to a decrease in the maximum usable frequency (MUF) and an increase in the lowest usable frequency (LUF) of the F2 region critical frequency, thereby resulting in a much smaller range of frequencies that can be used for HF communications. The severity of a geomagnetic disturbance at any time is represented by the magnetic indices K (a three-hourly quasi-logarithmic local index of geomagnetic activity) and A (a daily index of geomagnetic activity) (Rishbeth and Garriott, 1969; McNamara, 1994).

The International Reference Ionosphere (IRI) Model

The success of HF communications depends on the ability to predict ionospheric conditions, and requires up-to-date information on the state of the ionosphere. As discussed earlier, the key characteristics of particular concern for radio propagation conditions via the ionosphere are the maximum plasma frequency, foF2, maximum height (hmF2) and propagation factor M(3000)F2 for a distance of 3000 km. Over the years, several global, regional and station-specific models (Mikhailov et al., 1996; Bradley, 1999; Hanbaba, 1999; Poole and McKinnell, 2000; Bilitza, 1990, 2001; Liu et al., 2004) have been developed to predict ionospheric parameters. Among these, the International Reference Ionosphere (IRI) model is the most widely used. The IRI model has been developed to produce a global reference model, which is able to reproduce a number of ionospheric parameters. This model plays a significant role in application areas where radio signals are involved, such as ionospheric radio propagation and estimating the ionospheric effects on satellite signals. A significant efforts have been made in recent times to improve the IRI model (Bilitza et al., 2017). IRI model is recognised as a standard specification of ionospheric parameters by the Committee on Space Research (COSPAR) and the International Union of Radio Science (URSI). IRI is an international project jointly sponsored by COSPAR and URSI. The CCIR and URSI coefficients provide alternative maps of parameters, and are based on Fourier analysis and Legendre functions (spherical harmonic formulations) using monthly median values or worldwide values of foF2 for predicting ionospheric parameters (Bilitza et al., 2017). These organisations formed a Working Group in the late 1960s to produce an empirical standard model of the ionosphere. The IRI Working Group meets on an annual basis to discuss and implement improvements to the IRI model as new data and models become available and as old databases are fully evaluated and exploited. The IRI model (URSI and CCIR coefficients) is used as a benchmark to assess the success of the NN based models presented in this lecture.

Artificial Neural Networks

A Neural Network is an information-processing system that has certain performance characteristics in common with biological neurons and is modelled after the human brain, which computes some relationship between its input(s) and output(s) (Fausett, 1994; Haykin, 1994). The history of Neural Networks dates back to the early 1940s when McCulloch and Pitts (1943) developed simple models of biological neurons and their interaction systems. The most commonly used NN for various applications in many fields because of its capability to solve complex problems is the backpropagation NN otherwise known as the ***multilayer perceptron*** **or** ***multilayered feed-forward networks***. Examples of areas in which NNs have been successfully applied are **medicine, speech production, pattern recognition, control systems, speech recognition, business and ionospheric predictions** (Fausett, 1994). Very simply a NN is a computer program that is trained to learn the relationship between a given set of inputs and the corresponding output(s). The applications of the NN technique have been found to be successful for solving problems because it has the ability to describe non-linear phenomena by extracting patterns and detecting trends that are too complex to be noticed by classical methods and even humans when trained on real observed data (Williscroft and Poole, 1996; Altinay et al., 1997). A NN is made up of three basic components: weights, an activation function and a bias (Figure 8). There are three major layers in a NN. These are the input, hidden and output layers as shown in Figure 9.

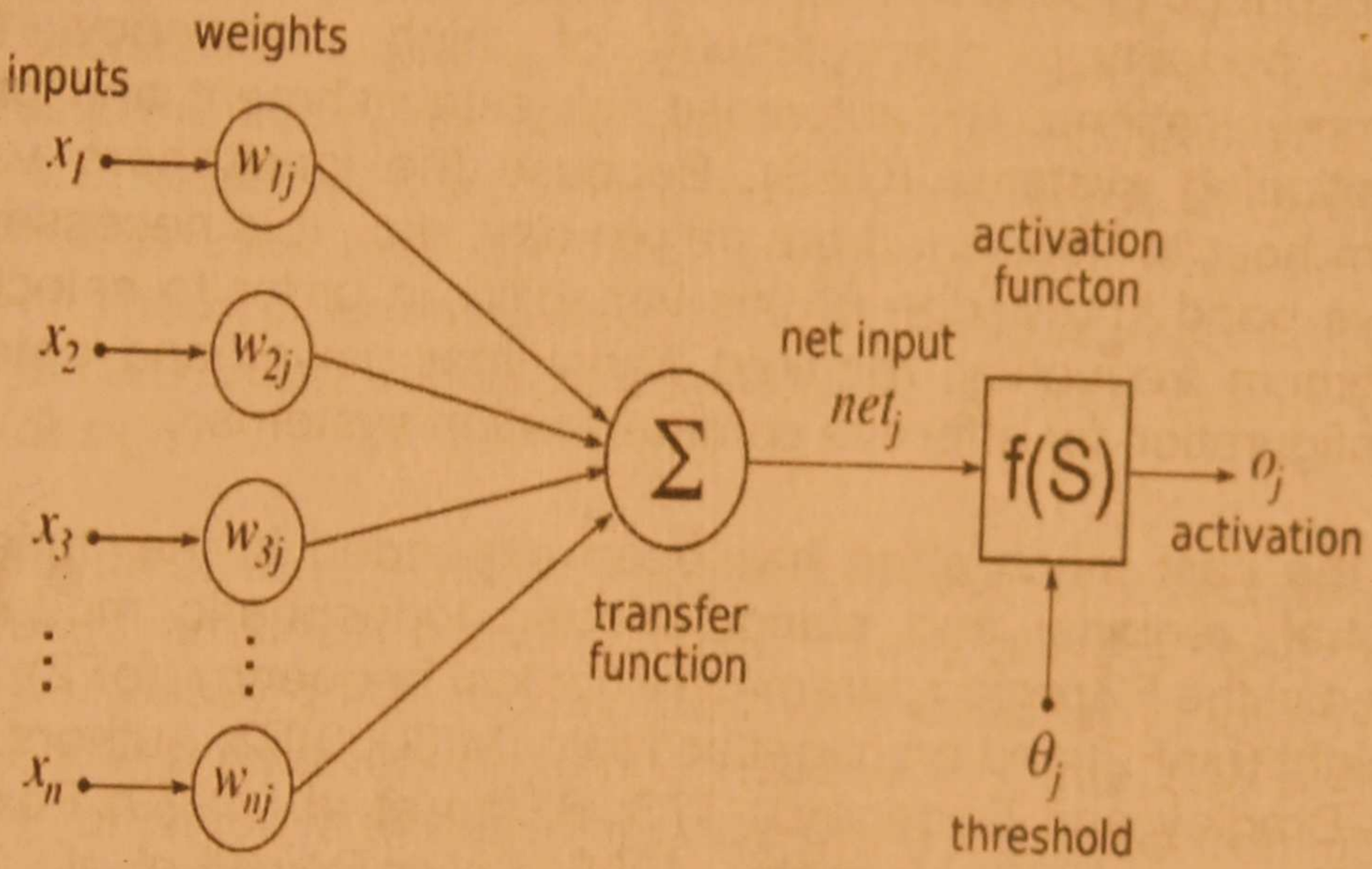

Figure 8: Basic elements of a network neuron

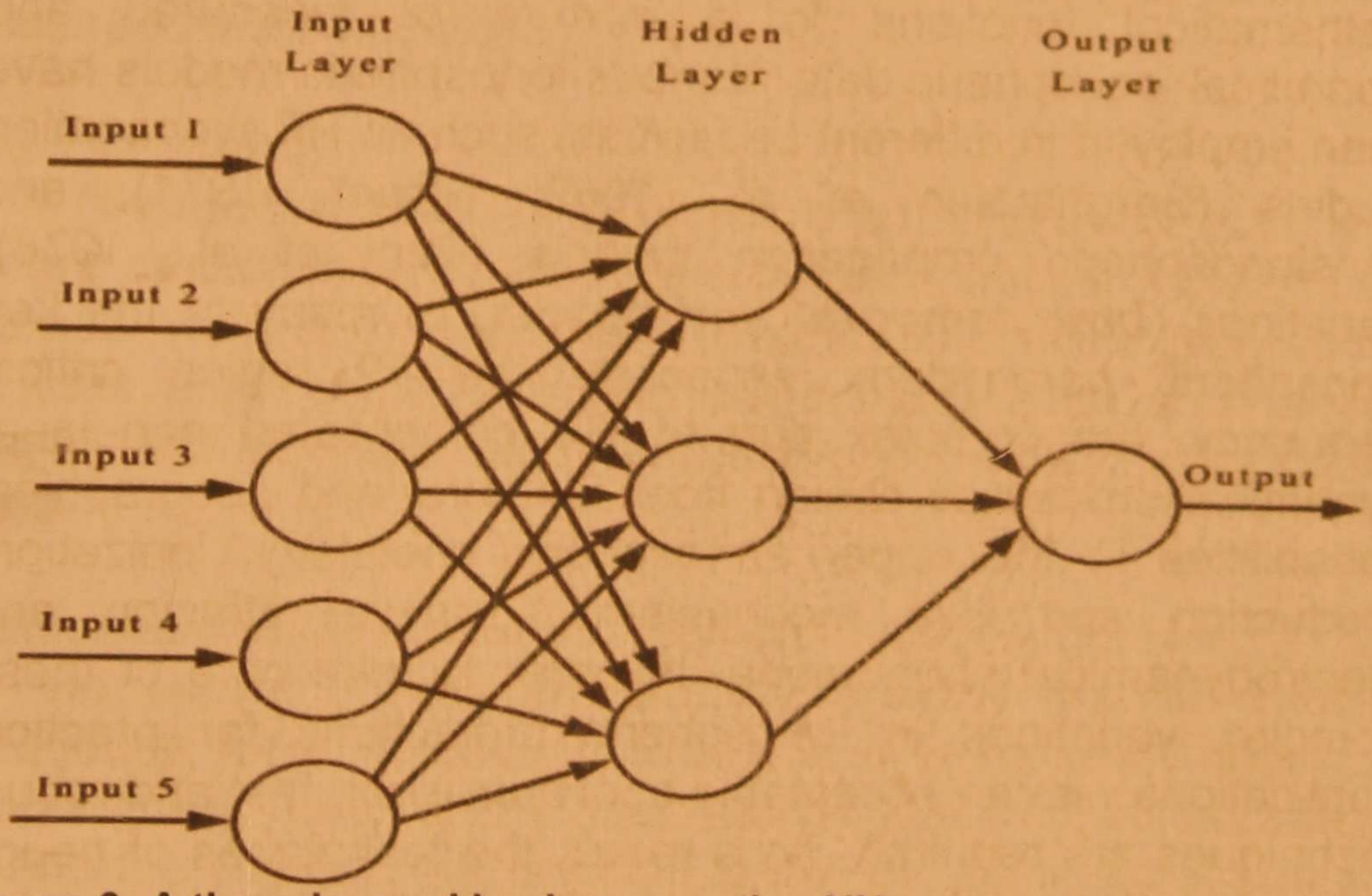

Figure 9: A three-layered backpropagation NN

MY RESEARCH FOCUS AND CONTRIBUTIONS TO KNOWLEDGE

Introduction

Mr. Vice Chancellor, Sir, permit me to give a short introduction on my research focus.

Ionospheric predictions are an important guide for the planning and frequency management of high frequency (HF) communications, HF automatic link establishment and global positioning systems (GPS). Because the ionosphere varies from hour to hour and from day to day, etc., it is necessary to have good knowledge of this variability in order to select the optimum frequency, required transmitter power and antenna configuration for effective communication systems.

In the past much effort has been expended in the quest for global, regional and station-specific ionospheric models to predict the F2 region parameters (critical frequency (foF2), peak height (hmF2) and propagation factor M(3000)F2. Authors such as Bradley and Dudeney, 1973; Bilitza et al., 1979; Fox and McNamara, 1988; Hanbaba, 1999; Fuller-Rowell et al., 2000; Bilitza, 1990, 2001 have used the standard approach of fitting mathematical functions to a mixture of measured and theoretical ionospheric data. Various ionospheric models have been employed in different capacities, such as HF propagation studies (Barghausen et al., 1969; Nisbet, 1971), and transionospheric propagation models (Bent et al., 1978). Variations (***both temporal and spatial***) of many of the key ionospheric parameters, especially the F2 region critical frequency, are complex due to the complicated non-linear dynamical processes arising from temporal and geographical variabilities in the upper atmospheric chemistry, ionization, production and loss mechanisms, particle diffusion and electrodynamical phenomena. In order to take care of these complex variations in ionospheric predictions for practical applications with an acceptable minimum error, fast and robust techniques are required. As a result, the techniques of neural networks (NNs) have been employed to develop global empirical models for the peak parameters of the F2 region of the ionosphere. Broadly speaking there are two types of predictions required.

(i) Relatively short-term frequency predictions are required by the circuit operator in order that he may be able to anticipate Maximum Usable Frequency (MUF) failure and thus increase the circuit reliability.

(ii) Long-term predictions are required for the planning of terminal installations. This involves both the circuit planner and the frequency allocator. The sorts of questions they are faced with are: What will be the range of usable frequencies over the next sunspot cycle? What is the minimum power necessary to fulfil the requirements of the circuit? What elevation angles must be used in antenna design?

To meet these requirements, I decided to develop four different NN based empirical global models. These are the foF2 NN model, M(3000)F2 NN model, short-term forecasting foF2 NN model, and a near-real time foF2 NN model. Data used in the training of these NN based models were obtained from the worldwide ionosonde stations spanning the period 1964 to 1986 based on availability, which included all periods of calm and disturbed magnetic activity.

Input Vectors

The NN input parameters which serve to define the location and time a prediction is required are solar and magnetic indices, day number (day of the year), universal time, location geographic latitude, angle of meridian relative to subsolar point, solar zenith angle, and inclination and declination of the Earth's magnetic field.

Earlier studies (Rishbeth and Garriott, 1969; Hargreaves, 1979) of the diurnal F2-region variation showed that its critical frequency, foF2, reaches its lowest level in the early hours of the morning, rises rapidly after sunrise due to photoionization during the day and starts to fall to low values again at sunset due to recombination. As a result, the hour number, HR (in Universal Time, UT) was considered to represent the diurnal variation of foF2 in the inputs to the NNs models. The choice of solar diurnal cycle (24 hours) (i.e. solar day) as a representative of diurnal variation (HR) of foF2 is based on the fact that its power amplitude (order of 5×10^9) is much higher when compared with that of the solar semidiurnal cycle (12 hours) (order of 7.5×10^7) and lunar semidiurnal cycle (12.42 hours)

Ionospheric predictions are an important guide for the planning and frequency management of high frequency (HF) communications, HF automatic link establishment and global positioning systems (GPS). Because the ionosphere varies from hour to hour and from day to day, etc., it is necessary to have good knowledge of this variability in order to select the optimum frequency, required transmitter power and antenna configuration for effective communication systems.

In the past much effort has been expended in the quest for global, regional and station-specific ionospheric models to predict the F2 region parameters (critical frequency (foF2), peak height (hmF2) and propagation factor M(3000)F2. Authors such as Bradley and Dudeney, 1973; Bilitza et al., 1979; Fox and McNamara, 1988; Hanbaba, 1999; Fuller-Rowell et al., 2000; Bilitza, 1990, 2001 have used the standard approach of fitting mathematical functions to a mixture of measured and theoretical ionospheric data. Various ionospheric models have been employed in different capacities, such as HF propagation studies (Barghausen et al., 1969; Nisbet, 1971), and transionospheric propagation models (Bent et al., 1978). Variations (***both temporal and spatial***) of many of the key ionospheric parameters, especially the F2 region critical frequency, are complex due to the complicated non-linear dynamical processes arising from temporal and geographical variabilities in the upper atmospheric chemistry, ionization, production and loss mechanisms, particle diffusion and electrodynamical phenomena. In order to take care of these complex variations in ionospheric predictions for practical applications with an acceptable minimum error, fast and robust techniques are required. As a result, the techniques of neural networks (NNs) have been employed to develop global empirical models for the peak parameters of the F2 region of the ionosphere. Broadly speaking there are two types of predictions required.

(i) Relatively short-term frequency predictions are required by the circuit operator in order that he may be able to anticipate Maximum Usable Frequency (MUF) failure and thus increase the circuit reliability.

(ii) Long-term predictions are required for the planning of terminal installations. This involves both the circuit planner and the frequency allocator. The sorts of questions they are faced with are: What will be the range of usable frequencies over the next sunspot cycle? What is the minimum power necessary to fulfil the requirements of the circuit? What elevation angles must be used in antenna design?

To meet these requirements, I decided to develop four different NN based empirical global models. These are the foF2 NN model, M(3000)F2 NN model, short-term forecasting foF2 NN model, and a near-real time foF2 NN model. Data used in the training of these NN based models were obtained from the worldwide ionosonde stations spanning the period 1964 to 1986 based on availability, which included all periods of calm and disturbed magnetic activity.

Input Vectors

The NN input parameters which serve to define the location and time a prediction is required are solar and magnetic indices, day number (day of the year), universal time, location geographic latitude, angle of meridian relative to subsolar point, solar zenith angle, and inclination and declination of the Earth's magnetic field.

Earlier studies (Rishbeth and Garriott, 1969; Hargreaves, 1979) of the diurnal F2-region variation showed that its critical frequency, foF2, reaches its lowest level in the early hours of the morning, rises rapidly after sunrise due to photoionization during the day and starts to fall to low values again at sunset due to recombination. As a result, the hour number, HR (in Universal Time, UT) was considered to represent the diurnal variation of foF2 in the inputs to the NNs models. The choice of solar diurnal cycle (24 hours) (i.e. solar day) as a representative of diurnal variation (HR) of foF2 is based on the fact that its power amplitude (order of 5×10^9) is much higher when compared with that of the solar semidiurnal cycle (12 hours) (order of 7.5×10^7) and lunar semidiurnal cycle (12.42 hours)

(order of 10 x 10^4) (see Figure 3) (Oyeyemi, 2005). Following Williscroft and Poole, (1996), in order to see 00h00UT and 23h000UT as two adjacent hours, HR input is split into its cyclic components according to equations 6a and 6b.

$$\mathrm{HRS} = \sin\left(\frac{2\pi \text{ x UT}}{24}\right) \qquad (6a)$$

$$\mathrm{HRC} = \cos\left(\frac{2\pi \text{ x UT}}{24}\right) \qquad (6b)$$

The 24-hour variation takes care of its harmonics (i.e. 12-, 8-, 6-hour, etc.).

The solar zenith angle (χ) dependence of diurnal and seasonal variations in the F2 region of the ionosphere has been well established (Rishbeth and Garriott, 1969; Hargreaves, 1979; Forbes et al., 2000). As a result, this parameter has been included as an input to the NNs models, and its values with respect to each geographical location were generated using the following relation:

$$\mathrm{Cos}(\chi) = \sin(\theta)\sin(\delta) + \cos(\theta)\cos(\delta)\cos(\lambda_s - \lambda_g) \qquad (7)$$

where λ_s (subsolar longitude) is given as $\lambda_s = 15\mathrm{H} - 180$ and δ is the subsolar latitude (i.e. the angle between the earth-sun line and the equatorial plane called the declination angle) given as:

$$\delta = 23.45\sin\left[\frac{360}{365}\left(\mathrm{N} + 284^0\right)\right] \qquad (8)$$

λ_g is the geographic longitude, θ is the geographic latitude, H is the hour number and N is the day number of the year.

Using the argument as for the hour number, HR, the solar zenith angle is converted as follows:

$$\mathrm{CHIS} = \sin\left(\frac{2\pi \text{ x CHI}}{360}\right) \qquad (9a)$$

$$\mathrm{CHIC} = \cos\left(\frac{2\pi \text{ x CHI}}{360}\right) \qquad (9b)$$

A comparison of the power amplitudes of monthly (27-day), semiannual (182.5-day) and annual (1 year) cycles of Grahamstown (33.3°S, 26.5°E) foF2 values, which are of the order of 7.7×10^5, 2.8×10^8 and 3.3×10^8 respectively. (Figure 3) also revealed that F2 region has a strong seasonal dependence. The inclusion of day number of the year, DN, (1 < DN < 365) (1 year cycle), which also represents the seasonal variation of foF2, as an input to NN is based on the fact that its power amplitude is greater than that of the 27-day cycle (Figure 3). The effect of the semiannual cycle variation has been taken care of by the annual cycle variation. Again, to avoid unrealistic discontinuity between December 31 and January 1, the seasonal variation (DN) is represented by the two quadrature components as follows:

$$\mathrm{DNS} = \sin\left(\frac{2\pi \text{ x DN}}{365}\right) \qquad (10a)$$

$$\mathrm{DNC} = \cos\left(\frac{2\pi \text{ x DN}}{365}\right) \qquad (10b)$$

The effects of neutral air winds on the dynamics of ionospheric F2 region have been well established (Jiuhou et al., 2003). The linkage between ionospheric morphology and thermospheric wind theory, both declination and inclination of the Earth's magnetic field were included in the inputs to the NNs to model the effects of thermospheric winds. The well-known vertical ion drift equation produced by horizontal neutral air winds is given as:

$$W = U\cos(\theta - D)\cos I \sin I \qquad (11)$$

where W is the vertical ion drift velocity, U is the horizontal wind velocity blowing at geographic azimuth θ, and D and I are the magnetic declination and inclination, respectively. This vertical ion drift velocity can vary markedly from one place to another. From equation 11, one can deduce that:

$$W \propto \cos(\theta - D) \text{ and} \qquad (12a)$$

$$W \propto \cos I \sin I \qquad (12b)$$

This implies that the phase of the diurnal variation of *W* depends on *D* (equation 12a) and the amplitude of the diurnal variation of *W* depends on *I* (equation 12b) (Challinor and Eccles, 1971). Following the expansion of the vertical ion drift equation, *D* is converted to two cyclic components according to

$$\mathrm{DS} = \sin\left(\frac{2\pi \text{ x } D}{360}\right) \quad \text{(D is in degrees)} \qquad (13a)$$

and

$$\mathrm{DC} = \cos\left(\frac{2\pi \text{ x } D}{360}\right) \qquad (13b)$$

while *I* is expressed as

$$\mathrm{IS} = \sin\left(\frac{2\pi \text{ x } 2I}{360}\right) \quad (I \text{ is in degrees}) \qquad (14)$$

The Local Time, LT, which is represented as the angle of the meridian relative to subsolar point M (i.e. angular equivalent of the location Local Time), accounts for the persistence of the ionosphere that is evidenced by the asymmetry of foF2 about noon at any geographical location. M is expressed as:

$$\mathrm{M} = (\mathrm{UT} - 12) \text{ x } 15 + \lambda_g \qquad (15)$$

where UT and λ_g are the Universal Time and geographic longitude respectively. Using the same argument as for the hour number HR, M is converted according to:

$$MS = \sin\frac{2\pi \times \mathrm{M}}{360} \qquad (16a)$$

$$MC = \cos\frac{2\pi \times \mathrm{M}}{360} \qquad (16b)$$

Other input parameters are the R2 (2-month running mean of the daily sunspot number) and A16 (2-day running mean of the 3-hourly magnetic index, a_p) as a measure of solar and magnetic activities, respectively. The results of FT on measured values of foF2 (Figure 3) revealed the 11-year periodicity of foF2 over a period of two solar cycles. This suggests that the F2 region is greatly affected by solar EUV flux. Magnetic index, a_p, takes care of the short-term (noncyclic) (1 to 4 days, typically) variations (i.e. ionospheric and geomagnetic storms) occurring randomly in such a way that makes them difficult to model. For the short-term and near-real time foF2 models, additional input parameters related to recent past observations of foF2 itself were included in the training of the NNs (Field and Rishbeth, (1997); Poole and McKinnell, (2000); Oyeyemi, (2005); Oyeyemi and Poole (2004), Oyeyemi et al. (2005a, 2005b, 2006, 2007)).

Global Models for F2 Region Ionosphere

A. F2 region critical frequency (foF2) NN based global model

Mr. Vice Chancellor, Sir, a global model of foF2 has been of major importance in various ionospheric models, providing a global distribution of F2 peak density (Nisbet, 1971; Bilitza, 2001). These models have been used in different capacities such as radio wave propagation studies and telecommunication applications. A basic requirement for developing a good NN model is the availability of a large database of reliable data that describes the history of a process. The foF2 data (Table 2) used in developing NNs based models were obtained from 59 ionospheric stations across the globe at various times from 1964 to 1986, on the basis of availability. This data covers both periods of calm and disturbed conditions. To test the success of this approach, two NN models were developed. The first NN model (NN1) was developed without data from 13 stations (Table 3), selected for their geographic remoteness, which could then be used to validate the predictions of the NN model for those remote coordinates. These stations were subsequently included in the final model (NN2). Figure 10a

illustrates a map of the geographical locations of the training and verification stations. The input vectors to the NN model consist of day number (day of the year), universal time, solar activity, magnetic activity, geographic latitude, angle of meridian relative to subsolar point, magnetic dip angle, magnetic declination, and solar zenith angle (Figure 10b).

In order to estimate the performance of the networks model, daily hourly values of foF2 predicted from NN1 and NN2 are compared with those obtained by the existing standard global IRI model using both the URSI and CCIR coefficients and experimental values of foF2 obtained from test stations (Tables 4a and 4b) and the root mean square error (RMSE) differences calculated using equation 17.

$$\mathrm{RMSE} = \sqrt{\frac{1}{\mathrm{N}}\sum_{i=1}^{N}\left(foF2_{obs} - foF2_{pred}\right)^2} \qquad (17)$$

The error differences are illustrated in Figures 11a and 11b respectively using bar graphs.

Table 2: Ionospheric Stations Used for the Training of NN1 and NN2 Networks

	Station Name	Latitude °N	Longitude°E
1.	Resolute Bay	74.7	265.1
2.	Kiruna	67.8	20.4
3.	Lycksele	64.6	18.7
4.	Narssarssuaq	61.2	314.6
5.	Uppsala	59.8	17.6
6.	Tomsk	56.5	84.9
7.	Moscow	55.5	37.3
8.	Kaliningrad	54.7	20.6
9.	Juliusruh/Rugen	54.6	13.4
10.	Goose Bay	53.3	299.2
11.	Irkutsk	52.4	104.0
12.	Slough	51.5	359.4
13.	Dourbes	50.1	4.6
14.	Winnipeg	49.8	256.6
15.	Lannion	48.5	356.7
16.	Freiburg	48.1	7.6
17.	St Johns	47.6	307.3

18.	Poitiers	46.6	0.4
19.	Ottawa	45.4	284.1
20.	Wakkanai	45.4	141.7
21.	Rome	41.8	12.5
22.	Boulder	40.0	254.7
23.	Akita	39.7	140.1
24.	Wallops Is	37.9	284.5
25.	Kokubunji	35.7	139.5
26.	Point Arguello	34.6	239.4
27.	Yamagawa	31.2	130.6
28.	Grand Bahama	26.6	281.8
29.	Okinawa	26.3	127.8
30.	Maui	20.8	203.5
31.	Dakar	14.8	341.6
32.	Djibouti	11.5	42.8
33.	Bogota	4.5	285.8
34.	Singapore	1.3	103.8
35.	Vanimo	-2.7	141.3
36.	Talara	-4.6	278.7
37.	Huancayo	-12.0	284.7
38.	Tahiti	-17.7	210.7
39.	La Reunion	-21.1	55.9
40.	Raratonga	-21.2	200.2
41.	Brisbane	-27.5	152.9
42.	Norfolk Is	-29.0	169.0
43.	Mundaring	-32.0	116.3
44.	Grahamstown	-33.3	26.5
45.	Salisbury	-34.7	138.6
46.	Canberra	-35.3	149.0
47.	Concepcion	-36.6	287.0
48.	Hobart	-42.9	147.2
49.	Christchurch	-43.3	172.8
50.	Kerquelen	-49.4	70.3
51.	Port Stanley	-51.7	302.2
52.	Campbell Is	-52.5	169.2
53.	South Georgia	-54.3	323.5
54.	Macquarie Is	-54.5	159.0
55.	Argentine Is	-65.2	295.7
56.	Casey	-66.3	110.5
57.	Terre Adelie	-66.7	140.0
58.	Halley Bay	-75.5	333.4
59.	Scott Base	-77.9	166.8

Source: *Oyeyemi et al. 2005a*

DONATED BOOK

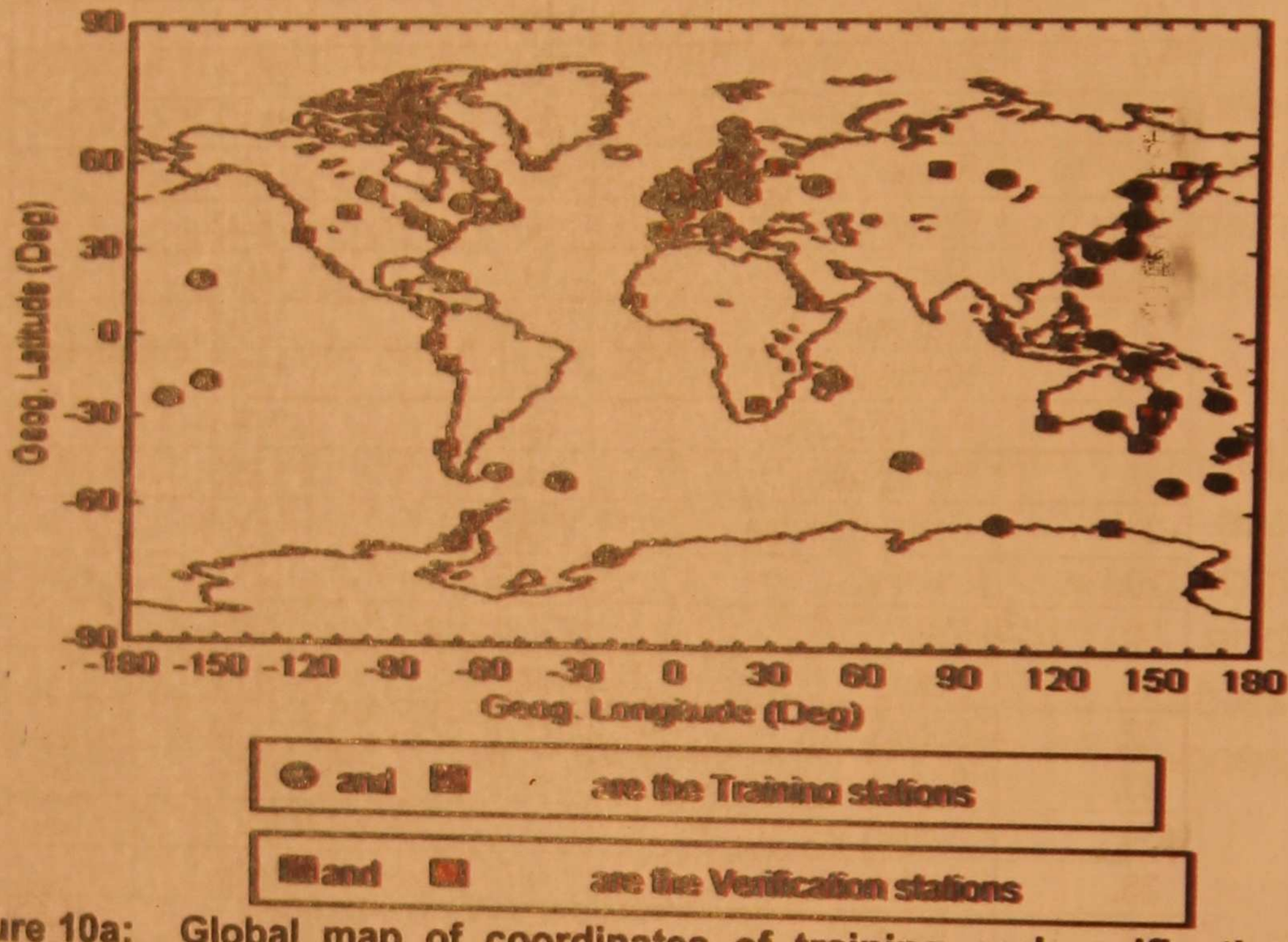

Figure 10a: Global map of coordinates of training and verification stations for NN1 and NN2

Source: *Oyeyemi et al., 2005a*

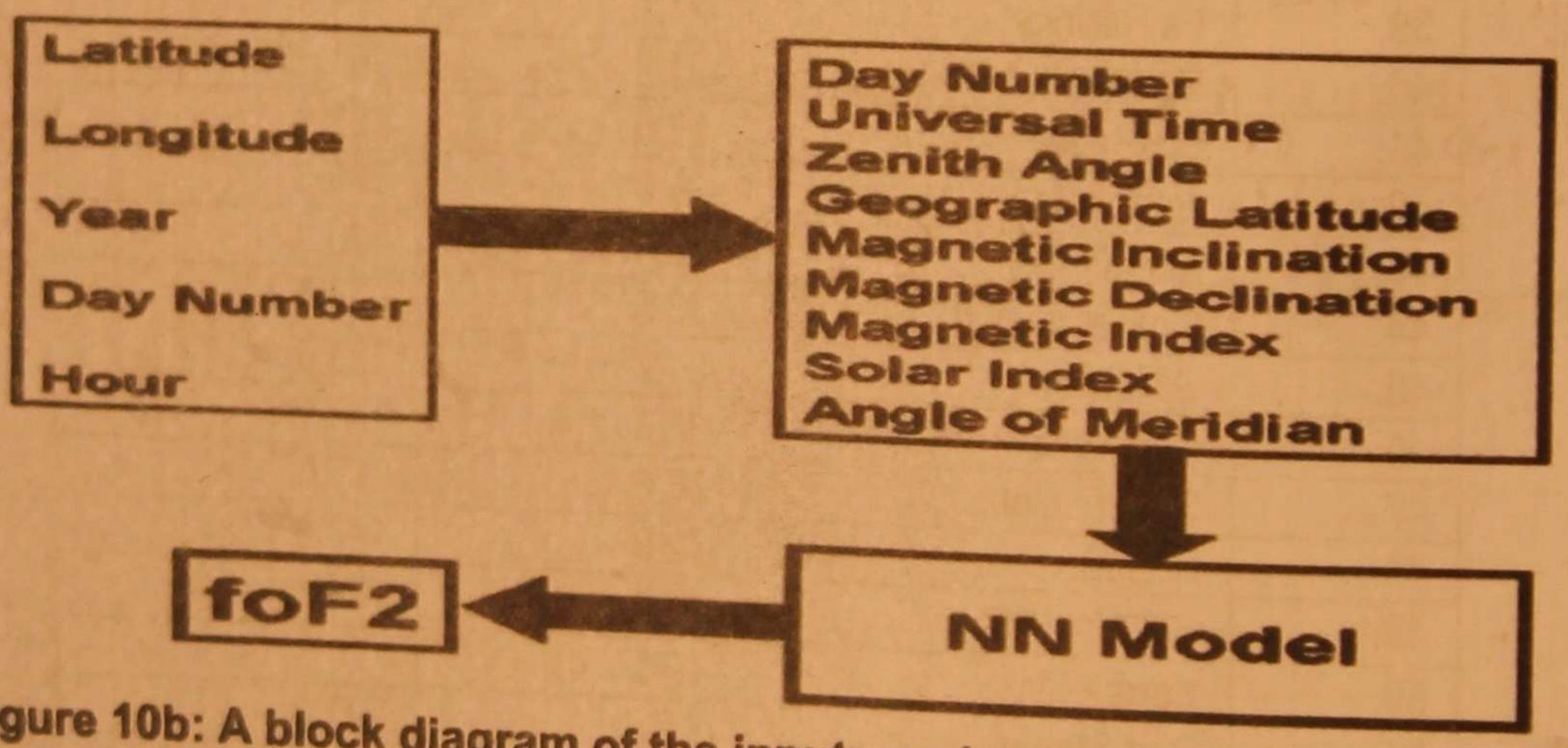

Figure 10b: A block diagram of the inputs and output to foF2 NN model

Source: *Oyeyemi et al., 2005*

Table 3: Ionospheric Stations Used for Verification of the NN1 and NN2 Models

	Station Name	Latitude °N	Longitude °E
1.	Singapore	1.3	103.8
2.	Dakar	14.8	341.6
3.	Huancayo	-12.0	284.7
4.	Talara	4.6	278.7
5.	Djibouti	11.5	42.8
6.	Grahamstown	-33.3	26.5
7.	Tomsk	56.5	84.9
8.	Terre Adelie	-66.6	140.0
9.	Concepcion	-36.6	287.0
10.	Narssarssuaq	61.2	314.6
11.	Argentine Is	-65.2	295.7
12.	Scott Base	-77.9	166.8
13.	Resolute Bay	74.7	265.1

Source: *Oyeyemi et al., 2005a*

Table 4a: The foF2 RMSE Difference (MHz) at the Verification Stations for Different Years during Solar Minimum Using URSI, CCIR, NN1 and NN2 Models

S/N	Station	Lat °N	Long °E	URSI (RMSE)	CCIR (RMSE)	NNI (RMSE)	NN2 (RMSE)	% diff between URSI and NN2	% diff between CCIR and NN2	Year
1.	Singapore	1.3	103.8	1.003	1.008	1.101	0.865	13.759	14.187	1964
2.	Dakar	14.8	341.6	1.242	1.123	1.244	1.053	15.217	6.233	1976
3.	Huancayo	-12.0	284.7	1.078	1.057	0.952	0.931	13.636	11.921	1974
4.	Talara	4.6	278.7	1.208	1.685	0.991	0.944	21.854	43.976	1965
5.	Djibouti	11.5	42.8	1.162	1.084	1.065	1.022	12.048	5.720	1974
6.	Grahamstown	-33.3	26.5	0.781	0.688	0.857	0.684	12.420	0.581	1977
7.	Tomsk	56.5	84.9	0.636	0.719	0.653	0.593	6.761	17.524	1977
8.	Terre Adelie	-66.6	140.0	0.717	0.784	0.845	0.675	5.858	13.903	1977
9.	Concepcion	-36.6	287.0	1.451	1.260	1.228	1.071	26.189	15.000	1965
10.	Narssarssuaq	61.2	314.6	0.572	0.594	0.568	0.525	8.217	11.616	1965
11.	Argentine Is	-65.2	295.7	0.846	0.916	0.766	0.703	16.903	23.253	1977
12.	Scott Base	-77.9	166.8	0.799	0.837	0.771	0.739	7.509	11.708	1977
13.	Resolute Bay	74.7	265.1	0.721	0.767	0.695	0.691	4.161	9.909	1977
	RMSE average			**0.940**	**0.963**	**0.903**	**0.807**	**14.080%**	**16.180%**	

Source: *Oyeyemi et al., 2005a*

Table 4b: The foF2 RMSE Difference (MHz) at the Verification Stations for Different Years around the Solar Maximum Using URSI, CCIR, NN1 and NN2 Models

S/N	Station	Lat °N	Long °E	URSI (RMSE)	CCIR (RMSE)	NN1 (RMSE)	NN2 (RMSE)	% difference between URSI and NN2	% difference between CCIR and NN2	Year
1	Singapore	1.3	103.8	1.503	1.513	1.531	1.151	23.420	23.926	1958
2	Dakar	14.8	341.6	1.418	1.405	1.504	1.207	14.880	14.093	1971
3	Huancayo	-12.0	284.7	1.273	1.296	1.145	1.124	11.705	13.272	1958
4	Tatera	4.6	278.7	1.402	1.670	1.272	1.173	16.334	29.760	1961
5	Djibouti	11.5	42.8	1.299	1.200	1.293	1.230	4.651	-2.500	1978
6	Grahamstown	-33.3	26.5	1.268	0.927	1.134	0.903	28.785	2.589	1979
7	Tomsk	56.5	84.9	1.262	1.166	1.275	0.996	21.078	14.580	1979
8	Terre Adelie	-66.6	140.0	1.203	1.206	1.154	1.092	9.227	9.577	1979
9	Concepcion	-36.8	267.0	1.732	1.539	1.368	1.193	31.120	22.482	1958
10	Narssarssuaq	61.2	314.6	1.061	1.076	1.042	0.965	9.048	10.316	1958
11	Argentine Is.	-65.2	295.7	1.419	1.398	1.019	1.000	29.478	28.469	1979
12	Scott Base	-77.9	166.8	1.402	1.319	1.182	1.163	17.047	11.827	1979
13	Resolute Bay	74.7	265.1	1.371	1.374	1.305	1.263	7.877	8.079	1979
	RMSE average			1.364	1.316	1.261	1.112	17.855%	15.398%	

Source: *Oyeyemi et al., 2005a*

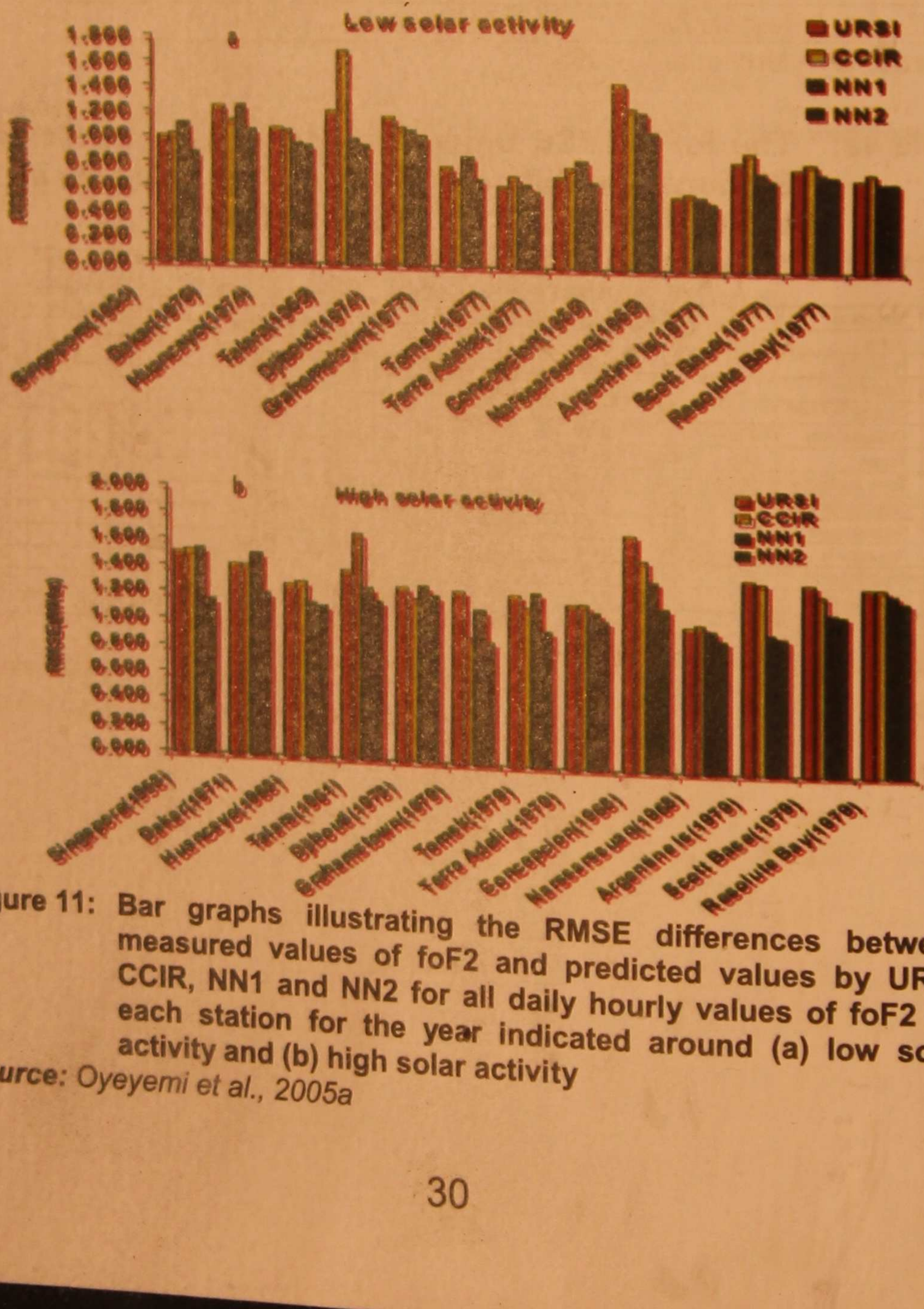

Figure 11: Bar graphs illustrating the RMSE differences between measured values of foF2 and predicted values by URSI, CCIR, NN1 and NN2 for all daily hourly values of foF2 for each station for the year indicated around (a) low solar activity and (b) high solar activity

Source: *Oyeyemi et al., 2005a*

The averages of the RMSE differences for all the years from the verification stations in Tables 4a and 4b for each of URSI, CCIR, NN1 and NN2 were also evaluated using RMSE average equation represented as:

$$RMSE_{average} = \frac{1}{k}\sum_{j=1}^{k}(RMSE)_j \qquad (18)$$

where k is the total number of stations used for verification (k =13).

The averages of the RMSE differences are illustrated using the bar chart of Figure 12. Also shown in Tables 4a and 4b are the percentage error differences between URSI, CCIR and NN2. These percentage error differences were evaluated according to equations (19) and (20) respectively. The overall percentage error difference of the verification stations during solar minimum activity between URSI and NN2 is 14.08%, and between CCIR and NN2 is 16.18% (Table 4a). For solar maximum activity, the percentage error differences are 17.86% and 15.40% respectively (Table 4b).

$$\left(\frac{URSI_{RMSE} - NN2_{RMSE}}{URSI_{RMSE}}\right) \times 100 \qquad (19)$$

$$\left(\frac{CCIR_{RMSE} - NN2_{RMSE}}{CCIR_{RMSE}}\right) \times 100 \qquad (20)$$

Figure 12: Bar graphs illustrating the RMSE average calculated for URSI, CCIR, NN1 and NN2 for (a) Low solar activity and (b) high solar activity, from Tables 4a and 4b respectively

Source: *Oyeyemi et al., 2005a*

Figure 13 shows examples of the diurnal variation of foF2 predicted by the NN2 model compared with URSI and CCIR, and the observed values starting at 00h00UT on the first of the days indicated in each case during the training period. Figure 14 illustrates a similar comparison of the diurnal variation of foF2 for selected stations not included in the training dataset, and for time periods that fell outside the training period.

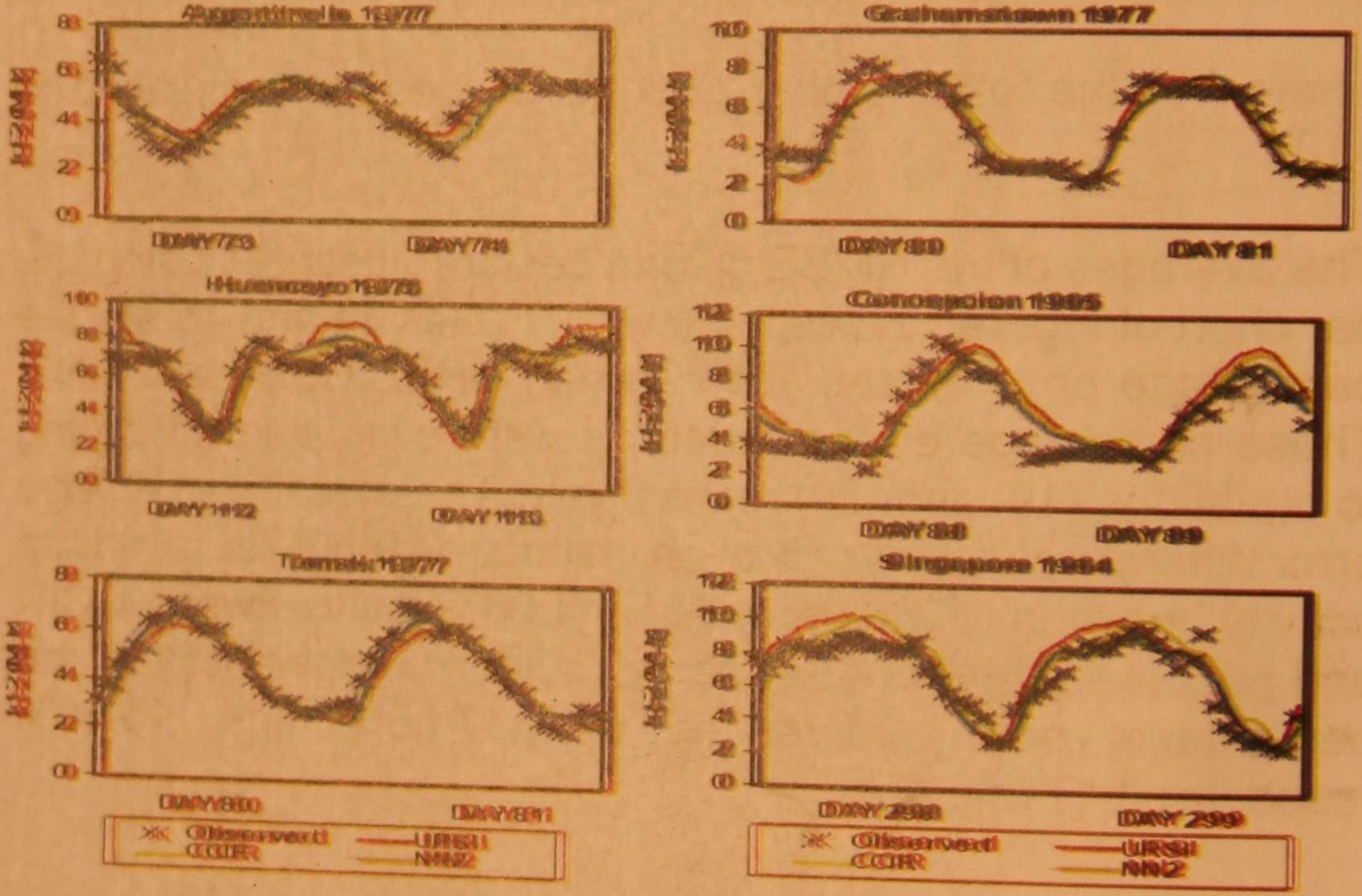

Figure 13: Comparisons of the diurnal behaviour of foF2 values predicted by the NN2, URSI and CCIR with observed values during solar minimum periods for 2 consecutive days starting at 00h00UT on the first day of the days as indicated

Source: *Oyeyemi et al., 2005a*

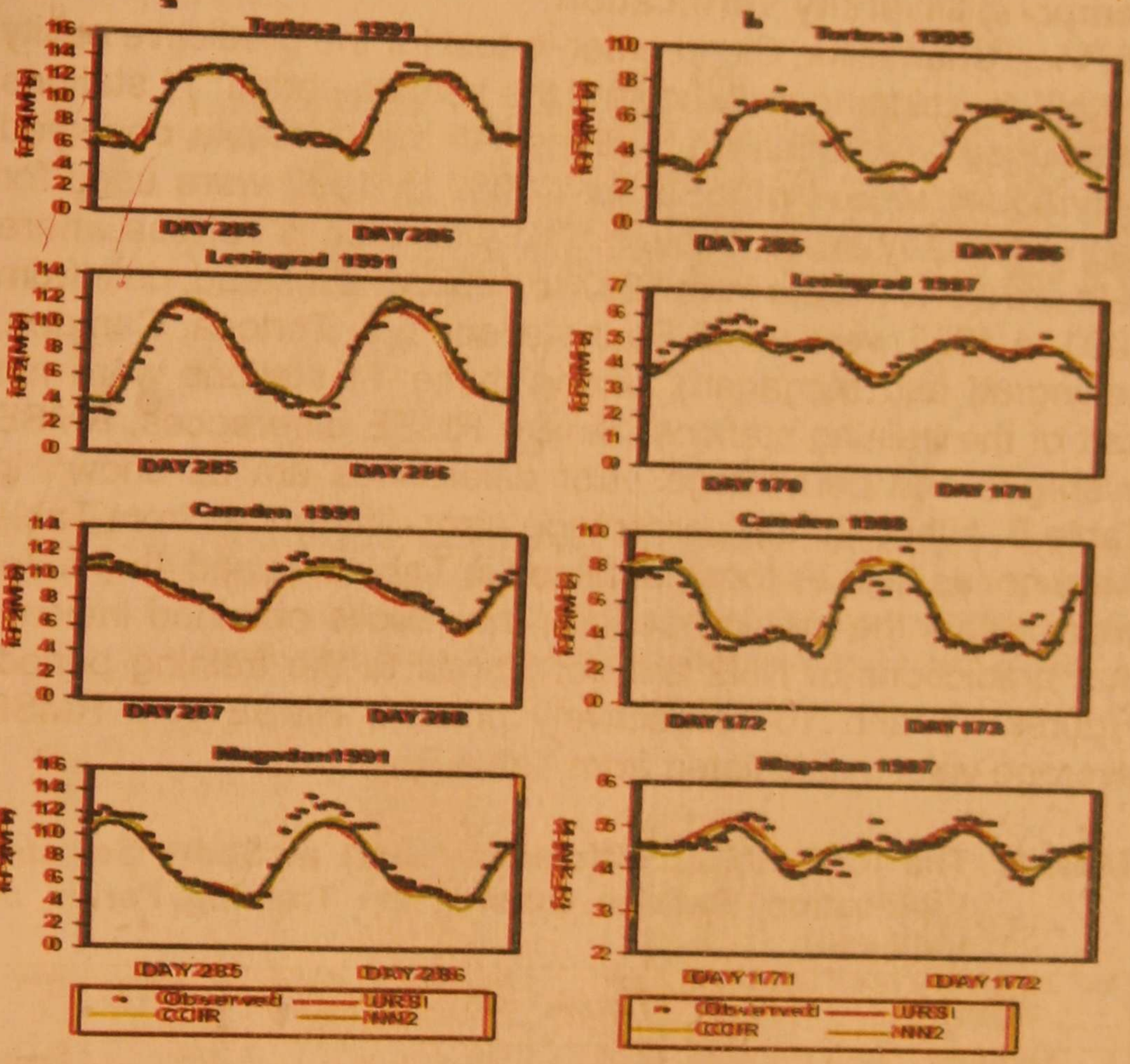

Figure 14: Similar to figure 13 by for stations not included in the training and also outside the training period for (a) solar maximum and (b) solar minimum periods

Source: *Oyeyemi et al. 2005a*

A close observation of these graphs also shows that all the three models successfully predict the general diurnal shape of foF2 behaviour. Such differences that do exist are short term (< ~ 3hrs) variations in foF2 which neither the NN models nor the IRI models are designed to predict. A comparison of NN2 results with URSI and CCIR show a very large improvement for Singapore, Talara, Concepcion, Argentine Is and Scott Base (Tables 4a and 4b). NN2 is always an improvement on either URSI or CCIR, an exception is Djibouti from Table 5b for which CCIR performs better than NN prediction.

Temporal Diversity Verification

Mr. Vice Chancellor, Sir, in order to test for the predictive ability of NN2 model *temporally* beyond the training period, 11 stations were used as verification stations. All the available observed daily hourly values of foF2 from 1987 to 1992 were used for each of the stations in Table 5. The exception is Tortosa where data are not available from 1987 to 1990, and instead, data from 1991 to 1995 were used. Four stations (i.e. Tortosa, Camden, Leningrad and Magadan) among these 11 stations were not part of the training stations. Similar RMSE differences, RMSE averages and percentage error differences are as shown in Table 5. Although, the percentage error differences from Table 5 are not as high as those obtained in Tables 4a and 4b (i.e. for years within the training period), the results obtained indicate that predictions of NN2 are not limited to the training period. Figures 15 and 16 respectively present RMSE and RMSE average values calculated from Table 5.

Table 5: The foF2 RMSE Difference (MHz) at Some Selected Verification Stations Outside the Training Period as Indicated

S/N	Station	Lat °N	Long °E	URSI RMSE (MHz)	CCIR RMSE (MHz)	NN2 RMSE (MHz)	% difference between URSI and NN2	% difference between CCIR and NN2	Period
1.	Point Arguello	34.6	239.4	1.193	1.131	1.111	6.873	1.768	1987-1992
2.	Camden	-34.0	150.7	1.178	1.167	1.081	8.234	7.369	1987-1992
3.	Uppsala	59.8	17.7	1.037	1.013	0.941	9.257	7.108	1987-1992
4.	Hobart	-42.0	147.0	1.069	1.041	0.934	12.629	10.279	1987-1992
5.	Leningrad	59.9	30.7	1.250	1.246	1.163	6.960	6.661	1987-1992
6.	Magadan	60.0	151.0	1.301	1.294	1.184	8.993	8.501	1987-1992
7.	Tortosa	40.0	0.3	1.070	1.040	0.988	7.664	5.000	1991-1995
8.	Canberra	-35.3	149.0	1.339	1.316	1.281	4.332	2.660	1987-1992
9.	Mundaring	-32.0	116.3	1.148	1.062	1.001	12.805	5.744	1987-1992
10.	Boulder	40.0	254.7	1.096	1.061	1.000	8.759	5.749	1987-1992
11.	Grahamstown	-33.3	26.5	1.219	1.062	1.023	16.079	3.672	1987-1992
	RMSE average			**1.173**	**1.130**	**1.064**	**9.248%**	**5.839%**	

Source: *Oyeyemi et al., 2005a*

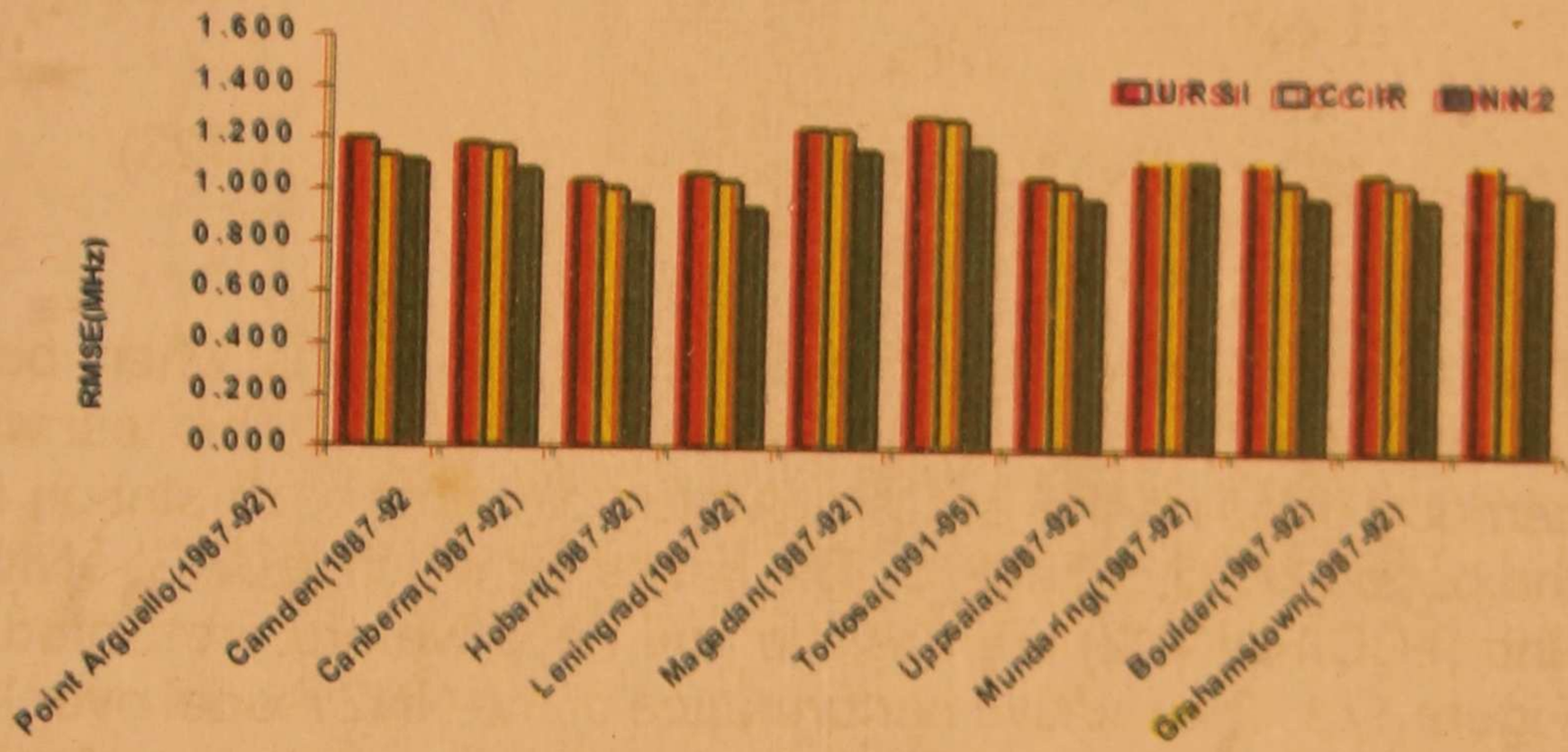

Figure 15: **Bar graph illustrating the RMSE differences between measured and URSI, CCIR and NN2 predictions for all daily hourly values of foF2 for each station for the period indicated (from Table 5)** ***Source: Oyeyemi et al., 2005a***

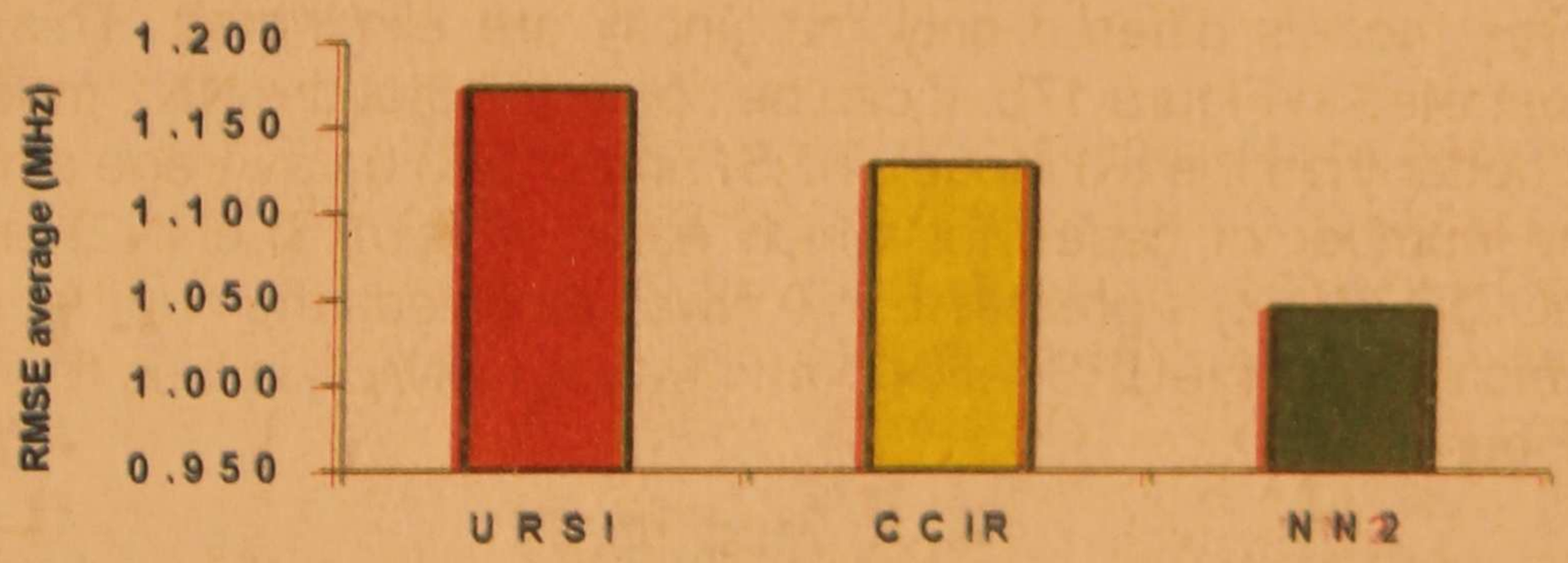

Figure 16: **Bar graph illustrating the RMSE average calculated for URSI, CCIR and NN2 for all the years indicated (from Table 5)**

Source: *Oyeyemi et al., 2005a*

The relative performance of NN2 over the IRI model (URSI and CCIR) was further verified with the observed data (outside the training period) from ionospheric stations in Table 5 using the relative error method from Houminer et al. (1993) and Richard et al. (2004). The relative errors eURSI, eCCIR and eNN2 for the URSI, CCIR and NN2 predicted values respectively were defined as:

$$eURSI = \frac{|foF2_{obs} - foF2_{URSI}|}{foF2_{obs}} \qquad (21)$$

$$eCCIR = \frac{|foF2_{obs} - foF2_{CCIR}|}{foF2_{obs}} \quad (22)$$

$$eNN2 = \frac{|foF2_{obs} - foF2_{NN2}|}{foF2_{obs}} \quad (23)$$

The NN2 model can be regarded as successful when both (eURSI-eNN2) > 0 and (eCCIR-eNN2) > 0 is true. This test was carried out on all the available data points for each station for the period listed in Table 5. The cases for which (eURSI-eNN2) and (eCCIR-eNN2) are positive and negative are presented in Figure 17a. The relative performance of the NN2 model over the IRI model is further clarified by considering only the number of cases for which the absolute values of (eURSI-eNN2) and (eCCIR-eNN2) in each case is greater than 0.05. This is done to ensure that those cases for which the performance of the three models differed only marginally are eliminated. This is illustrated in Figure 17b. It can be observed that the NN2 model is better than the IRI model (URSI and CCIR) on average since the number of cases for which each of (eURSI-eNN2) and (eCCIR-eNN2) is greater than 0 always exceeds the number for which each of (eURSI-eNN2) and (eCCIR-eNN2) is less than 0 (Figure 17a).

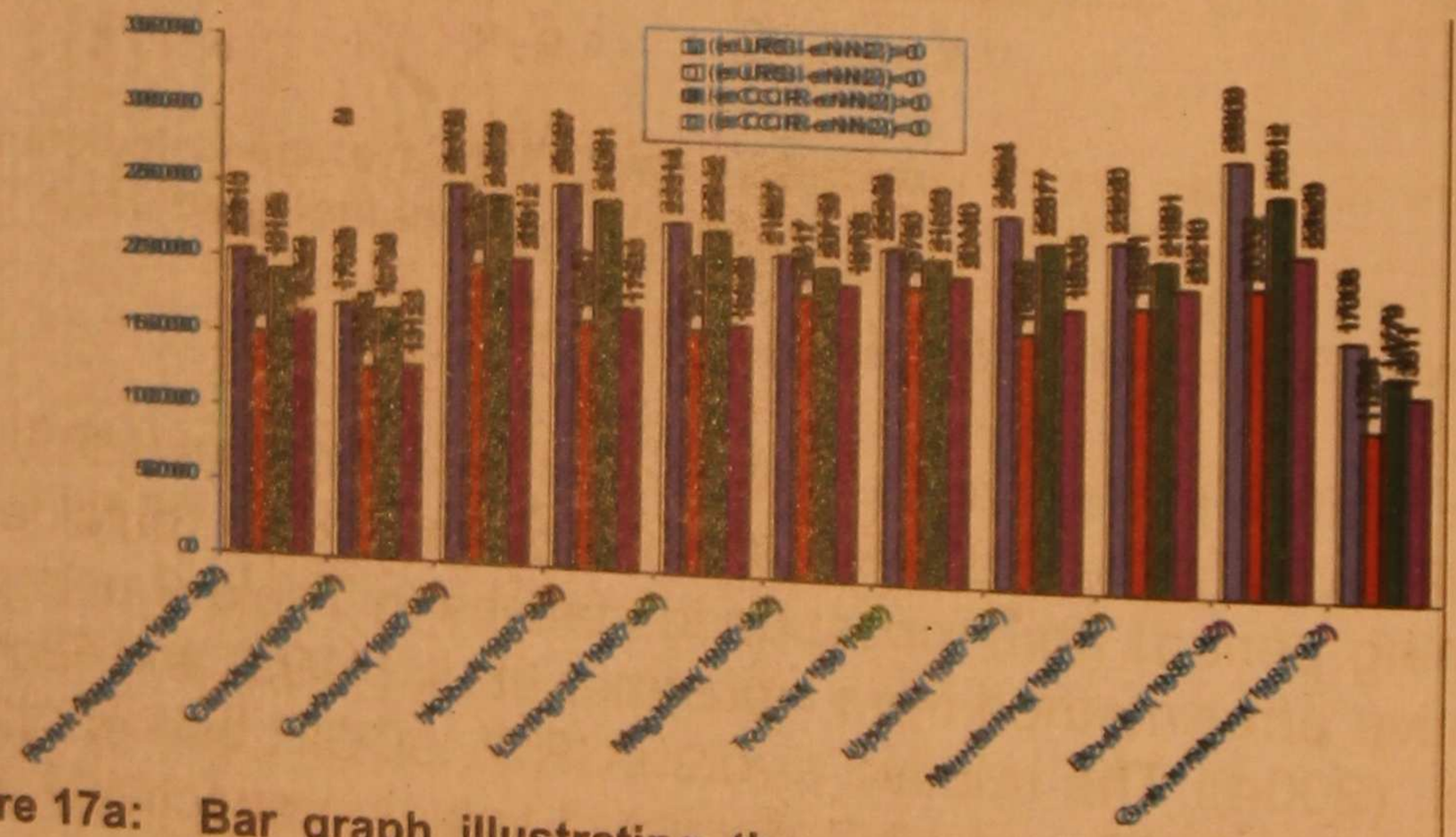

Figure 17a: **Bar graph illustrating the cases where the NN2 model performs better than the IRI model (URSI light blue, CCIR green) and where the NN2 model performs worse than the IRI model (URSI red, CCIR pink) for all the available hourly values of foF2 for each of the periods indicated**

Source: *Oyeyemi 2005*

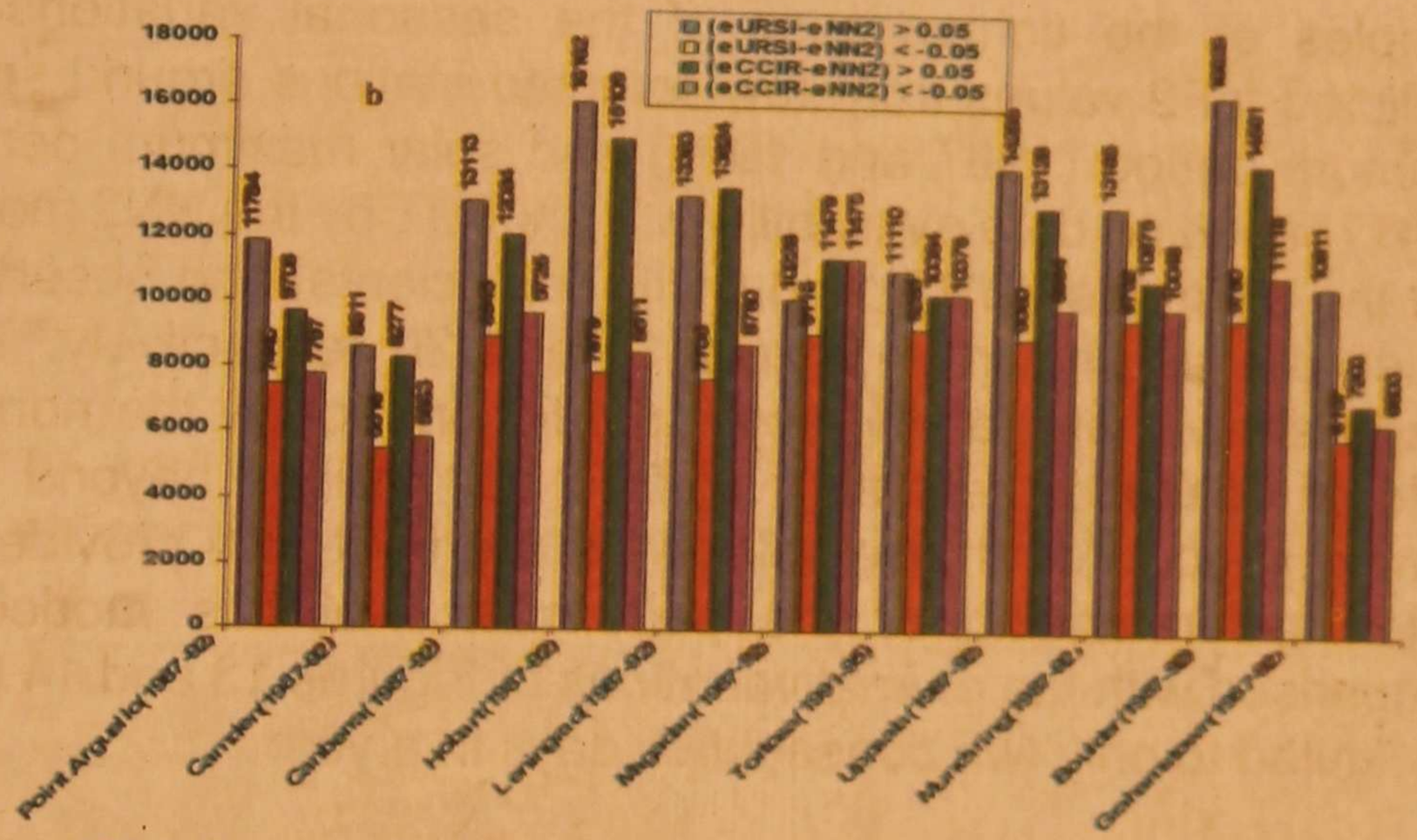

Figure 17b: Bar graph illustrating only cases where the difference in the absolute values of (eURSI-eNN2) and (eCCIR-eNN2) in each case is greater than 0.05.

Source: *Oyeyemi 2005*

Also, Figure 17b shows the number of cases for which each of (eURSI-eNN2) and (eCCIR-eNN2) is greater than 0.05 exceeds the number of cases for which each is less than - 0.05. The exceptions are for Magadan and Tortosa stations where the performance of the NN2 model and the IRI (CCIR option) are much the same (Figure 17b). A closer inspection of Figures 17(a & b) also reveals that the CCIR predictions are better than the URSI predictions.

Figures 18A (a, b and c) respectively show examples of the global distribution of foF2 values predicted by the NN2 model, URSI and CCIR coefficients for October 12, 1991 at 12h00UT for solar maximum. Values of foF2 were obtained using a scale size interval of 10 degrees for both geographic longitude and latitude. Figures 18B (a, b and c) illustrate a similar global variation of daily hourly values of foF2 for June 21, 1996 at 12h00UT during solar minimum. These maps are similar because the differences are not large but serve to show that the NN2 model does predict a similar global distribution of foF2 like the IRI model.

Samples of the comparisons of the seasonal variations of predicted foF2 values from few selected stations around solar minimum period (1987 and 1995) and solar maximum period (1991) based on data availability at 12h00UT by the NN2 model with the IRI model (URSI and CCIR coefficients) and observed values are as shown in figures 19 and 20 respectively. The results show that the NN model predictions follow the normal trend of seasonal behaviour of foF2 for periods beyond the training period from these selected stations. It also provides a better understanding of the performance of this model in comparison with the diurnal variations of Figures 13 and 14 that are limited to only two consecutive days in a year.

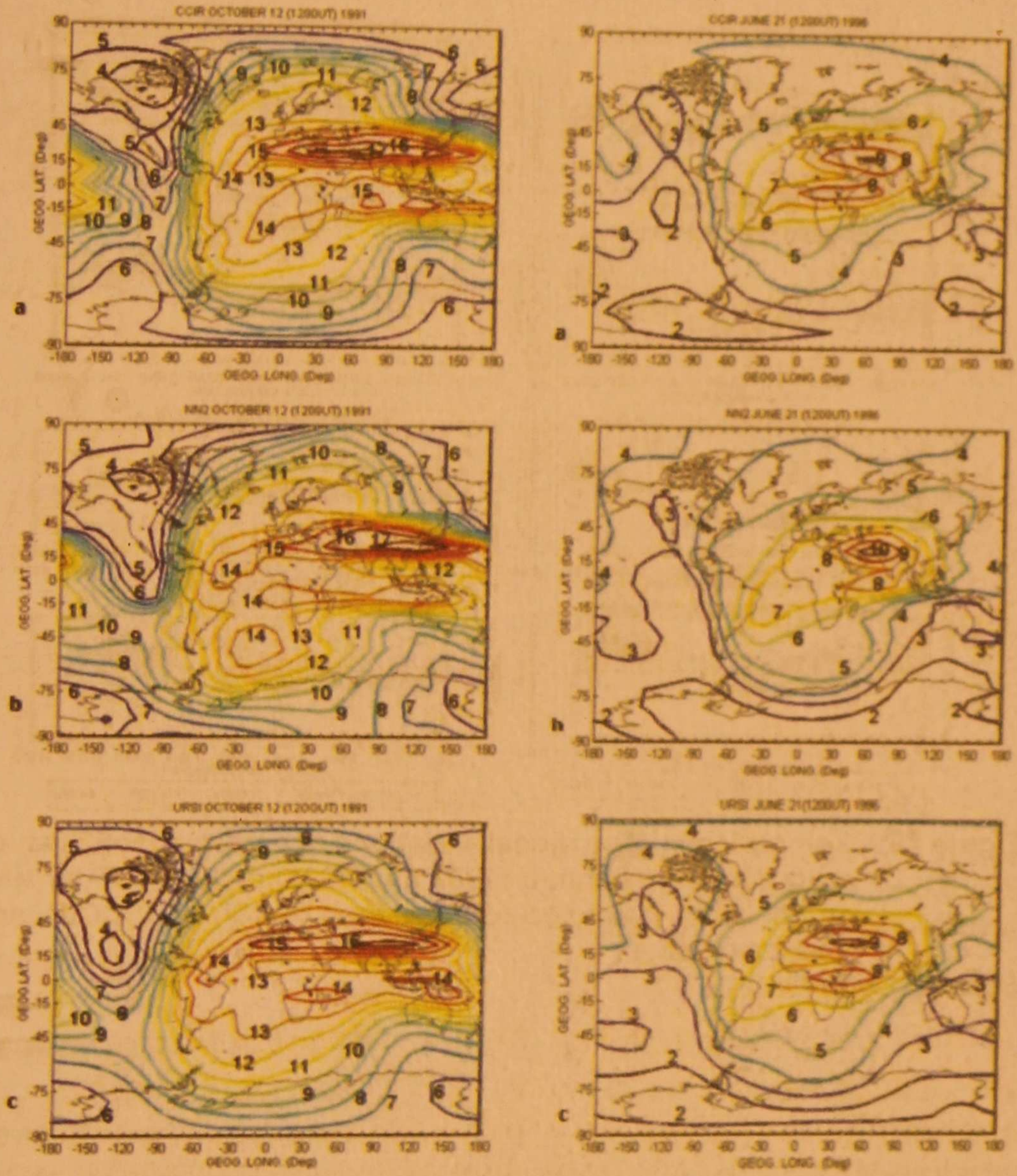

Figure 18: (A) Contour map of the global representation of foF2 values for October 12, 1991 at 12h00UT derived from (a) CCIR, (b) NN2 and (c) URSI models during high solar activity. (B) Contour map of the global representation of foF2 values for June 21, 1996 at 12h00UT derived from (a) CCIR, (b) NN2 and (c) URSI models during low solar activity

Source: *Oyeyemi et al., 2005a*

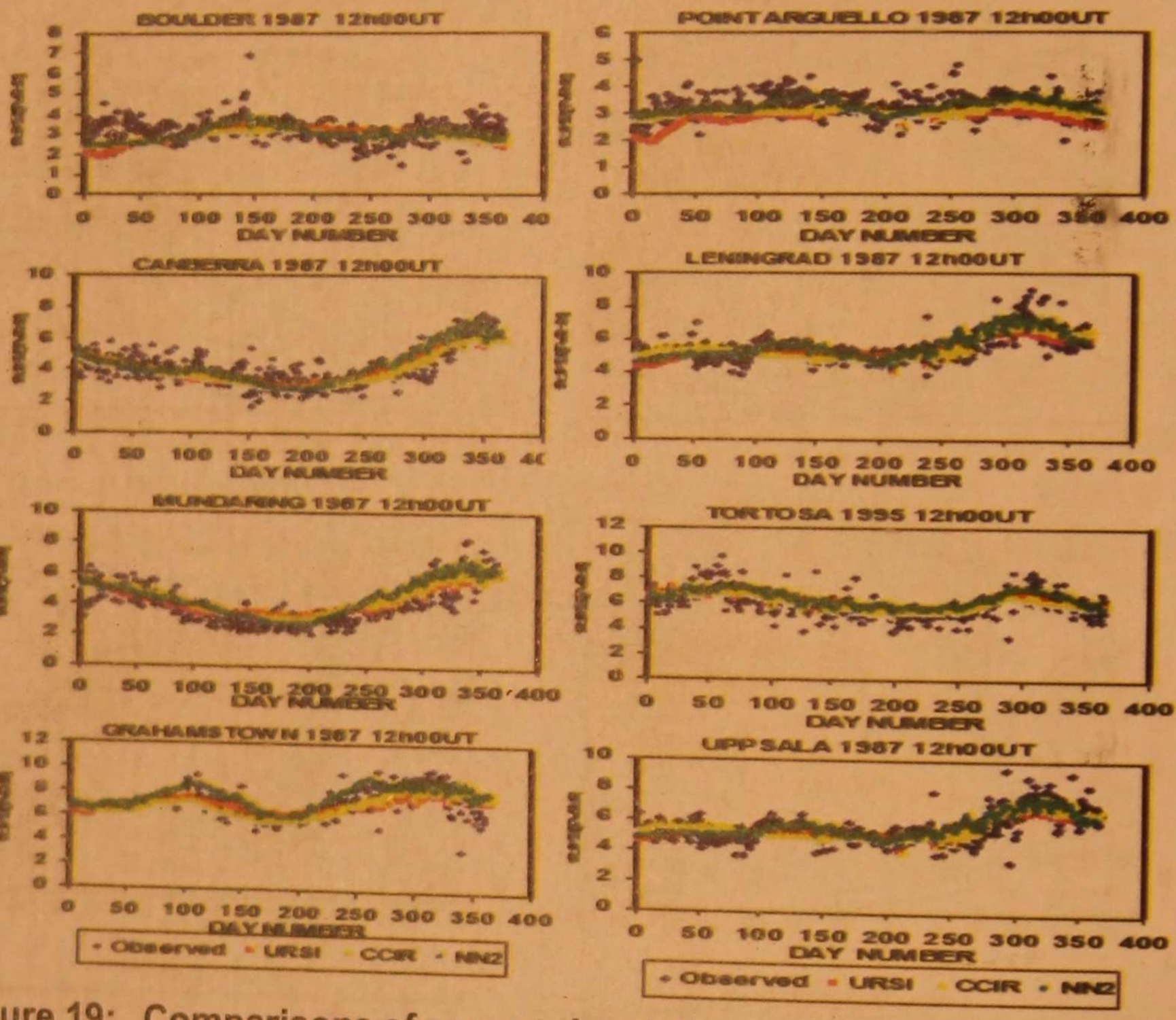

Figure 19: Comparisons of seasonal variations of predicted foF2 values around solar minimum (1987 and 1995) at 12h00UT by NN2 model with predicted values from URSI and CCIR and observed values

Source: *Oyeyemi 2005*

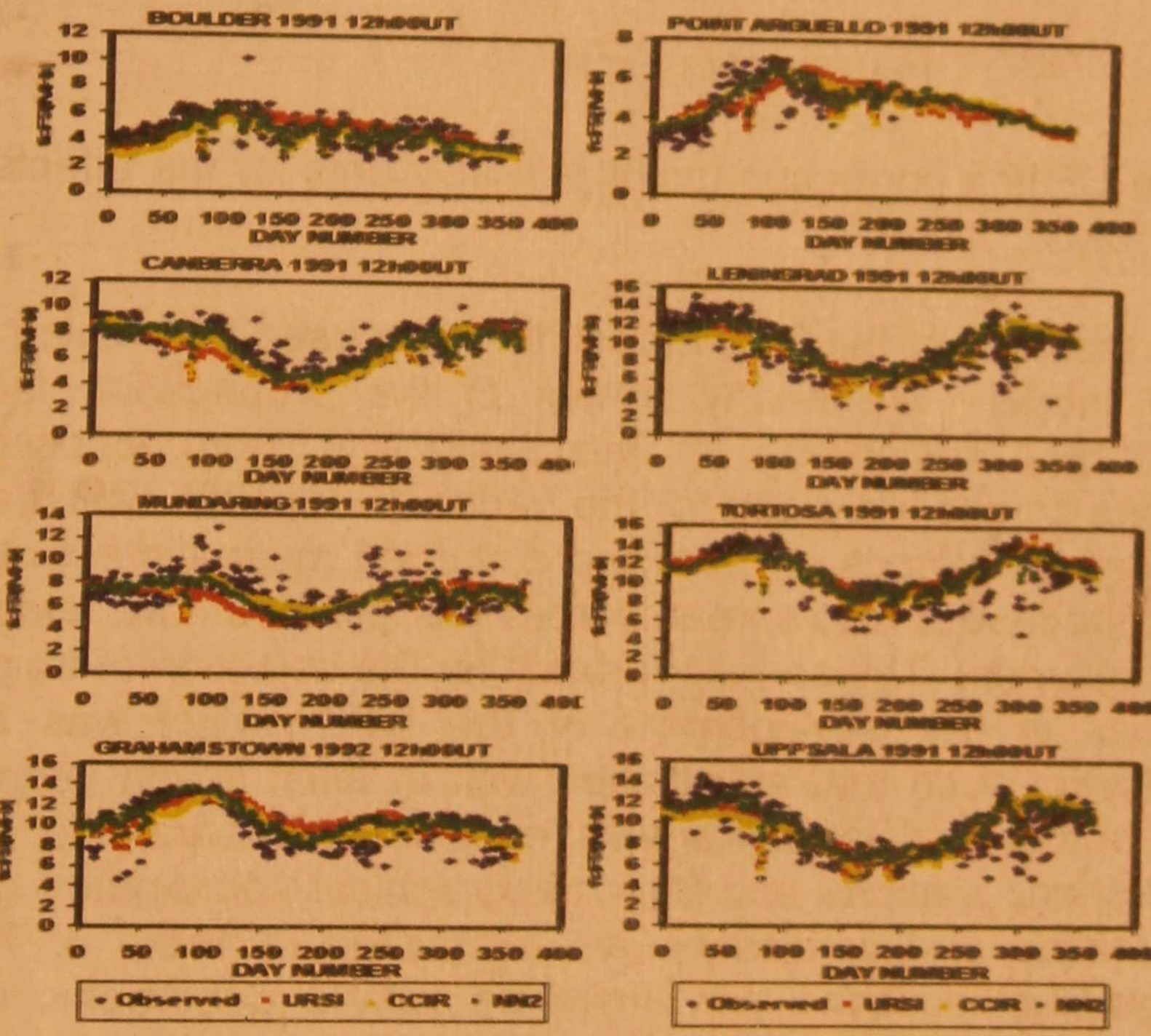

Figure 20: Comparisons of seasonal variations of predicted foF2 values around solar maximum (1991) at 12h00UT by NN2 model with predicted values from URSI and CCIR and observed values

Source: *Oyeyemi 2005*

Propagation Factor (M(3000)F2) NN Model (NNM)

Mr. Vice Chancellor, Sir, this section discusses the development of a global empirical model for the propagation factor M(3000)F2 using the same approach as that of the global foF2 empirical model discussed earlier. The M(3000)F2 parameter is related to the maximum usable frequency MUF(3000), which is defined as the highest frequency at which a radio wave can be received over a distance of 3000 km after refraction in the ionosphere (Bradley and Dudeney, 1973). Mathematically M(3000)F2 = MUF(3000)/foF2). Just like foF2, M(3000)F2 is another ionospheric parameter that is also important for frequency planning for various applications in HF radio communications and ionospheric models. For instance, the height of the F2 peak (hmF2) can be obtained from its close correlation with the propagation factor M(3000)F2 with the empirical formula:

$$\mathrm{hmF2} = \frac{1490}{[\mathrm{M(3000)F2} + \mathrm{CF}]} - 176 \qquad (24)$$

where CF is a correction factor that accounts for the effects of the E-layer.

As in the case of the foF2 model, the data used for training the NNM model are hourly values of the propagation factor M(3000)F2, depending on the availability, from ionosonde stations across the globe for the period 1964–1986 which also included all periods of calm and disturbed magnetic activities. The database is also spread across the latitudes (low, mid and high latitudes). The same approach for the selection of training stations in the development of the foF2 model was also employed, such that any station with at least seven years of data within a solar cycle was considered for training. The ionospheric stations and their geographical coordinates used for training and verification are presented in Table 6. Their geographic locations are illustrated with a geographic map shown in Figure 21. The basic structure of the NNM model employed in this work is a standard fully connected feedforward network with backpropagation. Figure 22 shows the block diagram of the NNM model with input and output parameters.

Table 6: Ionosonde Stations Used in the Training and Verification of NNM Model

S/N	Station Name	Lat °N	Lon °E	Verification station
1.	Resolute Bay	74.7	265.1	
2.	Kiruna	67.8	20.4	
3.	Lycksele	64.6	18.7	
4.	Magadan	60.0	151.0	B
5.	Uppsala	59.8	17.6	B
6.	Sverdlovsk	56.4	58.6	B
7.	Moscow	55.5	37.3	B
8.	Kaliningrad	54.7	20.6	
9.	Juliusruh/Rugen	54.6	13.4	
10.	Irkutsk	52.4	104.0	B
11.	Slough	51.5	359.4	
12.	Dourbes	50.1	4.6	
13.	Winnipeg	49.8	256.6	
14.	Lannion	48.5	356.7	

15.	St Johns	47.6	307.3	
16.	Poitiers	46.6	0.4	
17.	Ottawa	45.4	284.1	
18.	Wakkanai	45.4	141.7	B
19.	Tortosa	40.4	0.3	
20.	Boulder	40.0	254.7	B
21.	Akita	39.7	140.1	
22.	Wallops Is	37.9	284.5	B
23.	Kokubunji	35.7	139.5	
24.	Point Arguello	34.6	239.4	
25.	White Sands	32.3	253.5	
26.	Yamagawa	31.2	130.6	
27.	Okinawa	26.3	127.8	
28.	Maui	20.8	203.5	B
29.	Dakar	14.8	341.6	
30.	Vanimo	-2.7	141.3	B
31.	Huancayo	-12.0	284.7	B
32.	Tahiti	-17.7	210.7	
33.	La Reunion	-21.1	55.9	
34.	Raratonga	-21.2	200.2	
35.	Brisbane	-27.5	152.9	
36.	Norfolk Is	-29.0	169.0	
37.	Mundaring	-32.0	116.3	B
38.	Grahamstown	-33.3	26.5	B
39.	Salisbury	-34.7	138.6	
40.	Canberra	-35.3	149.0	
41.	Concepcion	-36.6	287.0	B
42.	Hobart	-42.9	147.2	
43.	Kerquelen	-49.4	70.3	
44.	Port Stanley	-51.7	302.2	
45.	Campbell Is	-52.5	169.2	B
46.	Macquarie Is	-54.5	159.0	B
47.	Argentine Is	-65.2	295.7	B
48.	Terre Adelie	-66.7	140.0	
49.	Mawson	-67.6	62.9	
50.	Halley Bay	-75.5	333.4	
51.	Scott Base	-77.9	166.8	

Source: *Oyeyemi et al., 2007*

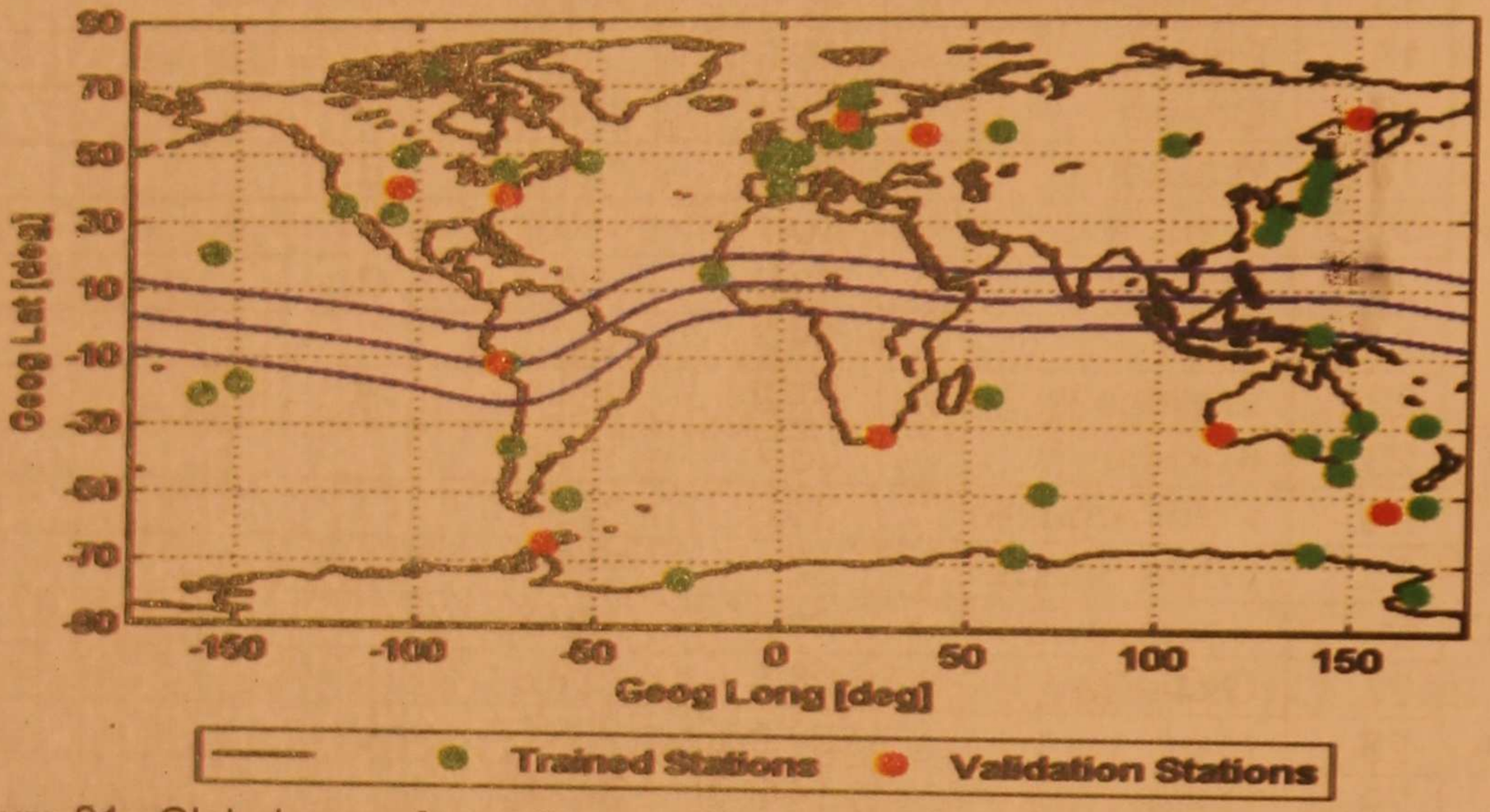

Figure 21: Global map of coordinates of training (green dots) and verifications (red dots) stations of NNM model

Source: Oyeyemi et al., 2007

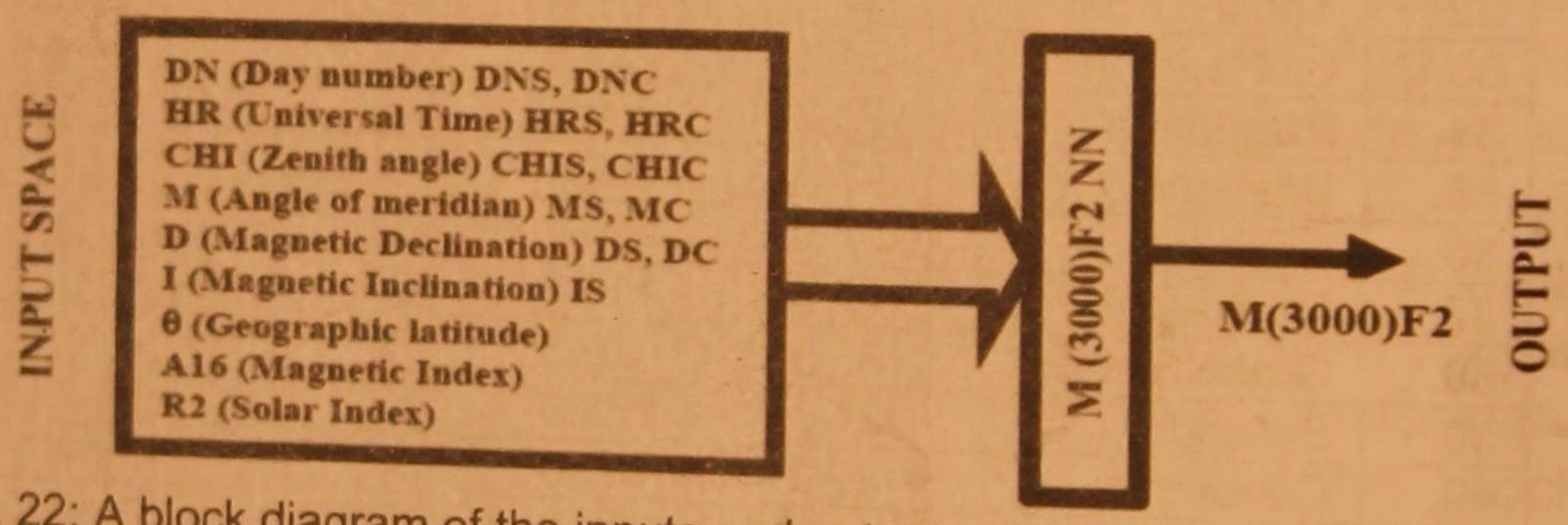

Fig. 22: A block diagram of the inputs and output to NNM

Source: *Oyeyemi et al., 2007*

The predictive ability of the NNM model temporally beyond the training period of 1964-1986 was carried out. The performance of the NNM model that was trained with M(3000)F2 values from all the stations in Table 6 was determined using equations 17 and 18 of RMSE and $RMSE_{average}$ respectively. Tables 7a and 7b show the error differences between measured and predicted values of M(3000)F2 by the NNM model and the IRI model for high and low solar activity periods respectively. As can be observed from Tables 7a and 7b, a comparison of error differences obtained for the IRI model and NNM model justify the potential of the NN techniques for M(3000)F2 predictions on a global scale, since in all cases the NNM model RMSE is smaller than that of the IRI model. The results obtained show that the NNM model can be successfully used for long-term

predictions. The NNM model is an improvement over the IRI model on average by a margin of the order of 6–20% in a number of cases as shown in Tables 7a and 7b. Evidence of this is clearly shown in Figures 23a and 23b where the error bars from NNM model predictions are smaller than that of the IRI model. Figures 24a and 24b illustrate the $RMSE_{average}$ from Tables 7a and 7b, respectively.

Table 7a: RMSE (MHz) in M(3000)F2 at Selected Verification Stations by the NNM and the IRI Model around High Solar Activity outside the Training Period

Source: Oyeyemi et al., 2007

Table 7b: RMSE (MHz) in M(3000)F2 at Selected Verification Stations by the NNM and the IRI Models around Low Solar Activity outside the Training Period

S/N	Stations	Lat °N	Long °E	IRI(RMSE) (MHz)	NNM (RMSE) (MHz)	% error difference between IRI and NNM	Period
1.	Magadan	60.0	151.0	0.195	0.181	7.179	1991
2.	Uppsala	59.8	17.6	0.176	0.165	6.250	1999
3.	Moscow	55.5	37.3	0.255	0.230	9.804	1992
4.	Boulder	40.0	254.7	0.196	0.154	21.429	2001
5.	Boulder	40.0	254.7	0.173	0.150	13.295	1991
6.	Wallops Is	37.9	284.5	0.245	0.241	1.633	1991
7.	Jicamara	-11.9	283.1	0.207	0.200	3.382	2002
8.	Mundaring	-32.0	116.3	0.173	0.164	5.202	1991
9.	Grahamstown	-33.3	26.5	0.241	0.192	20.332	2001
10.	Grahamstown	-33.3	26.5	0.215	0.175	18.605	1992
11.	Macquarie	-54.5	159.0	0.174	0.158	9.195	1992
12.	Agentine Is	-65.2	295.7	0.315	0.310	1.587	1992
	RMSE average			**0.214**	**0.193**	**9.552**	

Source: *Oyeyemi et al., 2007*

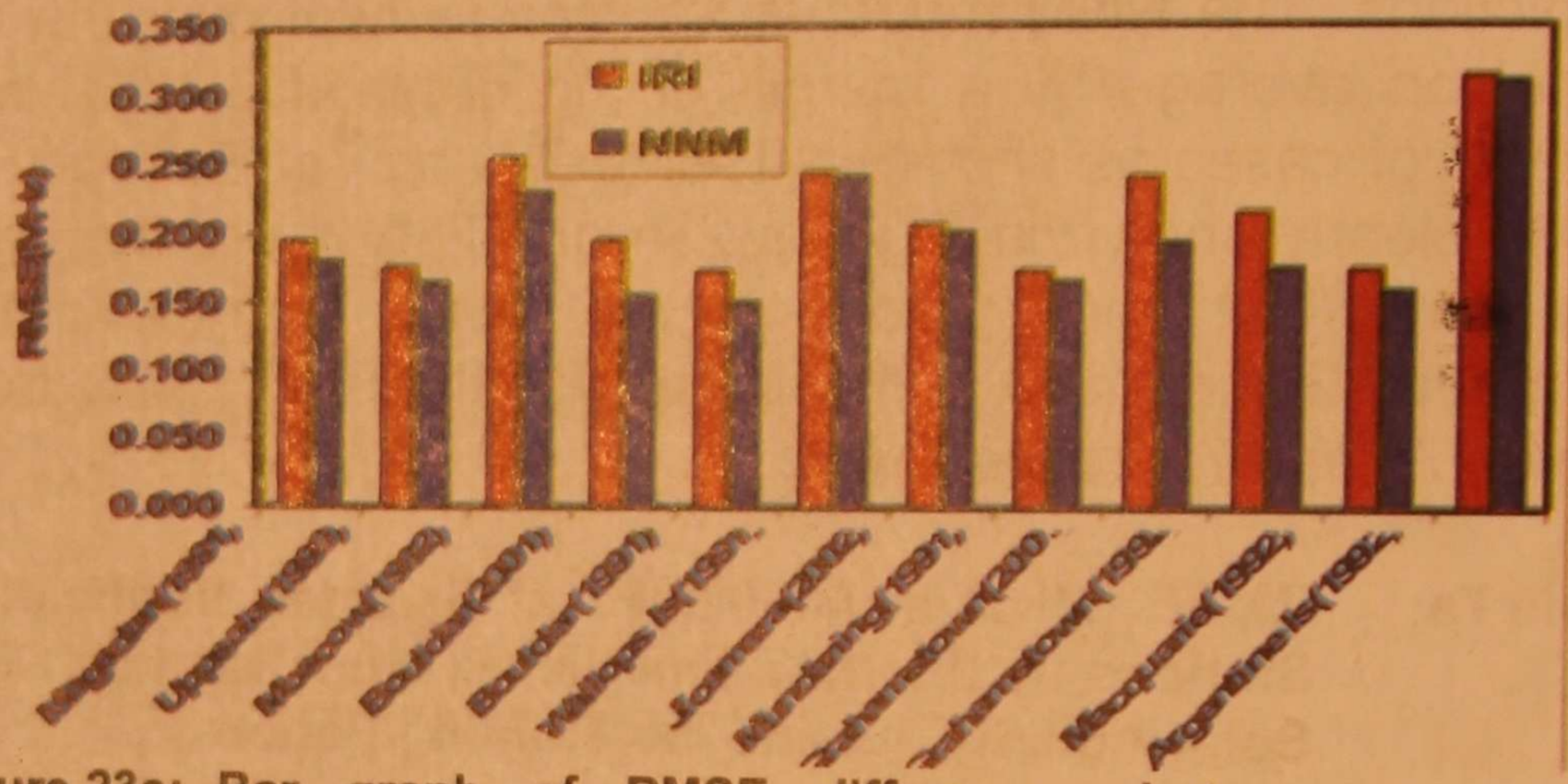

Figure 23a: Bar graph of RMSE differences between measured M(3000)F2 and predictions by NNM and IRI models for all daily hourly values of M(3000)F2 around high solar activity outside the training period

Source: *Oyeyemi et al., 2007*

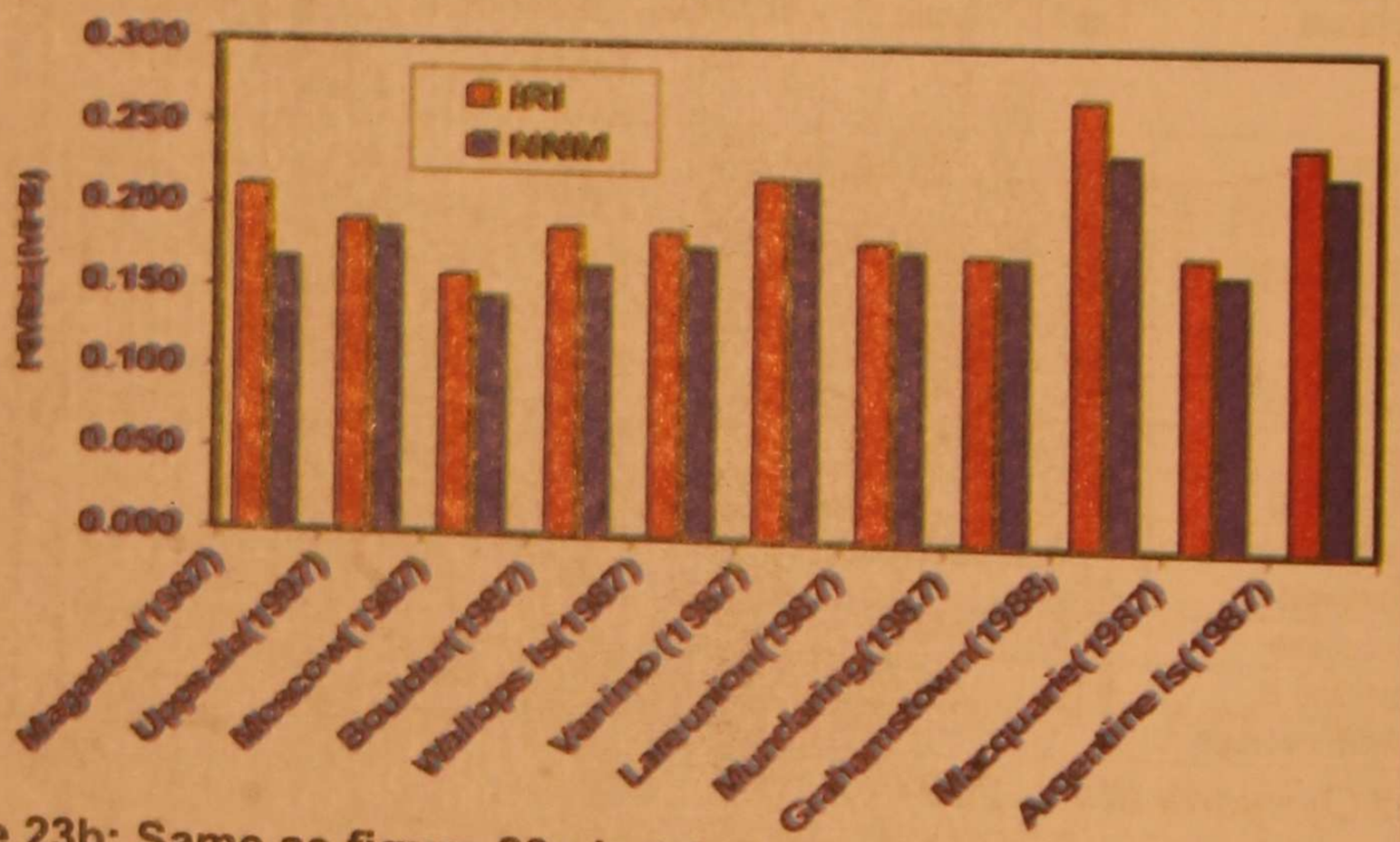

Figure 23b: Same as figure 23a but for low solar activity periods

Source: *Oyeyemi et al., 2007*

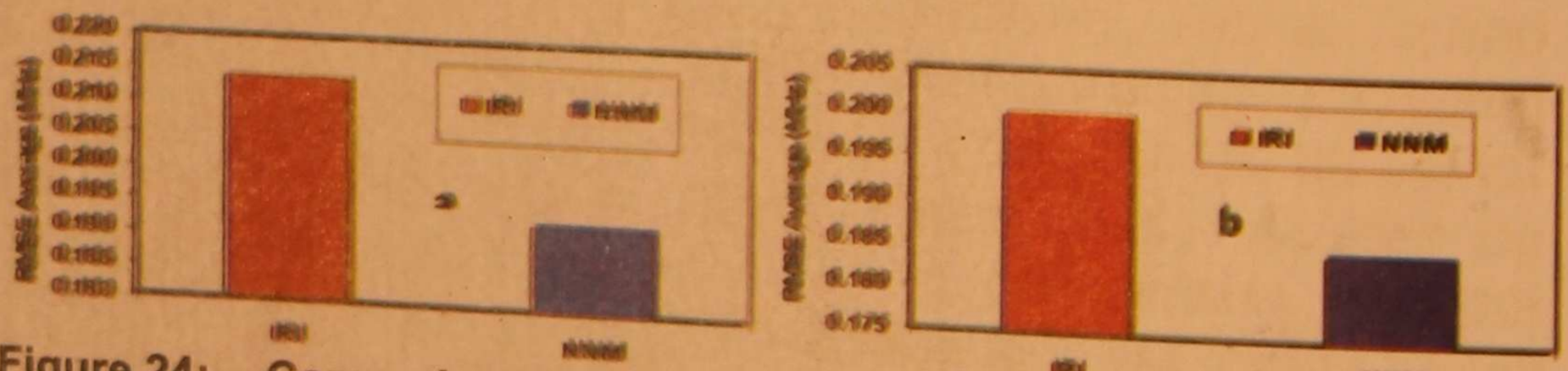

Figure 24: Comparisons of $RMSE_{average}$ between the NNM model and the IRI model using bar graph illustration ((a) and (b) from Tables 7a and 7b respectively)

Source: *Oyeyemi et al., 2007*

A comparison of the seasonal variation of M(3000)F2 NNM model predictions at 12h00 UT with the IRI model predictions and observed values around periods of low and high solar activity are shown in Figures 25a and 25b, respectively. These figures further exemplify the predictive ability of the NNM model for long-term prediction purposes, since the years for which the model was tested do not fall within the training period. It can be observed that the predictions from the two models fit the seasonal variation of M(3000)F2, and also, the NNM model compares favourably with the IRI model. There are a few cases, for instance, Argentine Is 1987 (Fig. 25a) and 1992 (Fig. 25b), where the models underestimate M(3000)F2 values, and Moscow 1992 (Fig. 25b) where the models overestimate.

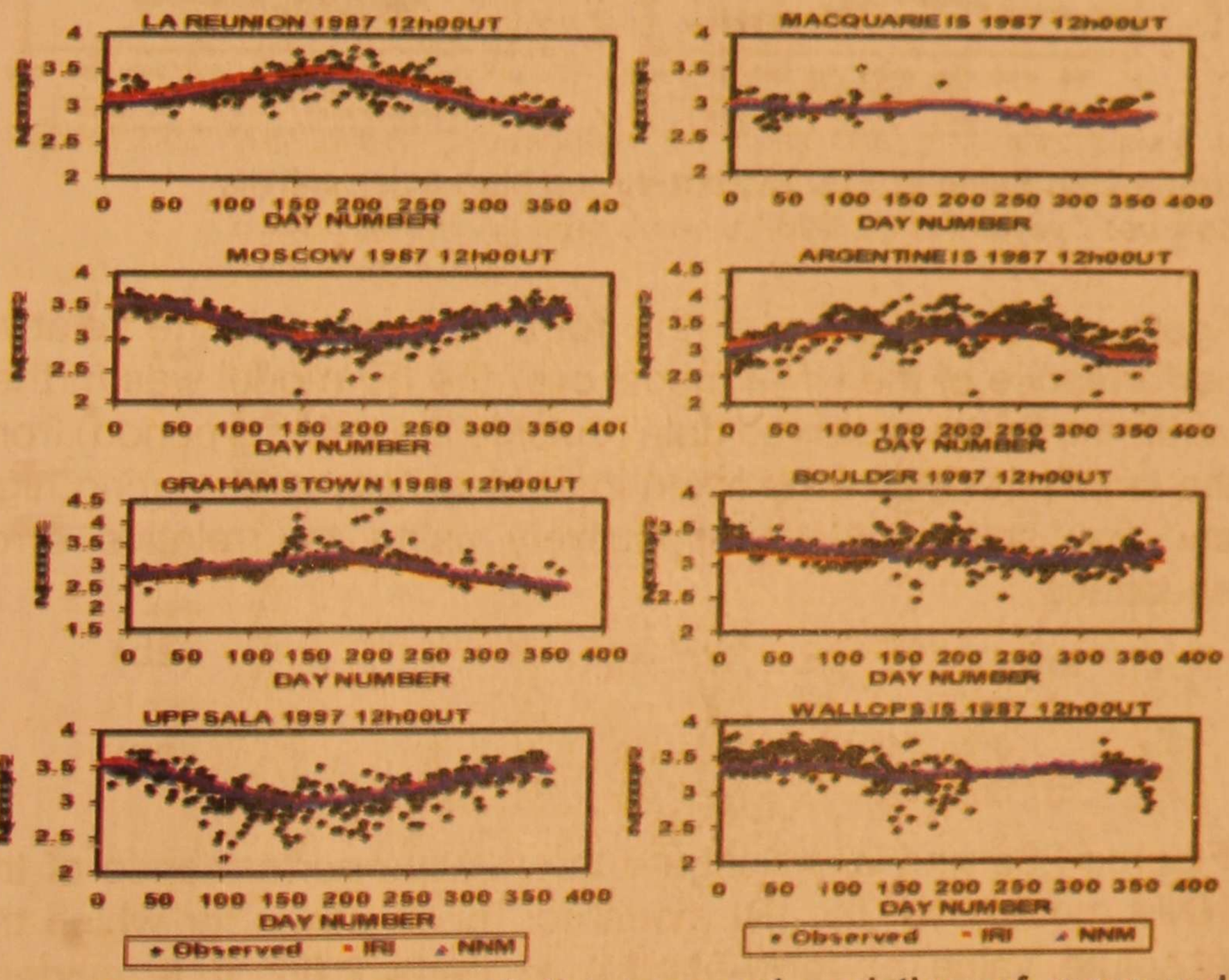

Figure 25: **Comparisons of the seasonal variation of measured M(3000)F2 (Observed) with the NNM model and the IRI model predictions during low solar activity at selected stations for 12h00UT. (Oyeyemi et al., 2007)**

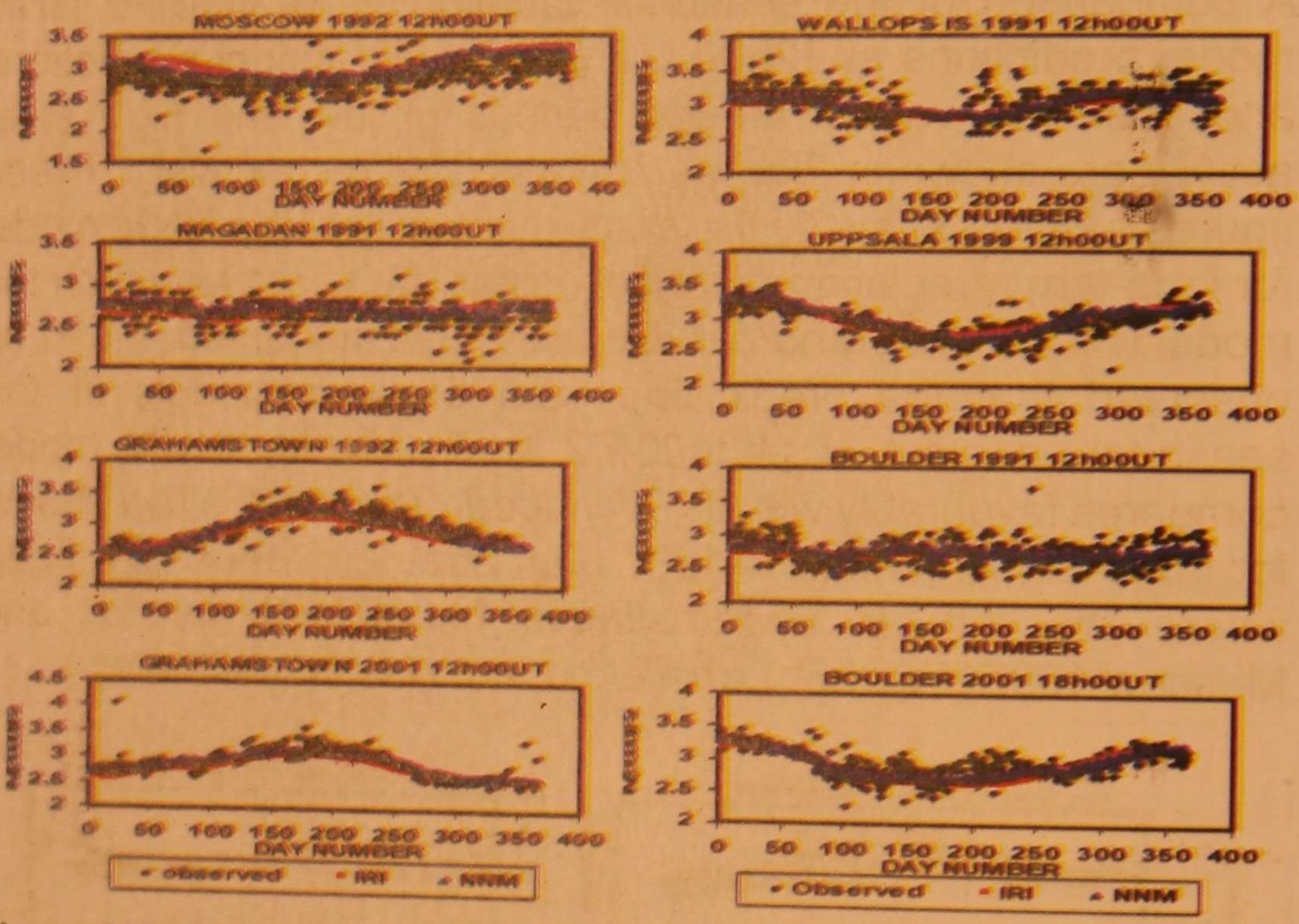

Figure 25b: Same as Fig. 25a but during high solar activity
Source: *Oyeyemi et al., 2007*

Again, as in the case of the foF2 NN2 model, the relative performance of the NNM model over the IRI model was further verified with the observed data (outside the training period) from the ionospheric stations listed in Tables 7a and 7b during high and low solar activity respectively using the relative error equations

$$\mathrm{eIRI} = \frac{|\mathrm{foF2}_{\mathrm{obs}} - \mathrm{foF2}_{\mathrm{IRI}}|}{\mathrm{foF2}_{\mathrm{obs}}} \qquad (25)$$

$$\mathrm{eNNM} = \frac{|\mathrm{foF2}_{\mathrm{obs}} - \mathrm{foF2}_{\mathrm{NNM}}|}{\mathrm{foF2}_{\mathrm{obs}}} \qquad (26)$$

Figures 26a and 26b illustrate the relative performance of the NNM model over the IRI model for those cases for which the absolute value of (eIRI-eNNM) exceeds 0.05. It is evident, particularly during high solar activity (Figure 26a), that the performance of the NNM model is relatively better when compared with that of the IRI model. During low solar activity (Figure 26b), the performance of the NNM model is still relatively better but the number of cases may be too small to be statistically significant except for Magadan, Boulder and

Argentine Is with a clear margin. The overall performance indicates the significance of the neural network technique for global predictions of M(3000)F2.

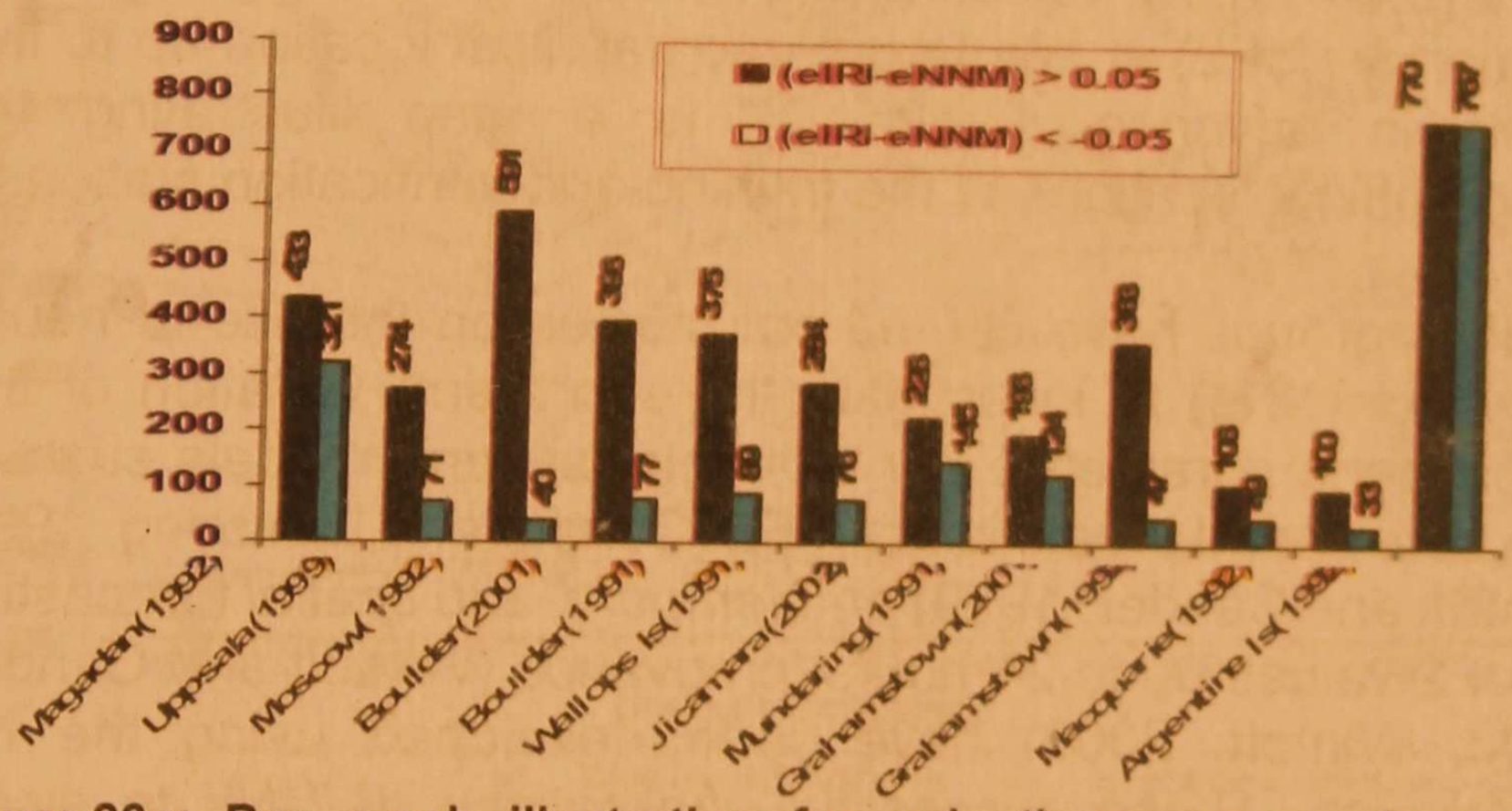

Figure 26a: Bar graph illustration for only those cases where the difference in the relative errors eIRI and eNNM is greater than 0.05 during high solar activity

Source: *Oyeyemi et al., 2007*

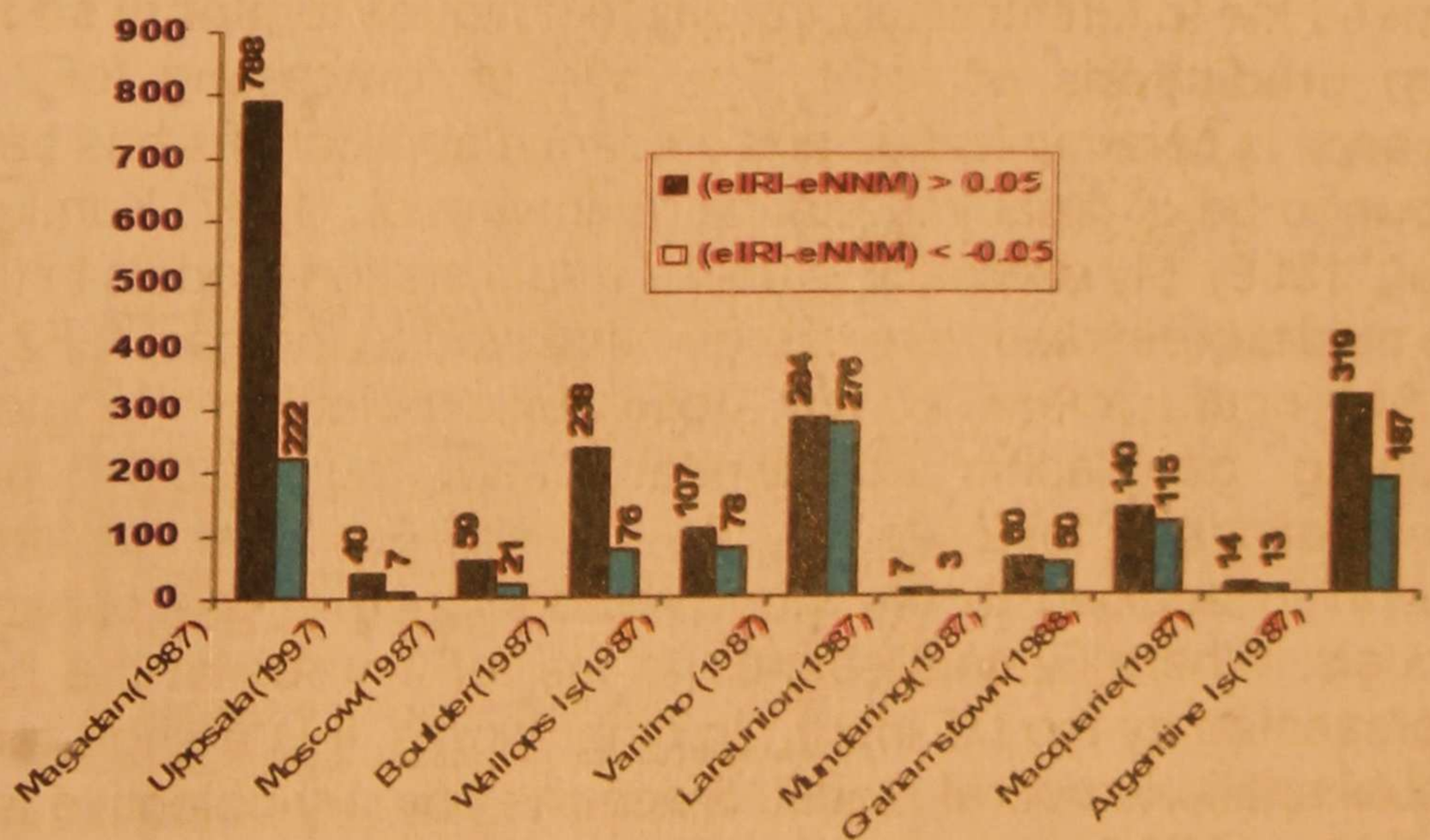

Figure 26b: Bar graph illustration for only those cases where the difference in the relative errors eIRI and eNNM is greater than 0.05 during low solar activity

Source: *Oyeyemi et al., 2007*

Global Short-term foF2 NN (STfoF2NN) Model up to 5 Hours in Advance

Mr. Vice Chancellor, Sir, neural networks (NNs) was employed to develop a global empirical model for short-term forecasting of the daily hourly values of the ionospheric F2 region critical frequency (foF2) at any target geographical location up to five hours in advance. Figure 27 is a map illustrating the geographical locations of the training and verification stations.

Various groups have carried out studies on the use of neural networks (NNs) to investigate the short-term variation of this ionospheric parameter. For example, several models such as one hour ahead prediction of foF2 (Cander and Lamming, 1997; Wintoft and Cander, 1999) and *temporal* and *spatial* forecasting of foF2 values up to 24 hours in advance (Wintoft and Cander, 2000; Wintoft, 2000) have been developed using the NN techniques. These successful applications of NNs to single station forecasting of foF2, together with my own successful applications of NNs to global modelling of foF2 and M(3000)F2 ionospheric parameters (discussed in the previous sections), inspired me to further apply the NN techniques to **global short-term predictions of foF2**. The role of forecasting foF2 in advance in communication and guidance applications has been shown to be of great importance (Altinay et al., 1997; Kumluca et al., 1999). My approach is unlike single station models in that the model presented here can be employed to forecast foF2 up to five hours ahead at any geographic point on the globe knowing geographic coordinates, and four recent past observations of foF2 (i.e. F_{-3}, F_{-2}, F_{-1} and F_0) from the target station in addition to the input vectors used in the previous models. Where F_0 corresponds to the foF2 value at the hour represented by the UT input. In other words, it is a short term, global spatio-temporal model. Since the primary objective is to develop a NN based model to forecast foF2 values up to five hours ahead at any geographic location globally, the outputs of the **STfoF2NN** model are F_{+1}, F_{+2}, F_{+3}, F_{+4} and F_{+5} representing the values of foF2 up to five hours ahead of F_0, foF2 at the hour UT. However, studies have shown that there is no restriction on the number of outputs when designing a NN of this type. The

input and output parameters to the **STfoF2NN model** are as illustrated in the block diagram of Figure 28.

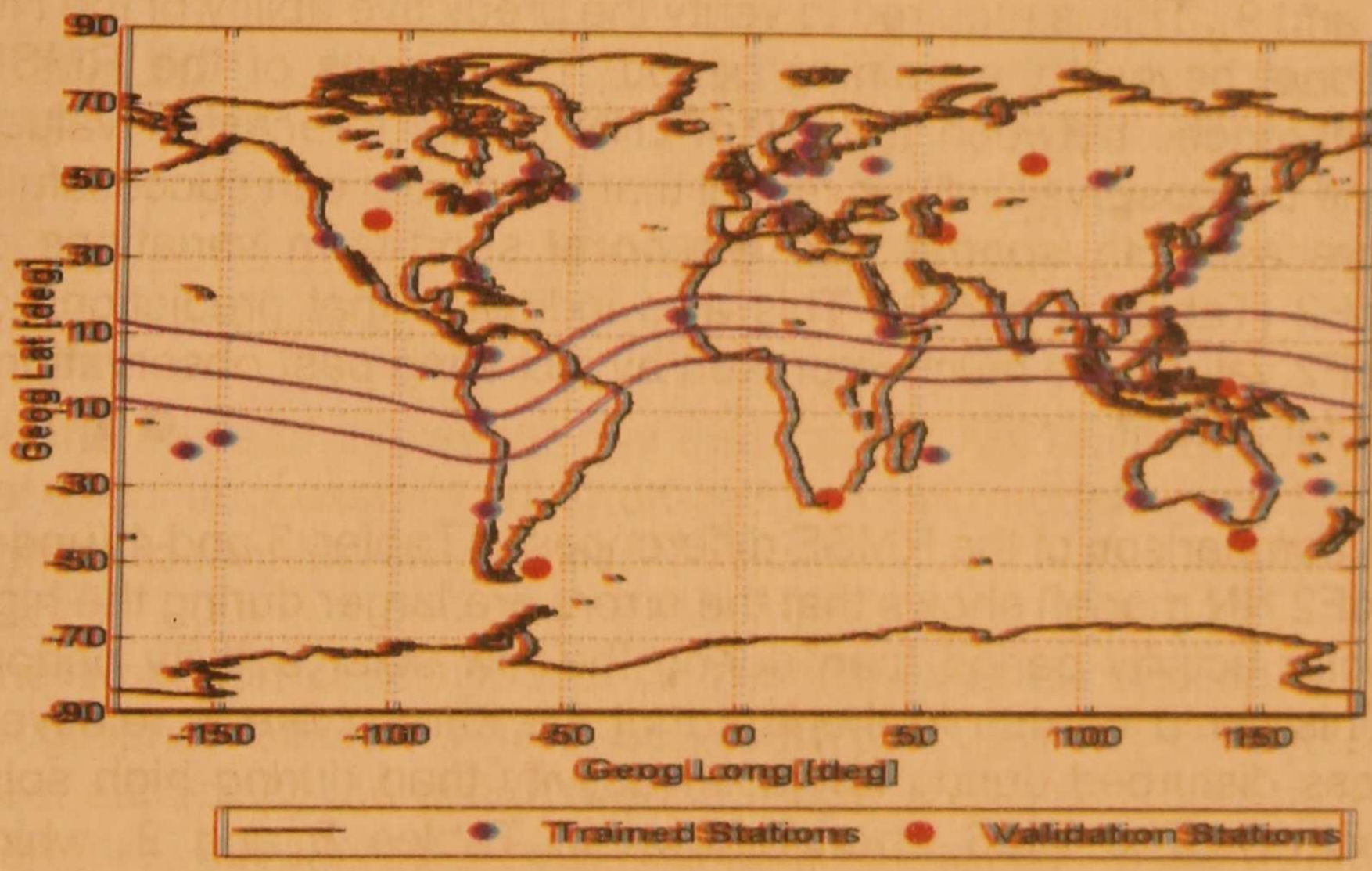

Figure 27: Map of geographical coordinates of raining and verification stations used for STfoF2NN model

Source: *Oyeyemi et al., 2005b*

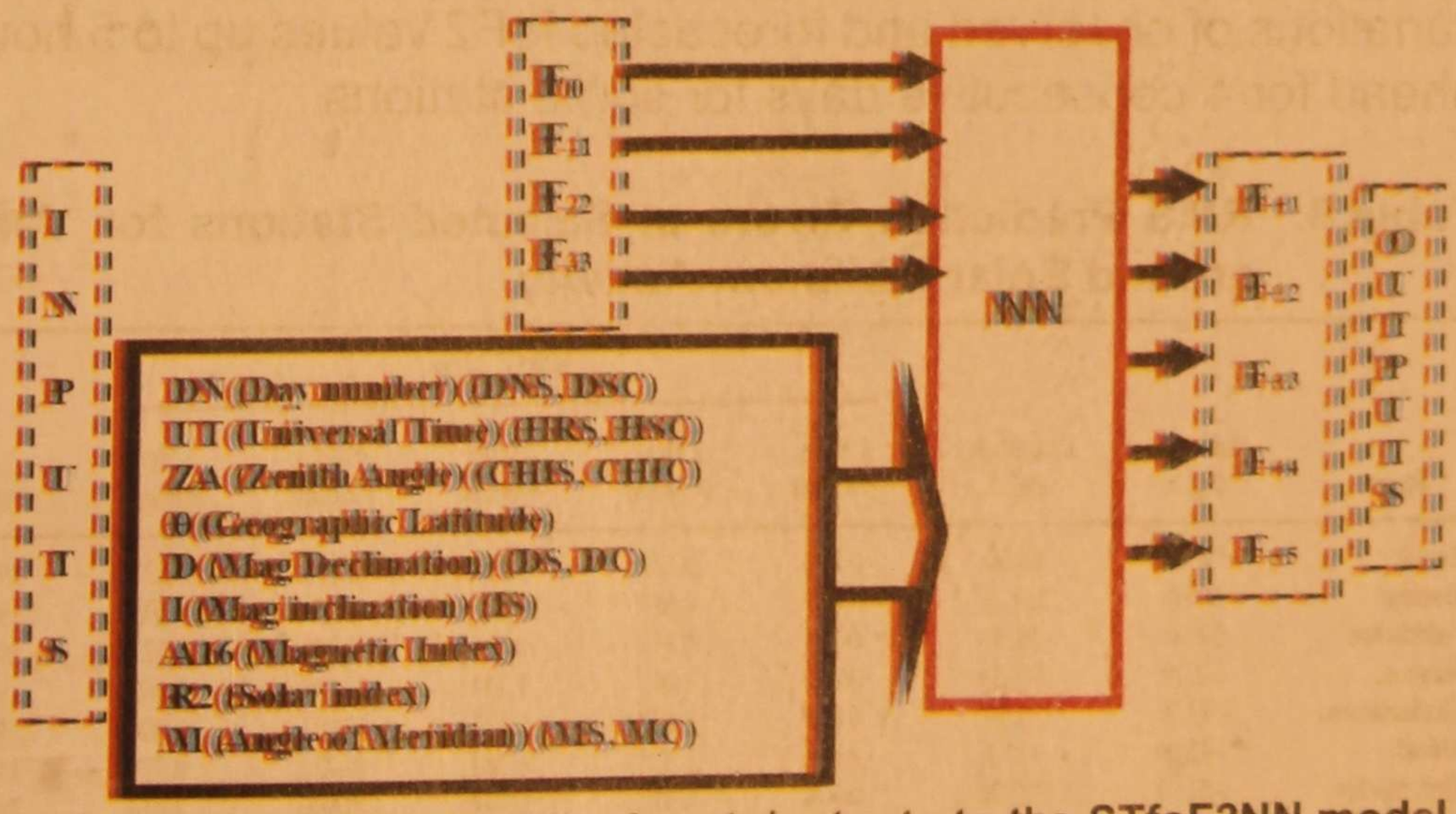

Figure 28: Block diagram of the inputs/outputs to the STfoF2NN model

Source: *Oyeyemi et al., 2005b*

The model presented here is applicable to any point on the globe provided the geographic coordinates and recent past observations of foF2 are known at that geographic point. Data from a few ionospheric stations (not included in the training and

outside the training period and during low and high solar activity periods) were used to verify the performance of the NN (Tables 8 and 9). This is required to verify the predictive ability of the NN model beyond the training period. The results of the RMSE differences between the **STfoF2NN** model forecasted values and the observed values reveal that the model can successfully forecast both ***spatial* and *temporal*** short-term variations of foF2 (Tables 8 and 9). This also indicates that predictions of foF2 values are much improved by including past observations of foF2 itself.

A comparison of the RMSE differences in Tables 3 and 4 (under foF2 NN model) shows that the errors are larger during the high solar activity period than during the low solar activity period. This could be due to the fact that the ionosphere is relatively less disturbed during low solar activity than during high solar activity. The RMS errors shown in Tables 8 and 9, which increase with increasing delay time, give the expected result that the NN will forecast 1 hour ahead with better accuracy than 5 hours ahead. Figures 29a and 29b show samples of daily variations of observed and forecasted foF2 values up to 5 hours ahead for 4 consecutive days for some stations.

Table 8: RMS Prediction Errors at Selected Stations for Years around Solar Minimum Activity

Station	Latitude, deg N	Longitude, deg E	RMSE, MHz					
			1 Hour Forecast	2 Hour Forecast	3 Hour Forecast	4 Hour Forecast	5 Hour Forecast	Period
Tomsk	56.50	84.90	0.446	0.511	0.553	0.589	0.627	1994
Boulder	40.00	254.70	0.417	0.519	0.590	0.631	0.693	1995
Ashkhabad	37.90	58.30	0.786	0.912	0.959	0.982	1.021	1994
Vanimo	−2.70	141.30	0.842	1.063	1.141	1.142	1.163	1994
Grahamstown	−33.30	26.50	0.459	0.623	0.724	0.801	0.804	1995
Hobart	−42.90	147.2	0.459	0.585	0.663	0.728	0.778	1992
Port Stanley	−51.70	302.20	0.844	0.873	0.944	0.960	1.014	1996

Source: *Oyeyemi et al., 2005b*

Table 9: RMS Prediction Errors at Selected Stations for Years

Station	Latitude, deg N	Longitude, deg E	RMSE, MHz 1 Hour Forecast	2 Hour Forecast	3 Hour Forecast	4 Hour Forecast	5 Hour Forecast	Period
Tomsk	56.50	84.90	0.430	0.552	0.657	0.752	0.850	2001
Boulder	40.00	254.70	0.425	0.612	0.757	0.844	0.889	2001
Grahamstown	−33.30	26.50	0.567	0.808	0.935	1.020	1.092	2001
Hobart	−42.90	147.20	0.494	0.642	0.735	0.815	0.874	1999
Port Stanley	−51.70	302.20	0.973	1.003	1.228	1.408	1.568	2001

Source: *Oyeyemi et al., 2005b*

On the basis of this study, it is evident that NN techniques can be used successfully in short-term global modeling of foF2 within reasonable error limits.

One limitation of this model is that it cannot be applied to a geographic location where observed data are not available, most especially the ocean areas. In view of this shortcoming, I, therefore, developed a near-real time NN based model, which does not require past observations of foF2 from the target location, but rather from only four control ionosonde stations that are known to have data in real time. This is the subject of the next section.

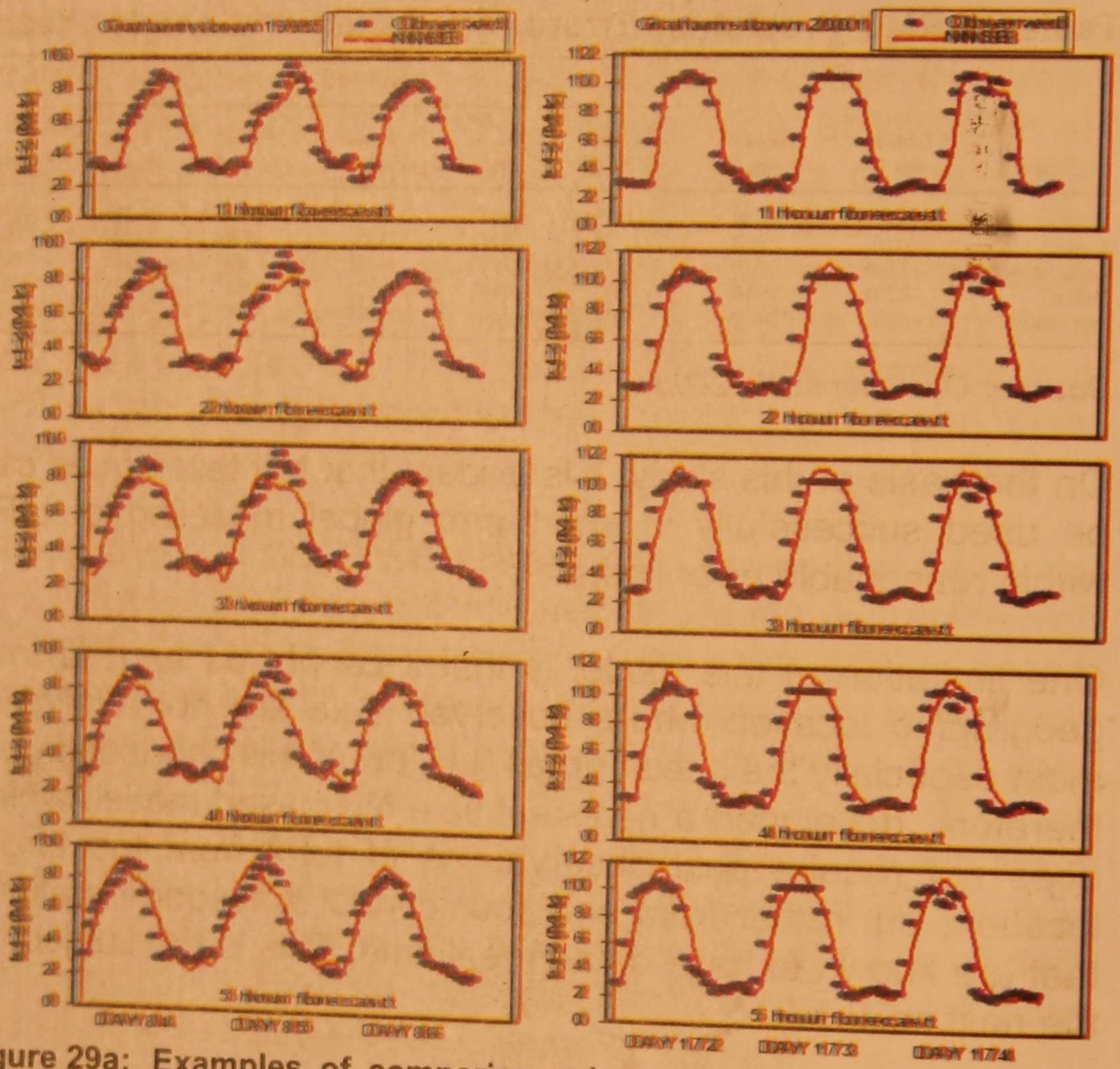

Figure 29a: **Examples of comparisons between observed and NNSB model predicted-values of foF2 (5 hours ahead) for 3 consecutive days for Grahamstown during low solar activity, (1995) and high solar activity, (2001)**

Source: *Oyeyemi et al., 2005b*

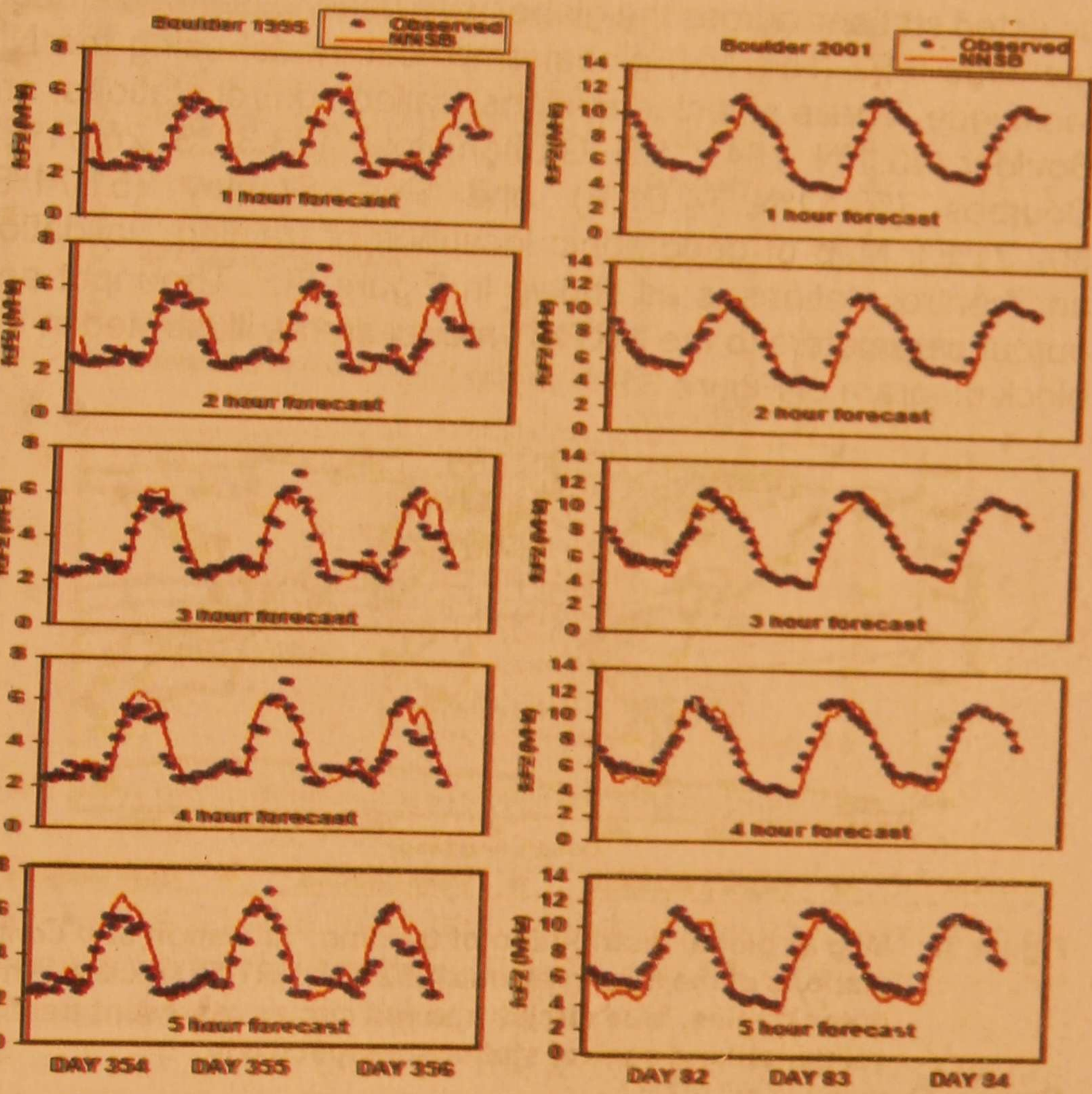

Figure 29b: Same as figure 29a but for Boulder station
Source: *Oyeyemi et al., 2005b*

Near-Real Time foF2 NN (NRTNN) Model

Oyeyemi et al., 2005b describes the applications of NNs for the development of a global empirical model for short-term forecasting of the ionospheric F2 region critical frequency (foF2) at any target geographical location up to 5 h in advance. This short-term model requires recent past observations of foF2 itself, and therefore, has the limitation in that it is not applicable to any geographic location where measured data are not readily available. In view of this, and considering the fact that ionospheric data is not available for vast areas of the globe, especially the ocean areas and where ionosonde stations are not available, recent past observations of foF2 from four

selected stations across the globe were used to develop a near-real time foF2 (NRTNN) global empirical model using the NN technique. These selected stations, called control stations, are Boulder (40.1°N, 254.71°E), Grahamstown (33.31°S, 26.51°E), Dourbes (50.11°N, 4.61°E) and Port Stanley (51.71°S, 302.21°E). Map of geographic locations of training, validation and control stations is as shown in Figure 30. The input and output parameters to the NRTNN model are as illustrated in the block diagram of Figure 31.

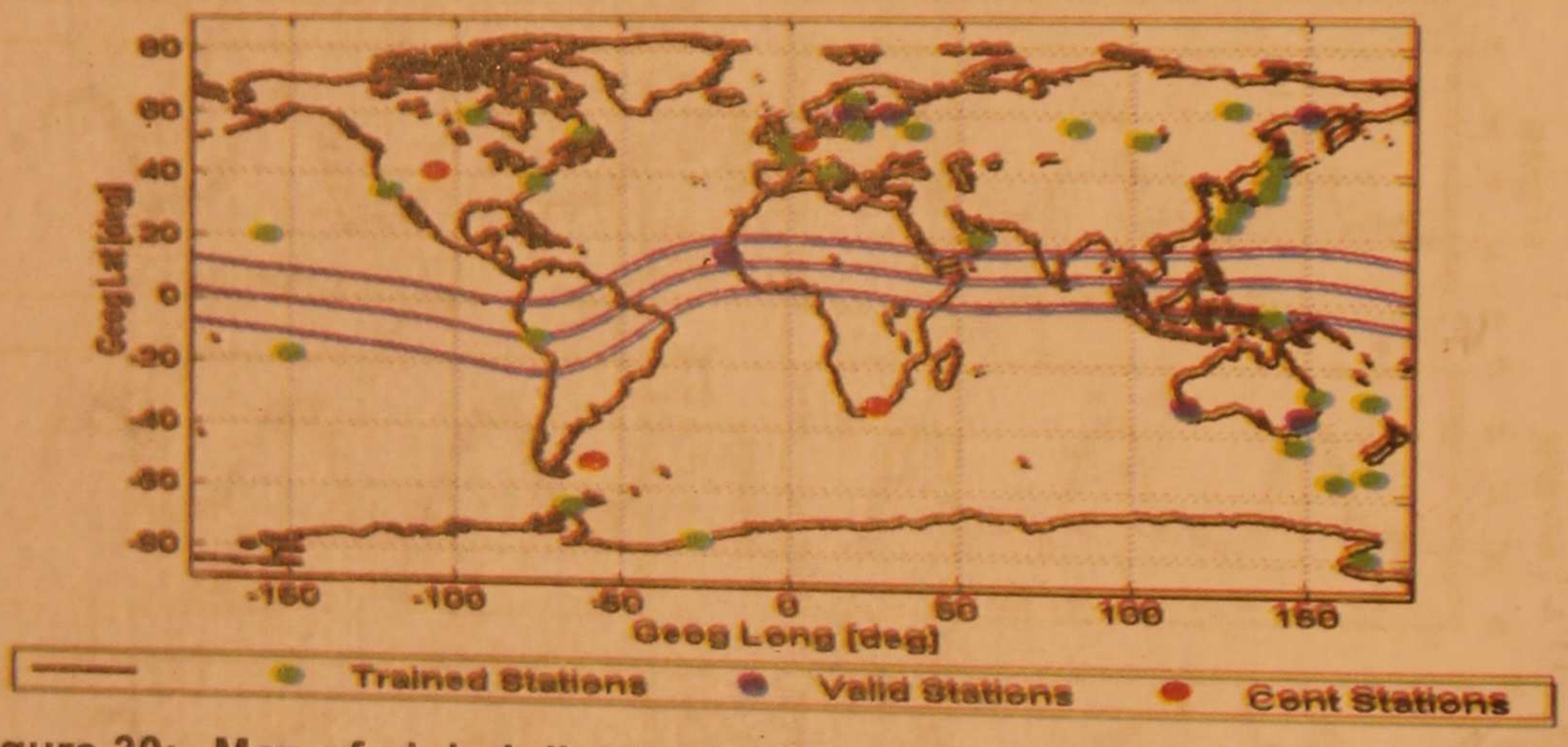

Figure 30: Map of global distribution of training, validation and control stations of the near-real time foF2 NN (NRTNN) model. Where green circles, blue circles and red circles represent training, validation and control stations, respectively

Source: *Oyeyemi et al., 2006*

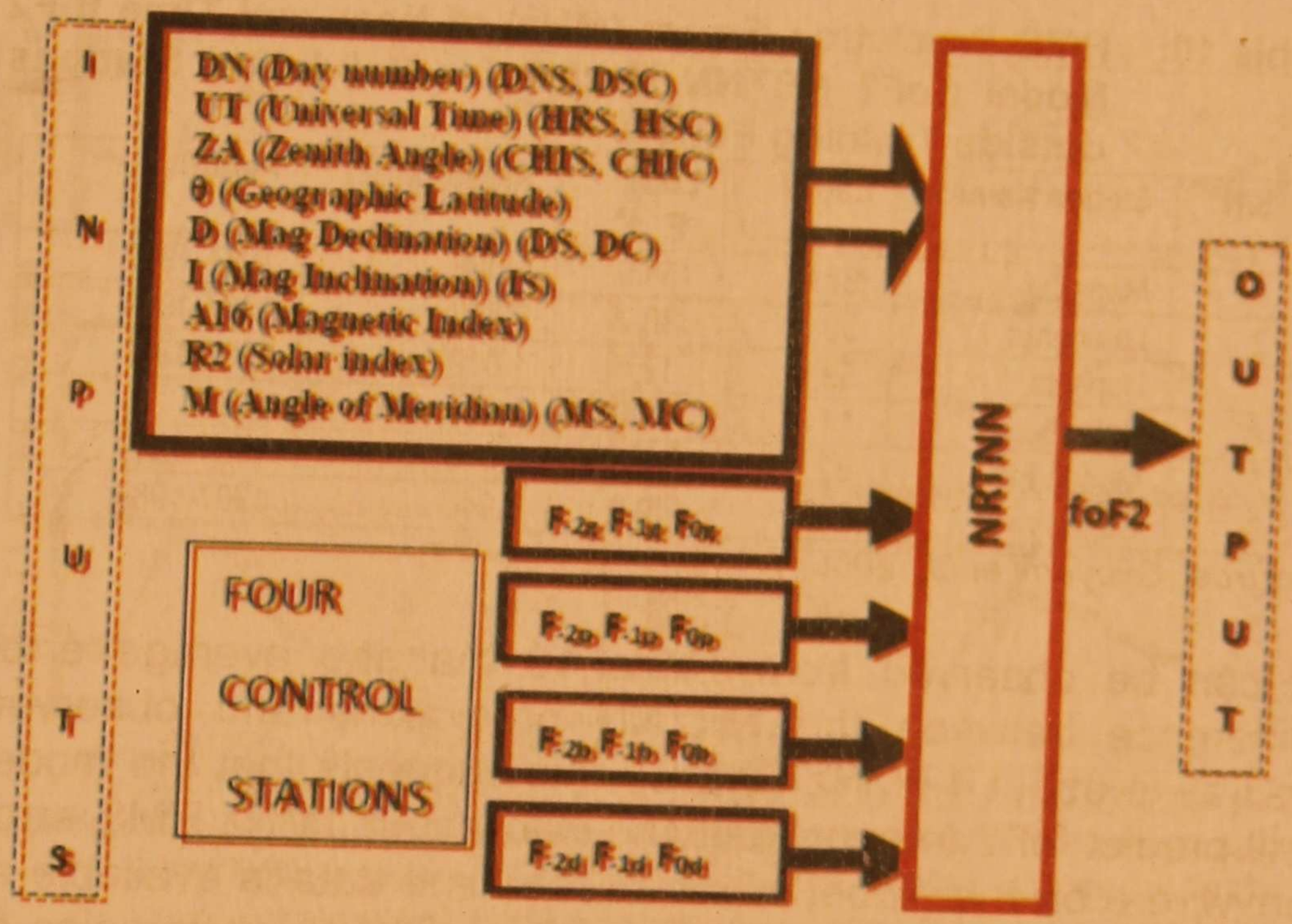

Figure 31: A block diagram of the NRTNN architecture
Source: *Oyeyemi et al., 2006*

From Figure 31, the foF2 related inputs are the 3 recent past observations of foF2 values: F_{-2}, F_{-1} and F_0, from each of the four selected stations. These are F_{-2p}, F_{-1p}, F_{0p}, F_{-2g}, F_{-1g}, F_{0g}, F_{-2b}, F_{-1b}, F_{0b}, F_{-2d}, F_{-1d} and F_{0d}. The letters p, g, b and d represent observations from Port Stanley, Grahamstown, Boulder and Dourbes stations respectively. The NN target output is the observed foF2 value from every other station used for training the NN corresponding to the most recent foF2 (i.e. F_{0p}, F_{0g}, F_{0b} and F_{0d}) from the four selected stations.

Table 10 shows error differences between the observed and predicted values of foF2 from selected validation stations. These stations were not included in the training of the NRTNN model and the validation was also carried out outside the training period of 1964 – 1986 to test for the predictability of the model.

Table 10: RMS Prediction Errors (MHz) of Near-real Time foF2 Model (foF2 NRTNN Model) for Validation Stations outside Training Period

S/N	Station Name	Lat °N	Long °E	RMSE (MHz)	Period
1.	Magadan	60.0	151.0	1.028	1987-1989
2.	Leningrad	59.9	30.7	0.856	1987-1989
3.	Uppsala	59.8	17.6	1.049	1987-1989
4.	Dakar	14.8	341.6	1.214	1987
5.	Mundaring	-32.0	116.3	0.945	1987-1989
6.	Canberra	-35.3	149.0	0.940	1987-1989

Source: *Oyeyemi et al., 2006*

It can be observed from Table 10 that the average error difference between the NRTNN predictions and observed values is about 1.0MHz RMSE. This suggests that the model will predict foF2 in near-real time with about 1MHz RMS error anywhere on the globe, provided real time data is available at the four control stations. Figures 32 and 33 show samples of comparisons between observed and predicted foF2 values illustrating diurnal and seasonal variations temporally beyond the training period respectively. These graphs serve to illustrate that the model successfully predicts the general diurnal and seasonal shape of foF2 behaviour.

From the results, it is evident that in addition to the geophysical information from any geographic location, recent past observations of foF2 from the four control stations could be used as inputs to a NN for the purpose of near-real time foF2 predictions.

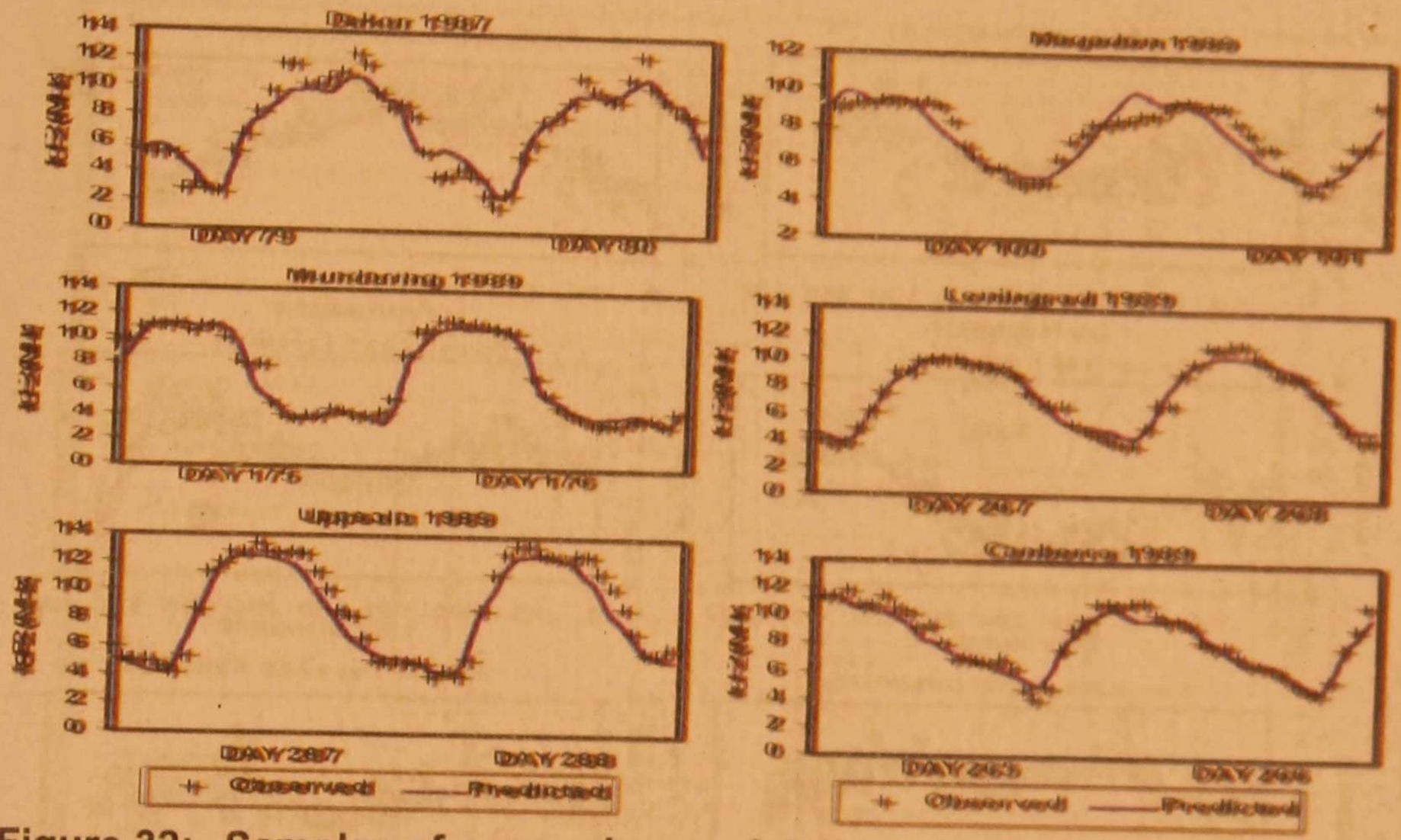

Figure 32: Samples of comparisons of daily variations of observed and NRTNN near-real time foF2 model predicted-values (outside training period) for 2 consecutive days starting at 00h00UT on the first of the days indicated for each station

Source: *Oyeyemi et al., 2006*

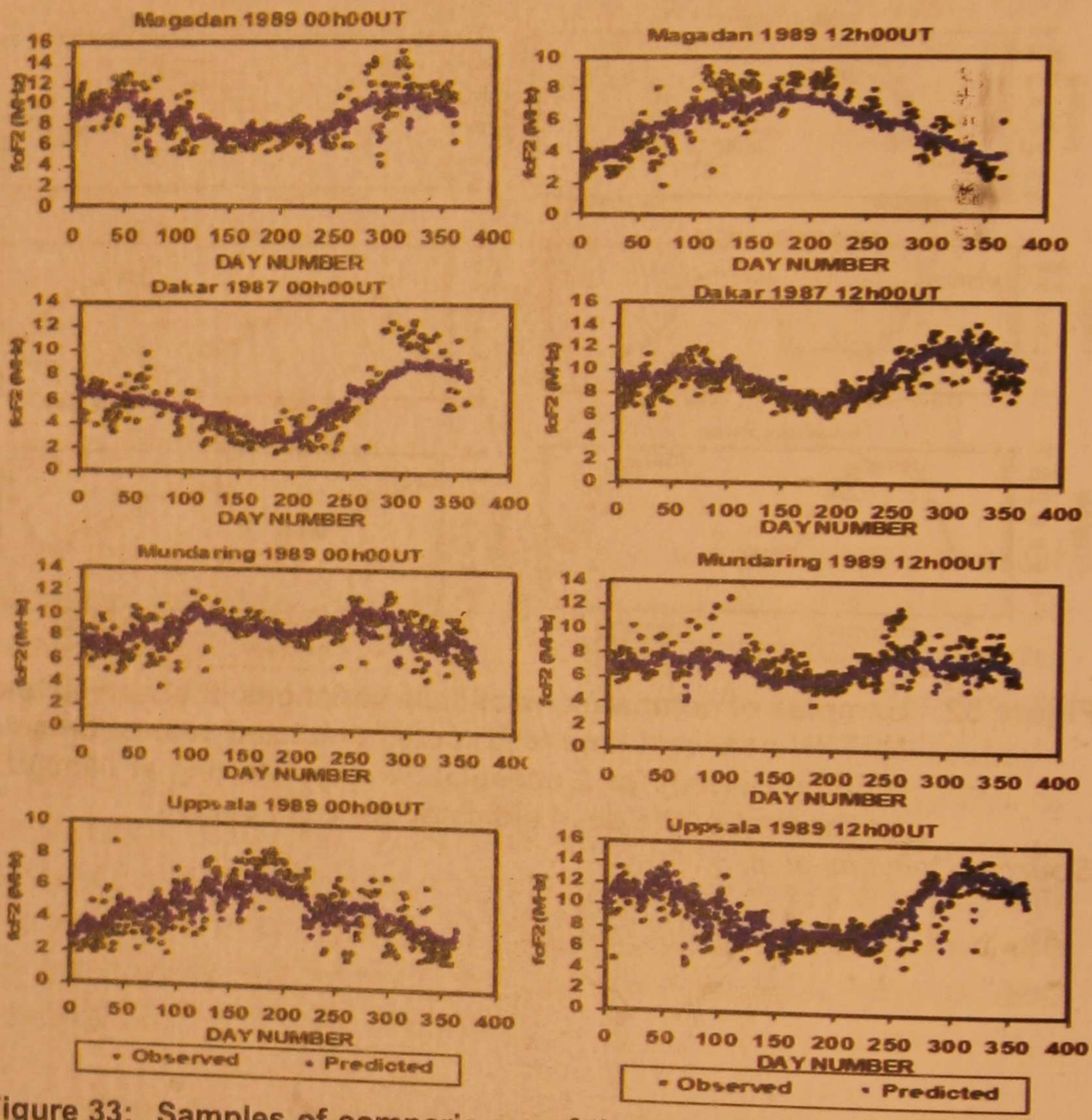

Figure 33: Samples of comparisons of the seasonal variation between measured (observed) and NRTNN near-real time foF2 model predicted values at 00h00UT and 12h00UT for selected verification stations (outside training period) for the year indicated

Source: *Oyeyemi et al., 2006*

A block diagram of all the components of the four models (i.e. foF2 NN model, M(3000)F2 NN model, short-term foF2 NN model and near-real time foF2 NN model) is shown in Figure 34. This block diagram illustrates how the end users would make use of each model by specifying the input vectors.

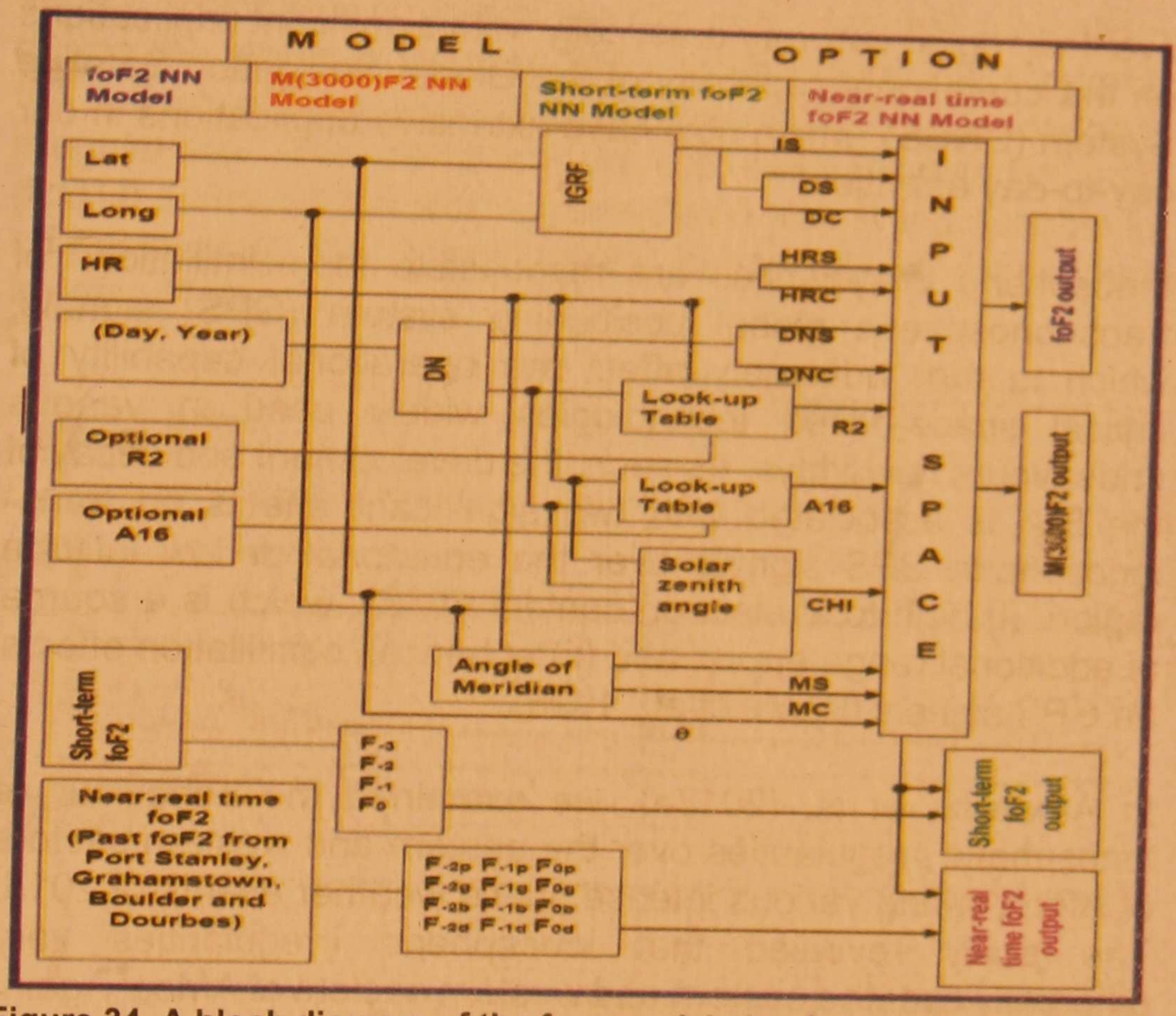

Figure 34. A block diagram of the four models implementation
Source: Oyeyemi 2005

Equatorial Ionosphere and irregularities (Dynamic of Equatorial Ionosphere)

The ionosphere, acting as a dispersive medium, has a great influence on the ground and space based communication and navigation systems, and the effect is directly proportional to the free electron density, which could change the phase and strength of electromagnetic radio frequency wave. In recent times, attention has been focused on the study of electrodynamics of the ***equatorial ionosphere*** because of the significant influence it has on HF communication, satellite navigation and space weather studies. The equatorial ionosphere is a densely populated region characterised by the Equatorial Ionization Anomaly (EIA) and the associated enhancement in ionization at about ±15° of the magnetic equator (Appleton, 1946; Wanninger, 1994). During disturbed geophysical conditions, the electrodynamics of the ionosphere

over this region can vary drastically, with significant implications on the operational capability of the Global Navigation Satellite System (GNSS), which now have extensive applications in our day-to-day activities.

Ionospheric Irregularities are responsible for scintillations of trans-ionospheric global positioning system (GPS) signals, which in turn adversely affect the operational capability of critical space-based technologies widely used in various endeavours nowadays. As such, the development and decay of the EIA is associated with two significant effects on trans-ionospheric GPS signals over the equatorial or low latitude region: (i) high total electron content (TEC), which is a source of additional range errors; and (ii) enhanced scintillation effects on GPS signals (Basu, et al., 1996).

In Amaechi, et al. (2018a), we examined the behaviour of ionospheric irregularities over the eastern and western sectors of Africa during various intense space weather events of 2015. The study revealed that ionospheric irregularities vary differently over the eastern and western sectors of Africa. Again, irregularities occurred predominantly over all stations in the post-sunset to midnight period and they were associated with total electron content (TEC) depletions/fluctuations which are a manifestation of equatorial plasma bubbles (EPB). This implied that critical GNSS technologies operating in both sectors will be impacted differently during geomagnetic storm periods. The study further found that storm time electric field over both sectors depends on the local time of southward turning of IMF Bz and inhibited/trigger irregularities during various phases of the storms. Differences in irregularities behaviour suggested the existence of further mechanisms probably from the lower atmosphere. Fig. 35 shows variations of vertical electron content, VTEC, (first panel), rate of change to total electron content, ROT (second panel) and rate of change of TEC index, ROTI index, (third panel) over (a) Addis Ababa (PRN 25) and (b) Malindi (PRN 29) during the storm of March 2015. TEC profile for both PRNs is characterised by depletions on 16 March while on 17 March it is relatively smooth. Figures 36a

shows examples of Interplanetary and magnetic conditions during the storm of October 2015, while Figure 36b illustrates the effect of the storm of October 2015 on ionospheric irregularities. The behaviour of the daily irregularity index (ROTI) during all the storms considered was found suitable for characterising the overall daily behaviour of ionospheric irregularities.

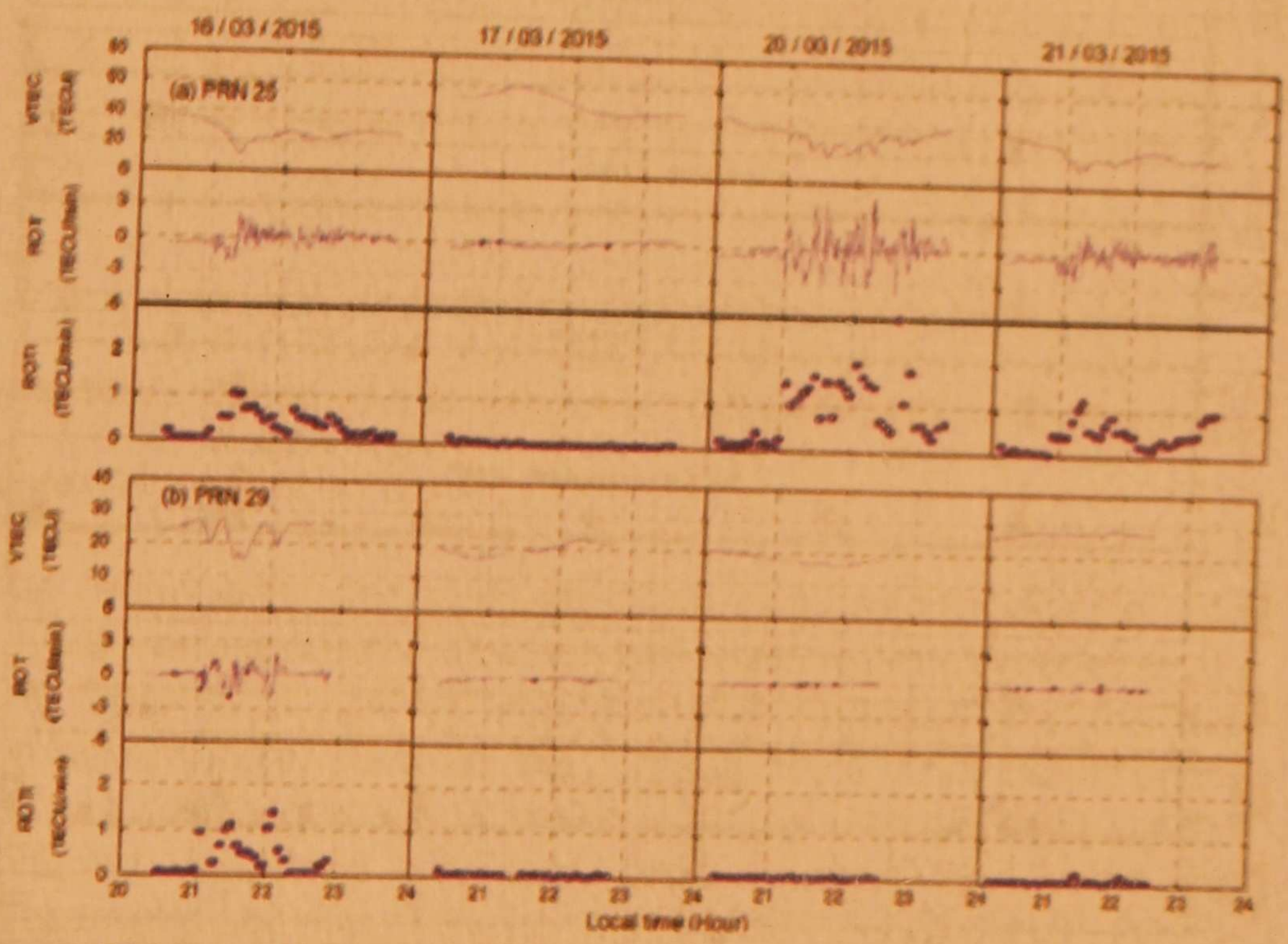

Figure 35: Variations of VTEC, ROT and ROTI over (a) Addis Ababa (PRN 25), (c) Malindi (PRN 29) during the storm of March 2015

Source: *Amaechi, et al., 2018a*

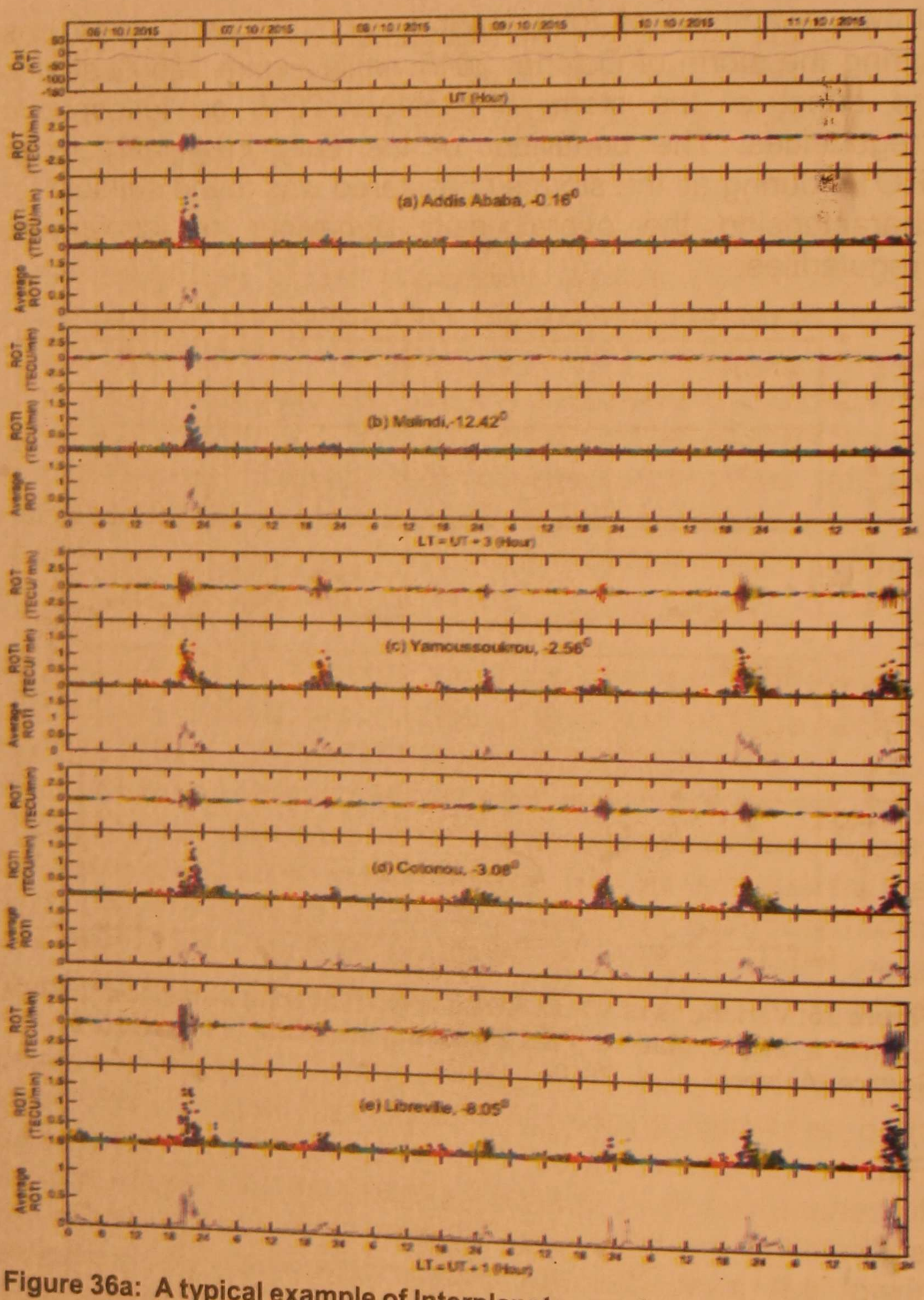

Figure 36a: A typical example of Interplanetary and magnetic conditions during the storm of October 2015

Source: *Amaechi, et al., 2018a*

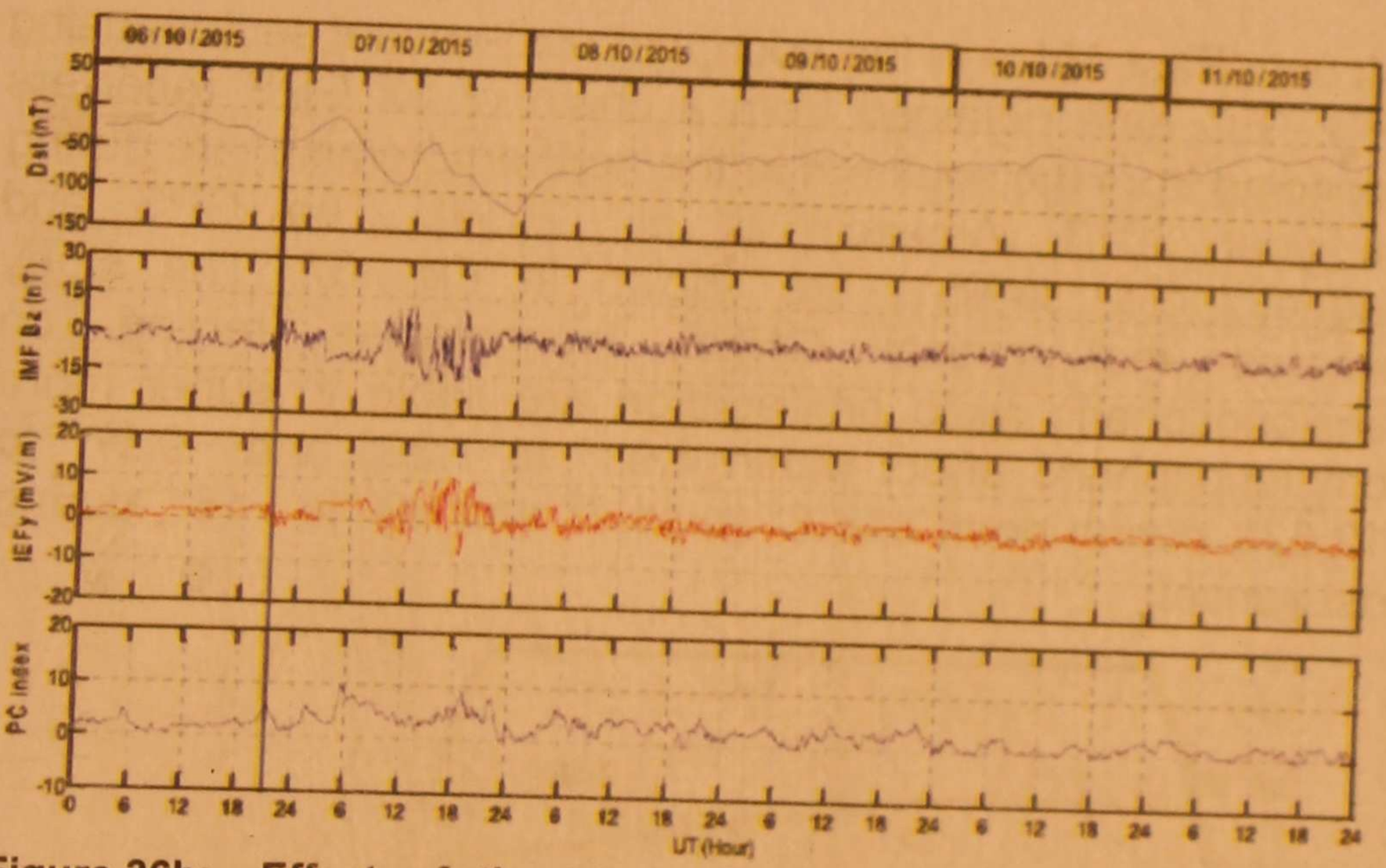

Figure 36b: Effect of the storm of October 2015 on ionospheric irregularities

Source: *Amaechi, et al., 2018a*

In the recent past decades, attention has been focused on the study of variations of EIA over various sectors (Walker et al., 1972, Opio et al., 2015). Results have revealed that the EIA main parameters, such as the magnitude, time of occurrence, locations of the crests, as well as crest to trough ratio exhibit significant variations with local time, season, and solar and geomagnetic activities (Walker and Ma 1972, Opio et al., 2015). EIA variability is driven by a change in composition (Rishbeth and Setty 1961), thermospheric wind and waves, and tidal forces of the lower atmospheric origin (Zou et al., 2000), changes in the equatorial electrojet (EEJ) (Ross 1966) together with the associated variations in $\boldsymbol{E} \times \boldsymbol{B}$ drift velocity (Scherliess and Fejer 1999); as well as changes in noon solar zenith angle in relation to the geometry of magnetic field lines (Liu et al., 2007, Wu et al., 2004). However, most of such studies have been carried over the Asian and American sectors with few studies over the African sector due to the paucity of GPS data over the African sector. The recent deployment of GPS receivers over the African sector has made it possible to carry out the variability of EIA over the African sector. We investigated the variations of the position and magnitude of the crests of the

EIA over East Africa in the noon and post-sunset sectors using GPS TEC data obtained from a chain of 12 GPS receivers extending from the southern to the northern hemisphere during the year 2013 (Amaechi et al., 2019). The GPS and magnetometer stations are shown in Fig. 37. The study revealed that critical GNSS technologies relying on transionospheric radio propagation are liable to suffer more from ionospheric effect within 4.91° to 7.36° and −9.17° to −12.62°, during noon and 8° to 11.7° and −9° to −16°, during post sunset.

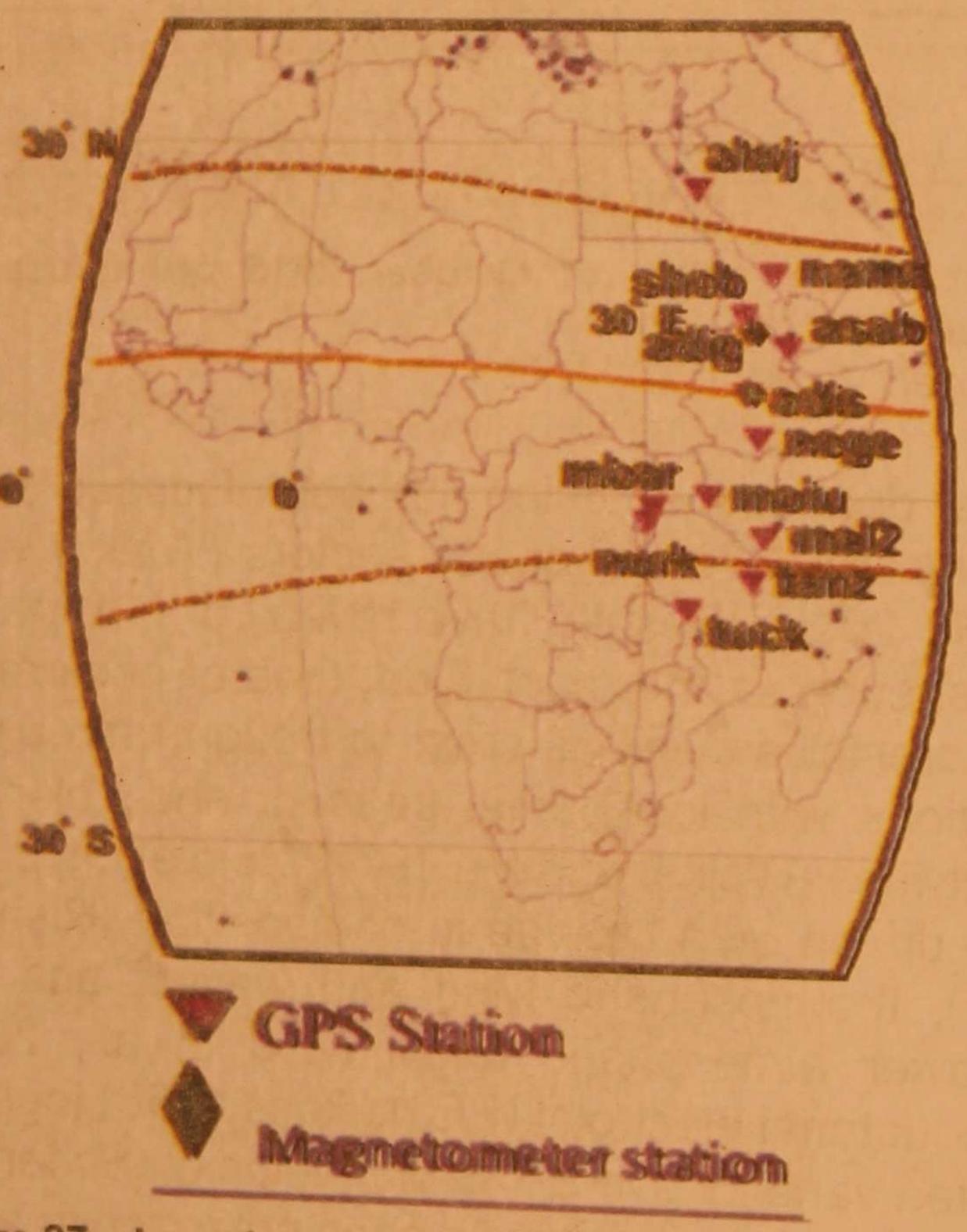

Figure 37: Location of the stations: the brown solid curve indicates the magnetic equator (dip = 0) while broken curves represent ±15° dip latitudes

Source: *Amaechi et al., 2019*

Figure 38 shows the TEC profile during the post-sunset period at about 2100 LT from January to December 2013. Clear variations of the position and magnitude of both crests are observed in this figure. Figure 39 shows contour maps of the

monthly mean diurnal variation of TEC for the year 2013 over the African EIA. The time of occurrence of maximum TEC as well as the latitudinal position of occurrence of such peak was used to define the time duration and position, respectively, of the EIA crests. From this figure, the time of occurrence of the crests was found to vary from 1400 local time (LT), to 1700 LT.

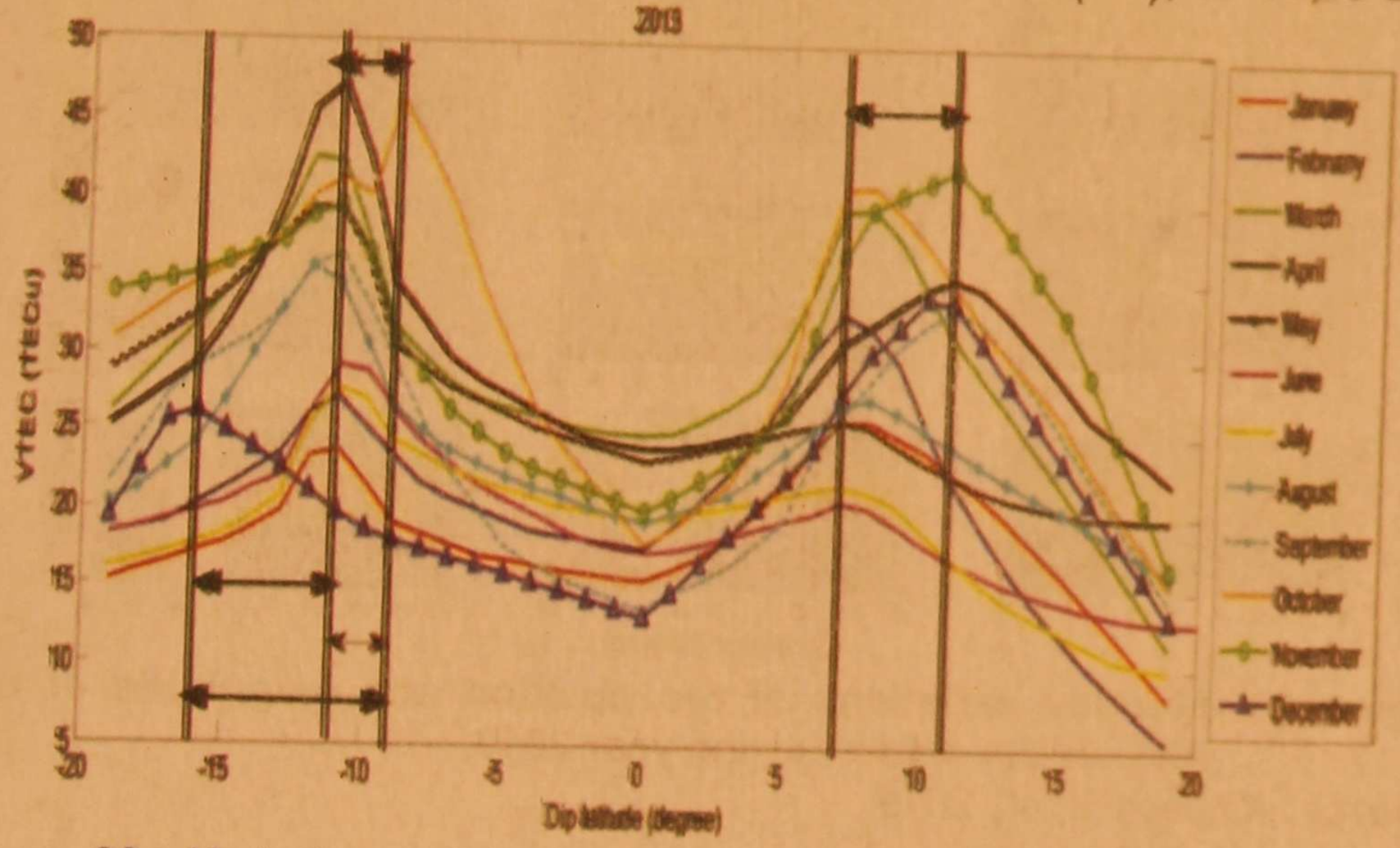

Figure 38: Variations of the position of the African EIA crests for 2013 during the post-sunset period (≈2100 LT). The double arrow shows the latitudinal extent of variation during this year.

Source: *Amaechi et al., 2019*

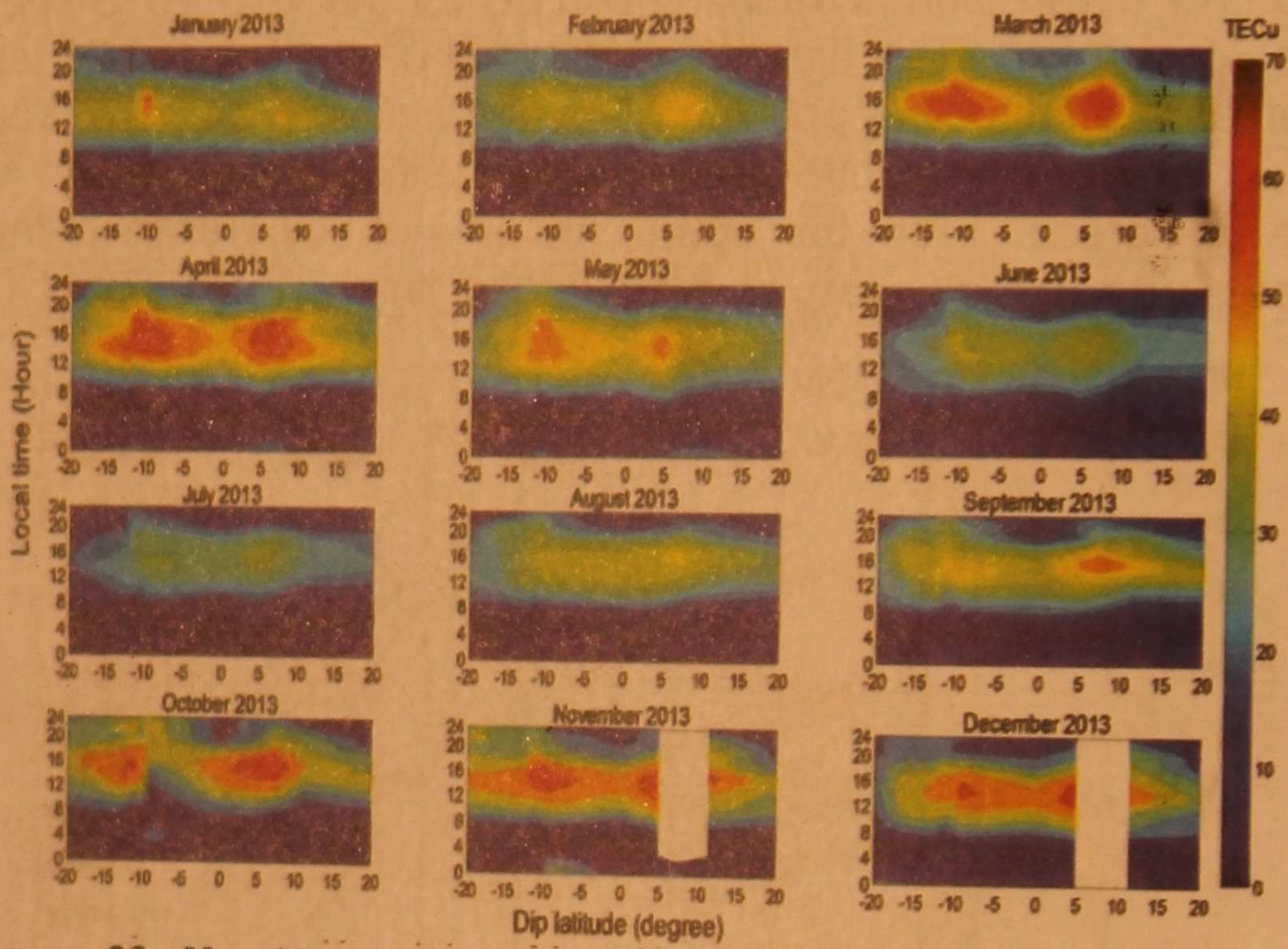

Figure 39: Monthly variations of the position and magnitude of the African EIA crests for the year 2013

Source: *Amaechi et al., 2019*

Figure 40 shows the seasonal variations of the EIA for the year 2013. The main seasons considered were represented by winter (November, December, January, February); summer (May, June, July, August); and equinoxes (March–April and September–October). The seasonal variations of equatorial electrojet (EEJ) ΔH are presented in Fig. 41. The contribution of the equatorial electrojet (EEJ) in controlling the formation of the EIA and the latitudinal extent of the crests' position was established. The computed time difference in the time of maximum EEJ and that of the occurrence of the crests of the EIA was found to be about 4 h during equinoxes and 2–3 h during solstices. The established seasonal variation of the crests over this region has given an insight into the seasonal pattern of wind over the African EIA (Figures 40 and 41).

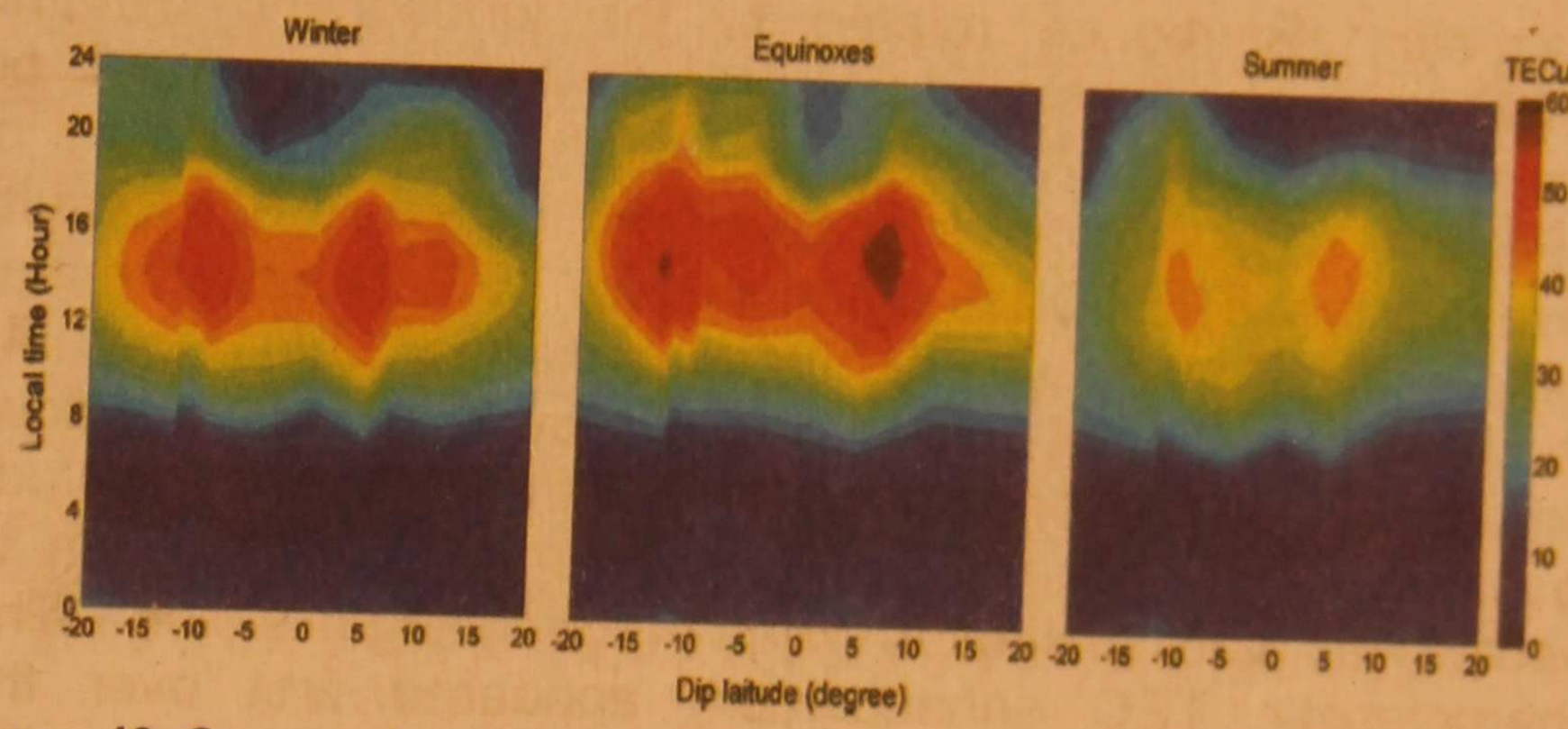

Figure 40: Seasonal variations of the EIA for the year 2013
Source: *Amaechi et al., 2019*

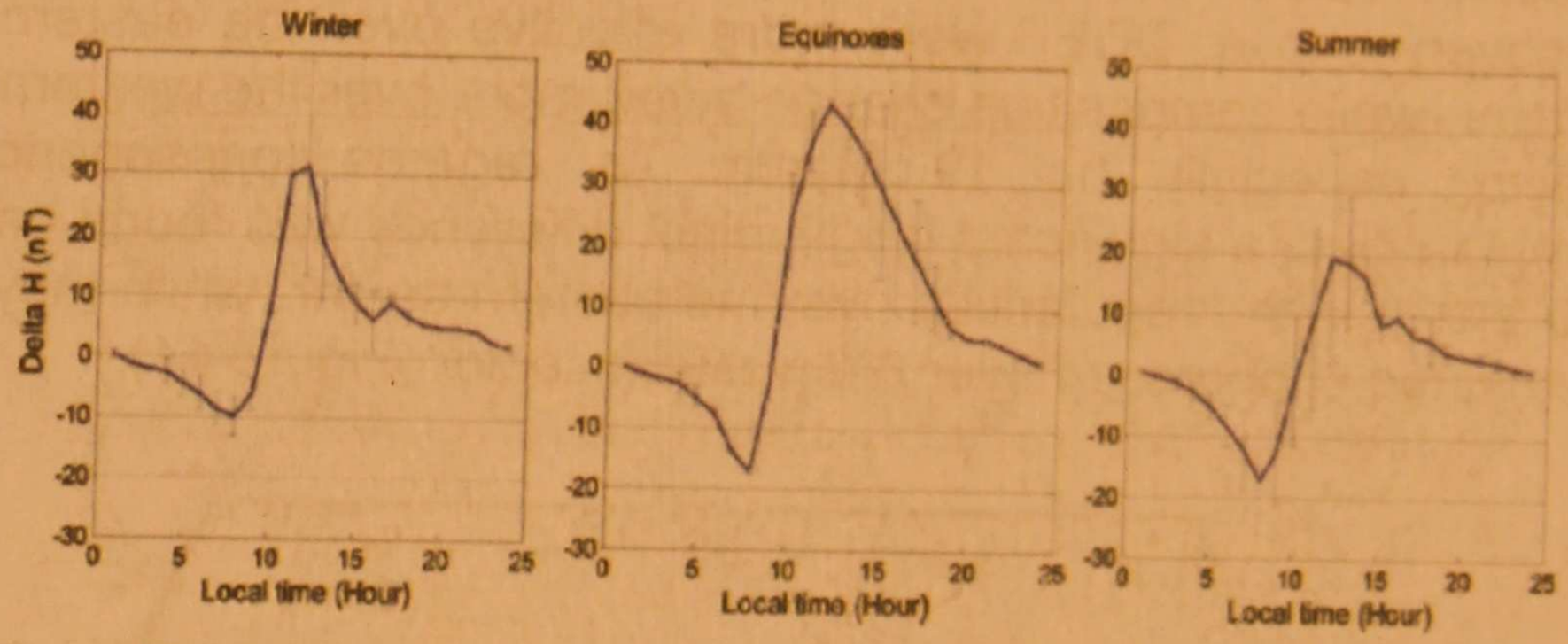

Figure 41: Seasonal variations of _H for the year 2013. The error bars represent the standard deviation used to demarcate the limit of day-to-day variability
Source: *Amaechi et al., 2019*

The electrodynamics of equatorial/low-latitude ionosphere during geomagnetic activity is quite complex. The complex behaviour of TEC under different geomagnetic conditions that can have deleterious impacts on space-based communication and navigation systems have been reported (Buonsanto, 1999; Lin et al., 2005; Carrano & Groves, 2007; Venkateswara Rao et al., 2013). In Amaechi, et al., (2018b), we investigated the response of the African equatorial/low-latitude ionosphere to the 2015 St. Patrick's Day geomagnetic storm during solar cycle 24. Prompt penetration of electric field (PPEF) and disturbance dynamo of electric field (DDEF) were isolated using their DP2 (i.e. magnetic disturbance related to PPEF) and Ddyn (i.e.

magnetic disturbance related to the ionospheric dynamo (DDEF)) magnetic signatures along with their impact on irregularities (Blanc & Richmond, 1980). Map of locations of GPS and magnetometers is as shown in Figure 42. Results revealed that PPEF was responsible for TEC enhancement as well as the expansion of the northern crest to 22°N. Figure 43 shows the variation of behaviour of EIA over the equatorial/low-latitude African sector from 16 to 22 March 2015. This study revealed a difference in the response from the eastern to western longitudinal sectors within Africa during this storm. The characteristic TEC enhancement appeared first over the eastern sector during the first PPEF, while it appeared over the western sector during the second PPEF. Also, during the recovery phase, DDEF were more effective over the eastern sector, while composition change acted more over the western sector especially on 19 March. As regards ionospheric irregularities, a significant longitudinal difference was found on 19 March with irregularities over the eastern sector, while they remained suppressed over the western sector (Figure 44).

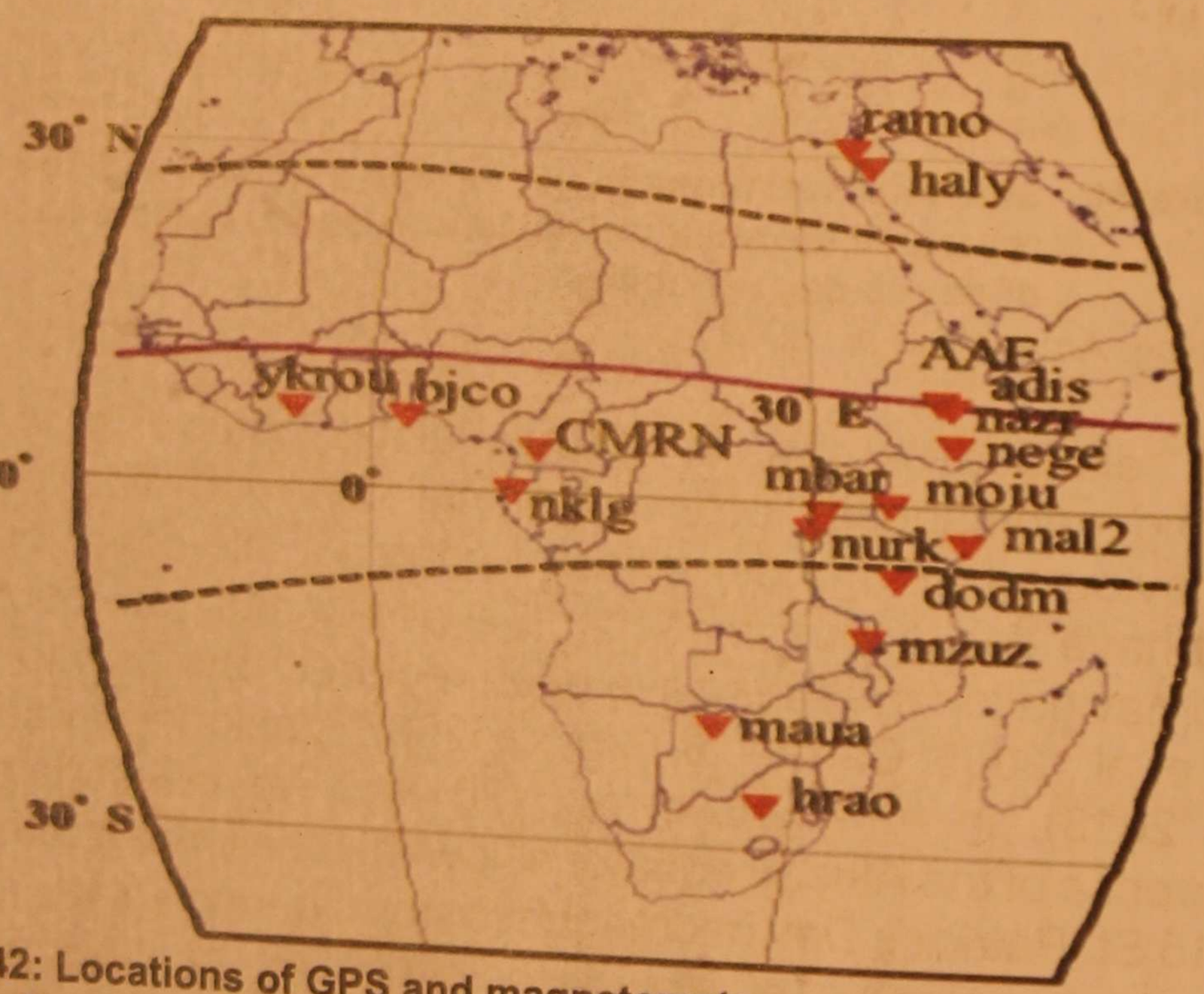

Figure 42: Locations of GPS and magnetometers
Source: *Amaechi, et al., 2018b*

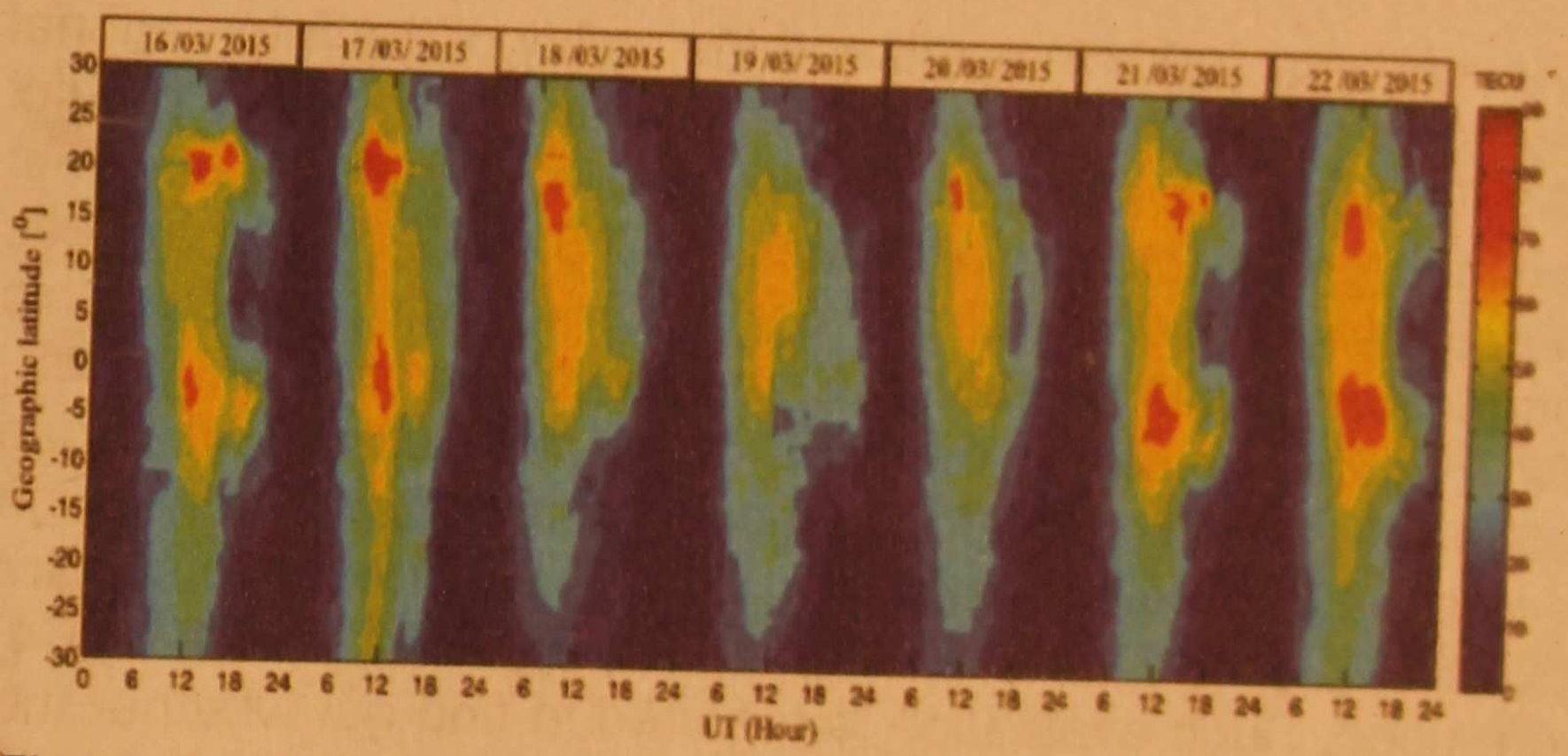

Figure 43: Variations of the equatorial ionization anomaly over the African eastern region for 16 – 22 March 2015

Source: *Amaechi, et al., 2018b*

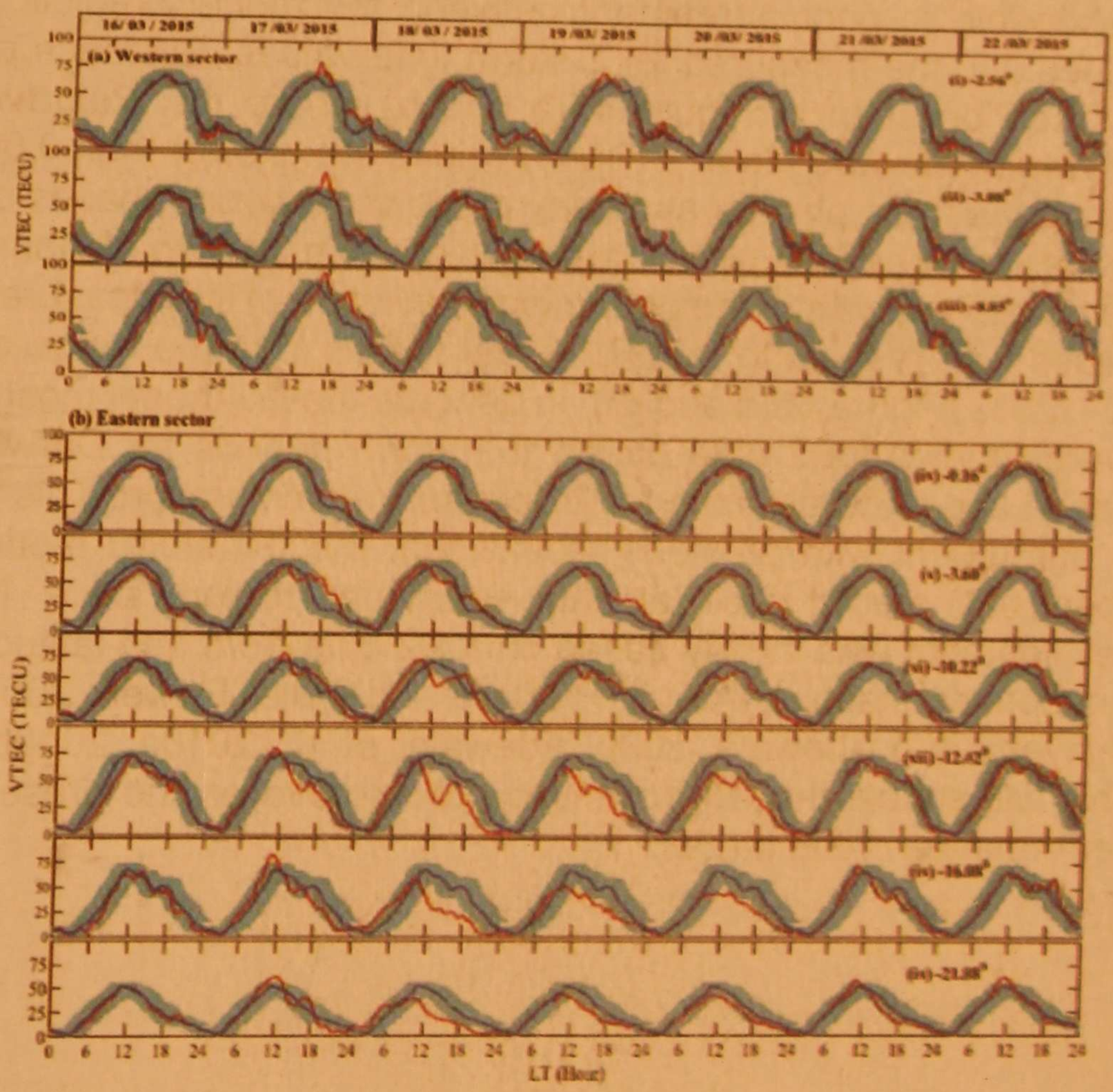

Figure 44: Variations of vertical total electron content (VTEC) over (a) the western sector and (b) the eastern sector

Source: *Amaechi, et al., 2018b*

Oyeyemi, et al., (2013) evaluated the ability of the International Reference Ionosphere IRI-2007 storm time model to predict foF2 ionospheric parameter from two low latitude stations: Vanimo (geographic coordinates, 2.7°S, 141.3°E, magnetic coordinates, 12.3°S, 212.5°E) and Darwin (geographic coordinates, 12.45°S, 130.95°E, magnetic coordinates, 22.9°S, 202.7°E) by comparing the foF2 measured values with those obtained by the IRI-2007 storm model. Data from nine geomagnetic storms (peak Dst $\leq 100nT$) occurring in the years 2000 (Rz12 = 119), 2001(Rz12 = 111) and 2003 (Rz12 = 64) were used. Such evaluation is required to find out whether the IRI storm model is able to capture the effects of the electric field effects on HF communication and navigation in the equatorial region of the ionosphere. The results show that there is reasonable to poor agreement between the model prediction values and the measured foF2 storm time values. Evidence of this can be seen in Figure 45(a and b) where the ***Relative Deviation Module Mean*** (RDMM) values are greater than 0.06 during the main phases and early stage of recovery phases of all the storm periods under investigation from the two stations. Sample of analysis of the percentage deviation of the measured values with respect to the IRI model values is in the range of 40–125% (Figure 46(a and b)). In general, the IRI model mostly overestimates foF2 data during the storm periods for Darwin station and underestimate foF2 data for Vanimo station. This is in agreement with previous results that the IRI storm model does not predict well at the equatorial region since its development was mostly based on foF2 data from mid-latitude ionospheric stations (Araujo-Pradere and Fuller-Rowell, 2003; Oyeyemi and Adewale, 2009, Adewale, et al., 2010a, 2010b). This will enable the IRI community to improve on the present performance of the model.

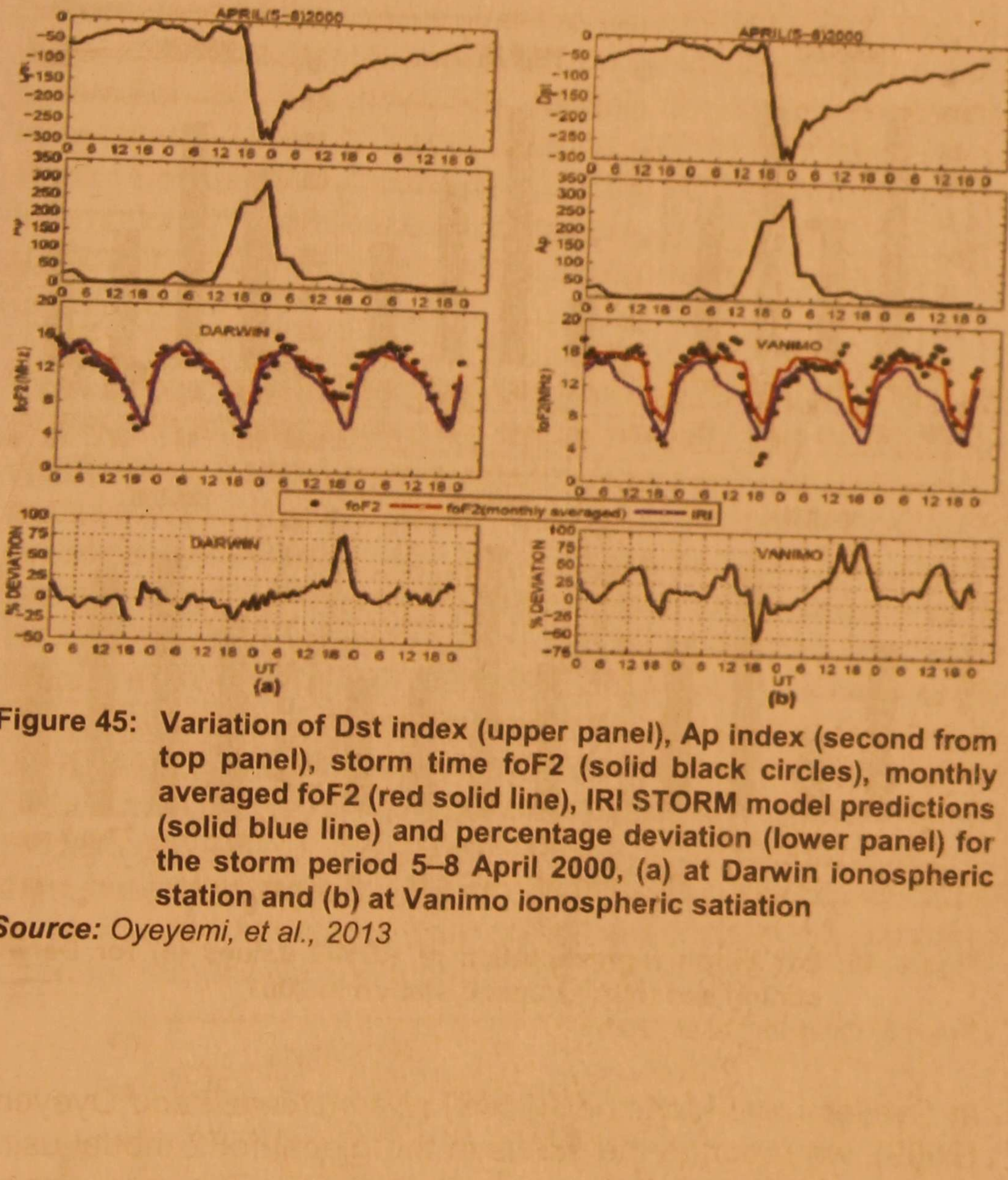

Figure 45: Variation of Dst index (upper panel), Ap index (second from top panel), storm time foF2 (solid black circles), monthly averaged foF2 (red solid line), IRI STORM model predictions (solid blue line) and percentage deviation (lower panel) for the storm period 5–8 April 2000, (a) at Darwin ionospheric station and (b) at Vanimo ionospheric satiation

Source: *Oyeyemi, et al., 2013*

Figure 46: Bar graph representation of RDMM values (a) for Darwin station and (b) for Vanimo station in 2001

***Source**: Oyeyemi, et al., 2013*

In Oyeyemi and McKinnell (2008) and McKinnell and Oyeyemi (2009), we reported the status of the global foF2 model using data from 85 global ionospheric stations. The two papers appealed for more data from particular areas, such as equatorial, high latitude, etc., in order to expand the database with which the model was developed. The equatorial region is known to be more complex because of its electrodynamical nature and therefore identified as problematic within the IRI peak prediction setup. After this report, the global database has been expanded to include 135 stations, shown in Figure 47. As a result, McKinnell and Oyeyemi (2010) developed a new version of the global foF2 NN based model to evaluate the

performance of the model over the equatorial region. The aim is to show the improvement in the predictions of the foF2 parameter by the new NN model as compared to the International Union of Radio Science (URSI) and International Radio Consultative Committee (CCIR) model options of the International Reference Ionosphere (IRI) and to also demonstrate the requirement for additional foF2 data from the equatorial zone.

The stations from the equatorial region used in the development of the model are shown in Table 11 with their geographic coordinates. Table 12 shows stations used in the analysis of the performance of the global model with their geographic coordinates. Figures 49 and 49 show the bar graphs representing the ranges of % *improvement* of NN based model over the IRI model options. It should be noted that the results from Vanimo, Fortaleza and Sao Luis stations correspond to unseen data, since the database for developing the model only used data up to 2005 and did not include data from Fortaleza or Sao Luis. Our results show, in general, an improvement in predicting the foF2 value over the equatorial region, however, these improvements would be more significant if additional much needed equatorial data could be added to the database used for the development of the NN based model.

Figure 47: Global map illustrating the locations of the 135 stations used in the development of the NN based global foF2 model

Source: *McKinnell and Oyeyemi 2010*

Table 11: The Geographic Coordinates of the Stations within the Equatorial Region whose Data were Used in the Development of the Global foF2 Model.

Station	Lat	Long
Port Moresby	–9.4	147.1
Ascension	–7.9	12.4
Talara	–4.6	278.7
Vanimo	–2.7	141.3
Singapore	1.3	103.8
Bogota	4.5	285.8
Trivandrum	8.5	77.0
Kwajalein	9.1	167.2

Source: *McKinnell and Oyeyemi 2010*

Table 12: The Geographic Coordinates of the Stations from the Equatorial Region Used to Verify the Ability of the Global foF2 Model to Predict in this Region.

Station	Lat	Long
Port Moresby	–9.4	147.1
Ascension	–7.9	12.4
Vanimo	–2.7	141.3
Fortaleza	–3.8	322.0
Sao Luis	–2.6	315.8

Source: *McKinnell and Oyeyemi 2010*

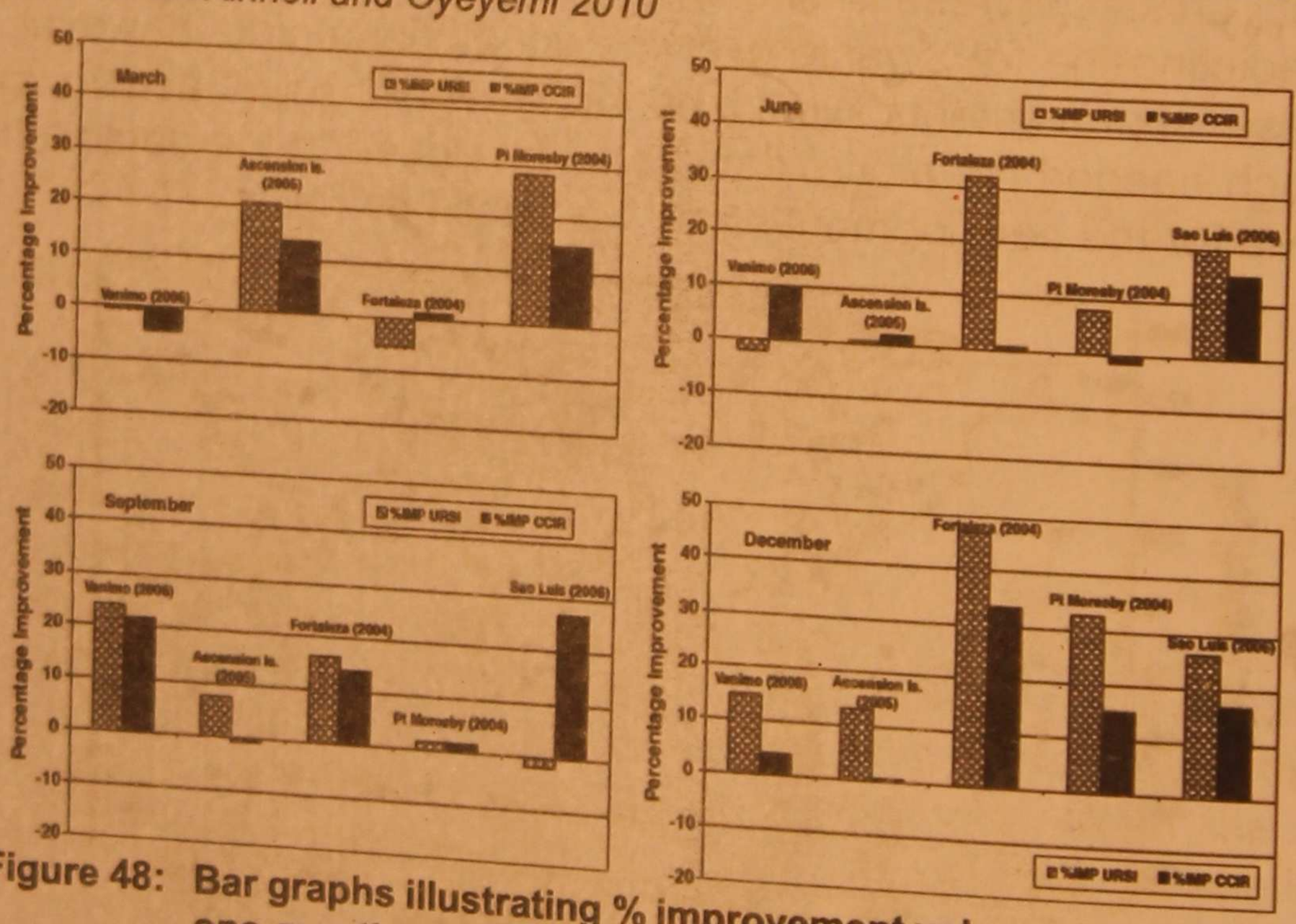

Figure 48: Bar graphs illustrating % improvement values obtained from one month of hourly values of foF2 for 4 different months (March, June, September and December) during low solar activity periods (2004, 205 and 2006)

Source: *McKinnell and Oyeyemi 2010*

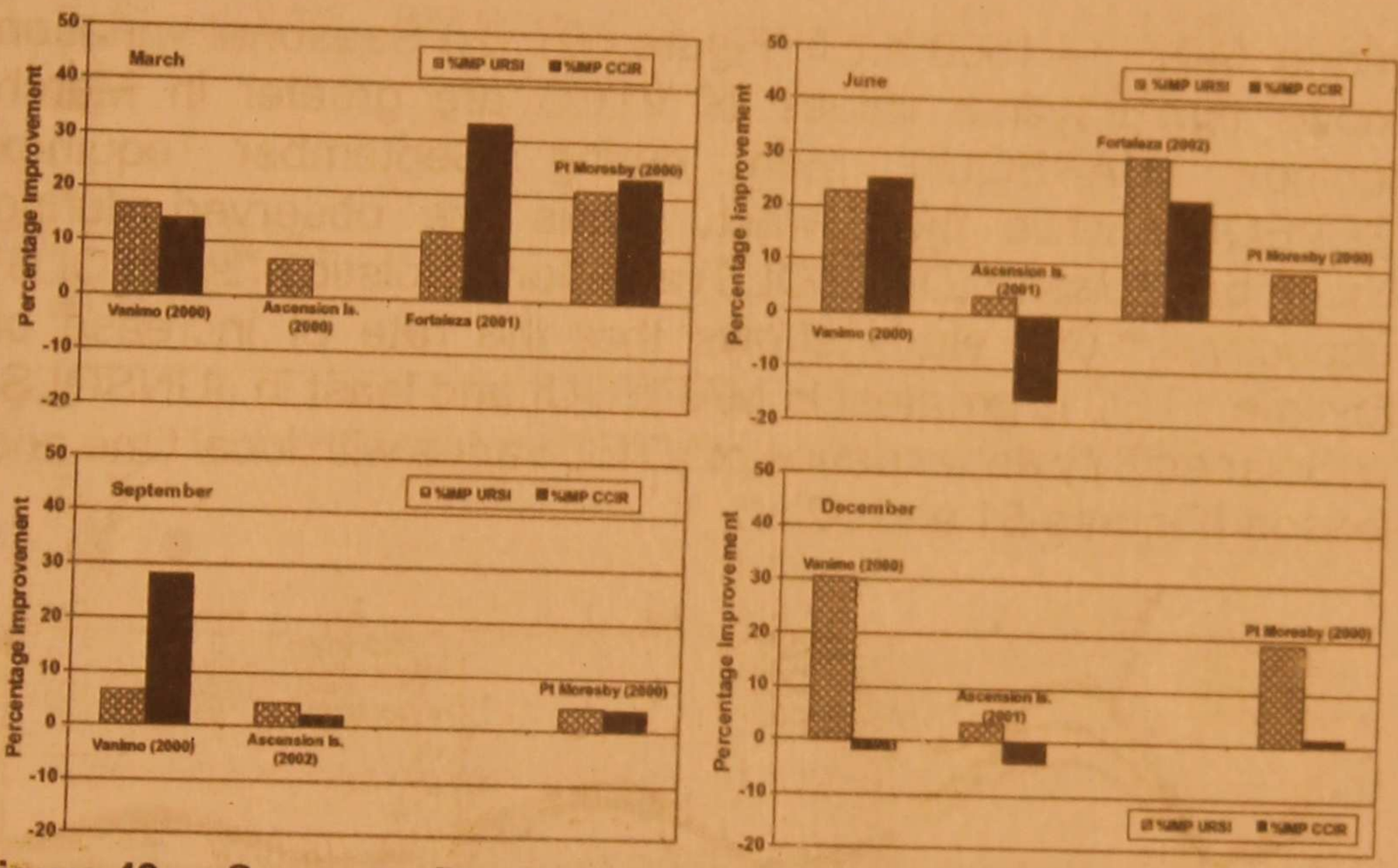

Figure 49: Same as figure 4 but during high solar activity periods (2000, 2001 and 2002)

Source: *McKinnell and Oyeyemi 2010*

Solar Extreme Ultraviolet Variability (EUV) and X-ray radiations provide the primary energy sources for producing plasma in the Earth's upper atmosphere. Consequently, the total electron content (TEC) of the ionosphere is also expected to reflect these variations (Huang and Cheng, 1995; Chen et al., 2008). Studies revealed that much work has not been carried out on the solar activity dependence of electron density over the equatorial region of the African continent due to the paucity of data. The effect of this is that our understanding of the electrodynamics of this region is limited with respect to HF communication. In Adewale et al. (2012), we investigated diurnal, seasonal and solar activity (10.7 cm radio flux (F10.7) and sunspot number (R)) dependence of GPS-TEC observed data at an equatorial station, Mbarara, Uganda (geographic coordinates: 0.60°S, 30.74°E; geomagnetic coordinates: 10.22°S, 102.36°E) during the period 2001–2009. Results show that (i) Vertical total electron content (VTEC) is generally higher during high solar activity (HSA) period than low solar activity (LSA) for all the seasons; (ii) VTEC has higher values during daytime compared with nighttime values. VTEC values generally increase from 0600 h LT in all the seasons and reache their maximum value

during 1400 h – 1500 h LT (Figure 50), (iii) Seasonal variation shows that daytime values of VTEC are greater in March equinox (MAREQUI) than during September equinox (SEPEQUI) while the lowest values are observed during December Solstice (DECSOLS) and June Solstice (JUNSOLS) respectively. Our study shows that the rate of increase of daytime VTEC is greatest in MAREQUI and least in JUNSOLS, (iv)Solar activity dependence of VTEC varies with local time and season (Figures 51 and 52).

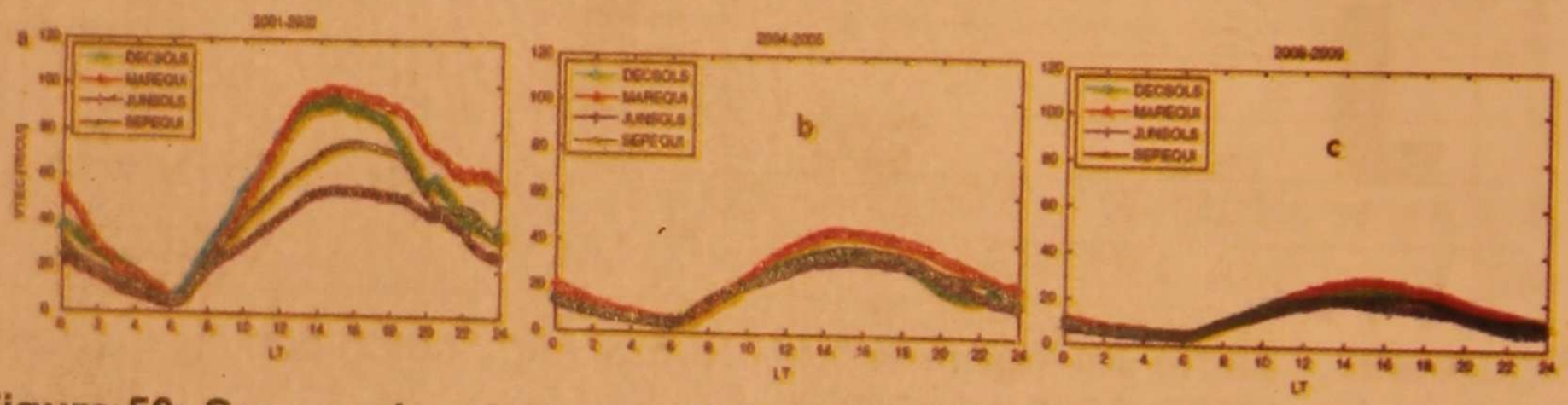

Figure 50: Seasonal variation of VTEC for (a) HSA, (b) MSA and (c) LSA
Source: *Adewale et al., 2012*

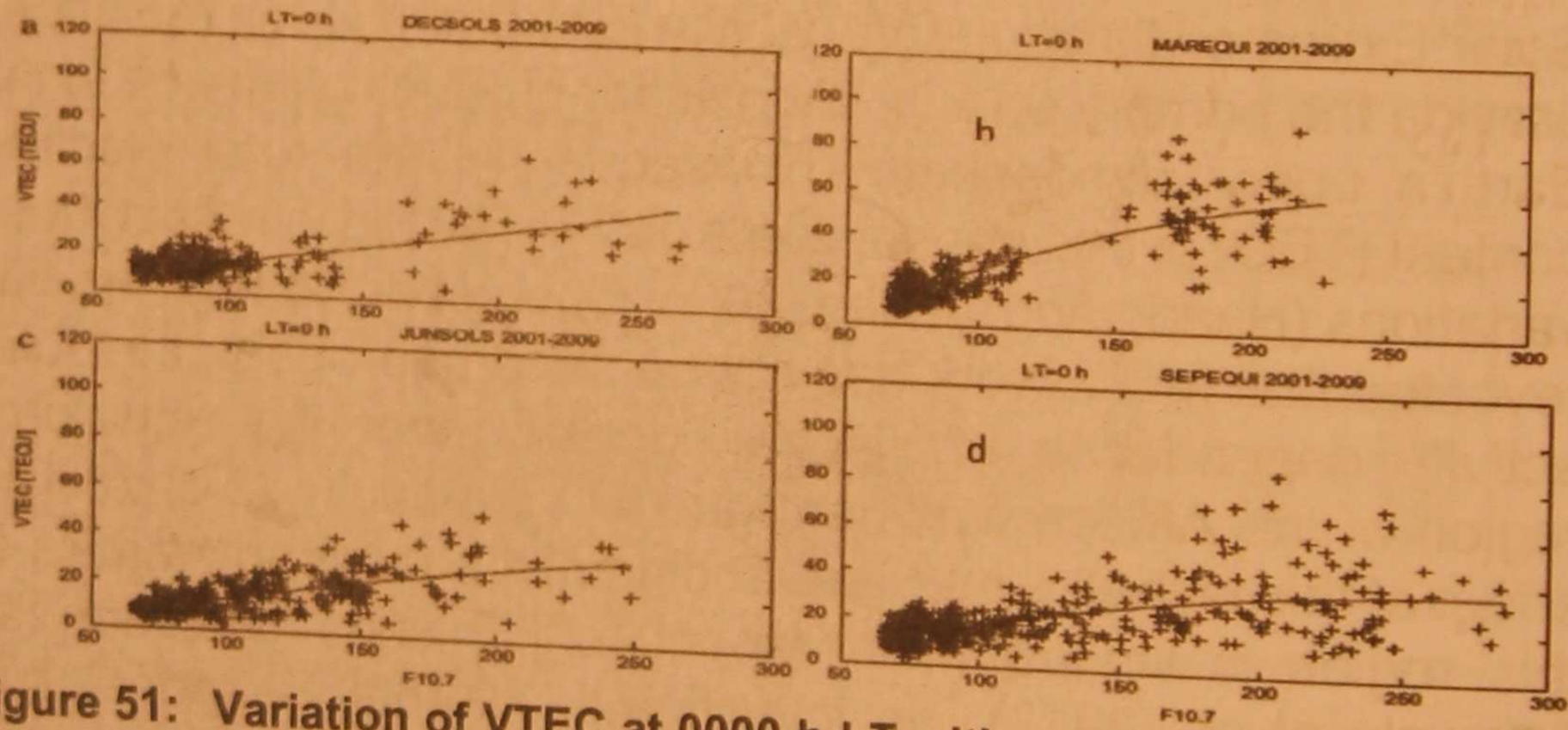

Figure 51: Variation of VTEC at 0000 h LT with solar flux (F10.7) for (a) DECSOLS, (b) MAREQUI, (c) JUNSOLS, and (d) SEPEQUI
Source: *Adewale et al., 2012*

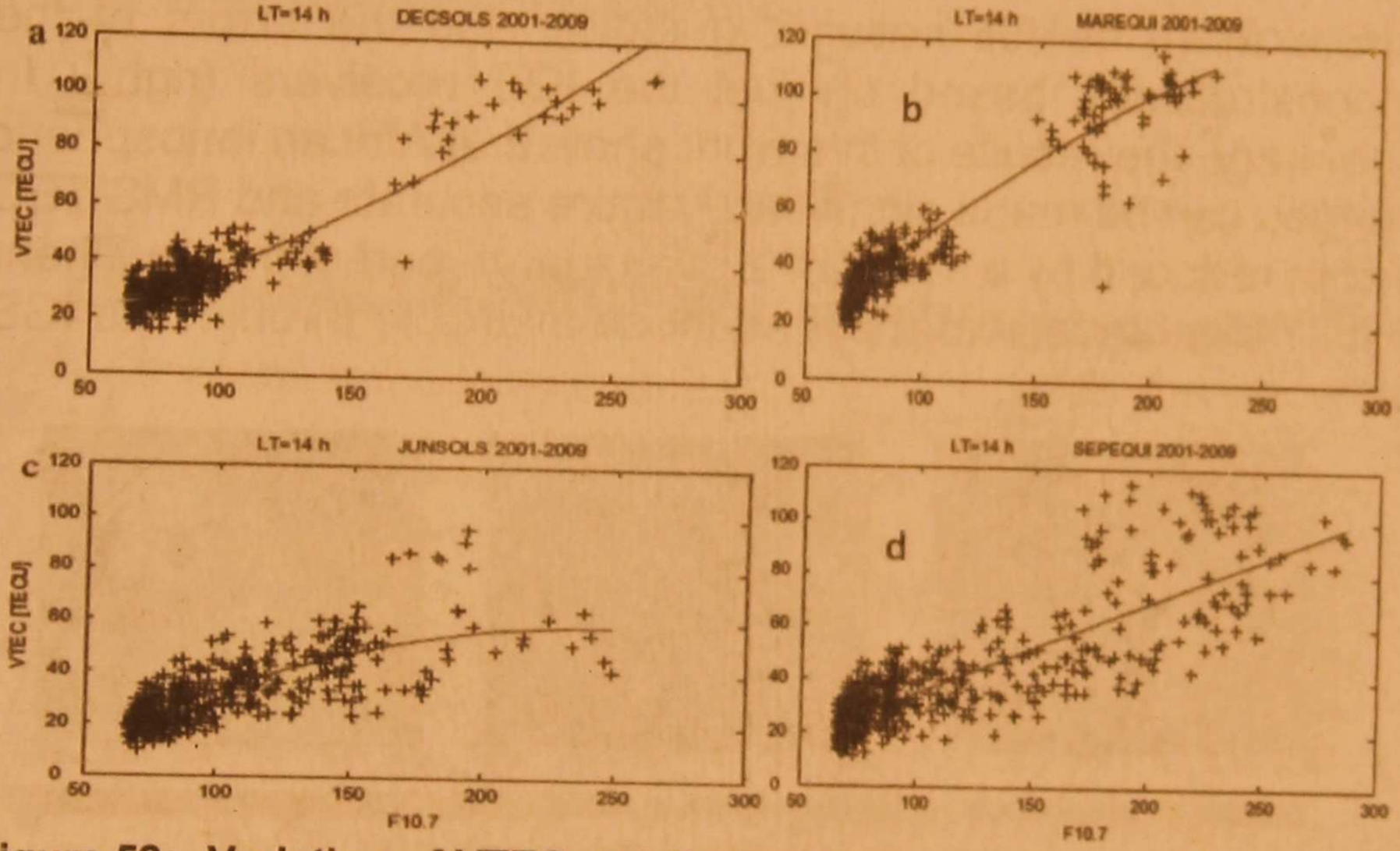

Figure 52: Variation of VTEC at 1400 h LT with solar flux (F10.7) for (a) DECSOLS, (b) MAREQUI, (c) JUNSOLS, and (d) SEPEQUI

Source: *Adewale et al., 2012*

Human activities such as radar detection and satellite positioning are affected by ionospheric electron densities. Ionospheric imaging could be used to estimate the effects on these activities in the African sector. As such, accurate ionospheric specification is necessary for improving human activities such as ***radar detection***, ***navigation***, and ***Earth observation***. This is of particular importance in Africa, where strong plasma density gradients exist due to the equatorial ionization anomaly. In Alex et al., (2014), we assessed the accuracy of three-dimensional ionospheric images over the African region using differential Global Positioning System (GPS), slant total electron content observations and a time-dependent tomography algorithm. Results show that the inclusion of observations from the African Geodetic Reference Frame (AFREF) archive significantly reduces ionospheric specification errors across the African sector, especially in regions that are poorly served by the permanent network of GPS receivers. Spatially distributed root-mean-square (RMS) errors are calculated based on the errors of the entire period (2–16 December 2012) and plotted (Figure 53). Figure 53 shows the reconstructions based on the fictional network (left), the

errors from the full network (middle), and the errors of the reconstructions based on just the IGS receivers (right). In summary, the results of this work show that African ionospheric images can be made significantly more accurate and RMS TEC errors reduced by a factor of 2 over a large part of the continent if additional receivers (beyond those available through the IGS network) are used.

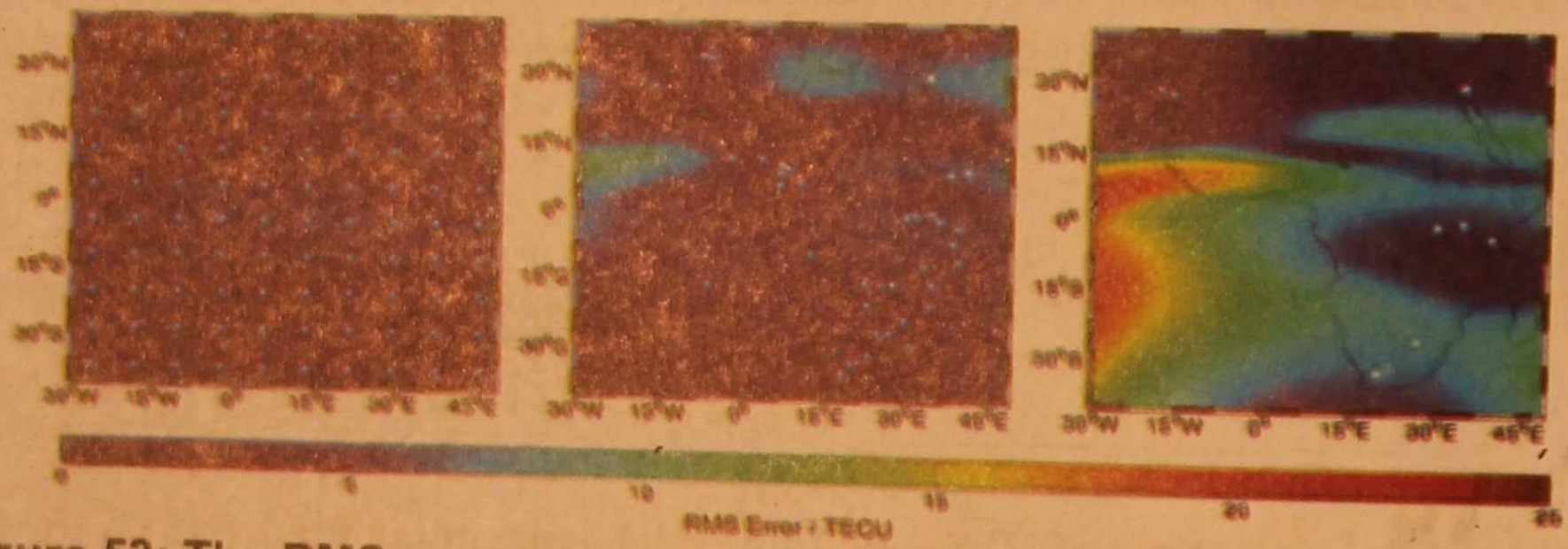

Figure 53: The RMS errors of three sets of simulated reconstructions
Source: *Alex et al., 2014*

GPS observation data obtained from the GSV4004B GPS Ionospheric Scintillation and TEC Monitor (GISTM) installed in the Department of Physics, University of Lagos (6.5°N, 3.4°E; magnetic latitude 3.03°S), Nigeria was used to present the first study of L-band scintillations and total electron content in Lagos (Adewale et al., 2012). The GPS receiver can track up to 11 GPS satellites at the L1 and L2 frequency simultaneously and measures both phase and amplitude at a 50-Hz rate for each satellite tracked on L1 from which both amplitude index (S_4) and phase scintillation index (σ_ϕ) are calculated. The results show that the presence of some large-scale depletions of TEC or plasma bubbles may be noted during the evening hours and that TEC depletions correspond to an increased rate of change of TEC (ROT). This confirms that plasma bubbles are associated with large scale irregularities (Dandekar and Groves, 2004). It was also established that enhanced amplitude scintillation (S_4) corresponds quite well with TEC depletions and increases in ROT (Figure 54).

A typical equatorial non-scintillation day is illustrated in Figure 55 where S_4 index is generally below 0.2, whereas an S4 index of 0.4 and above is indicative of scintillation events.

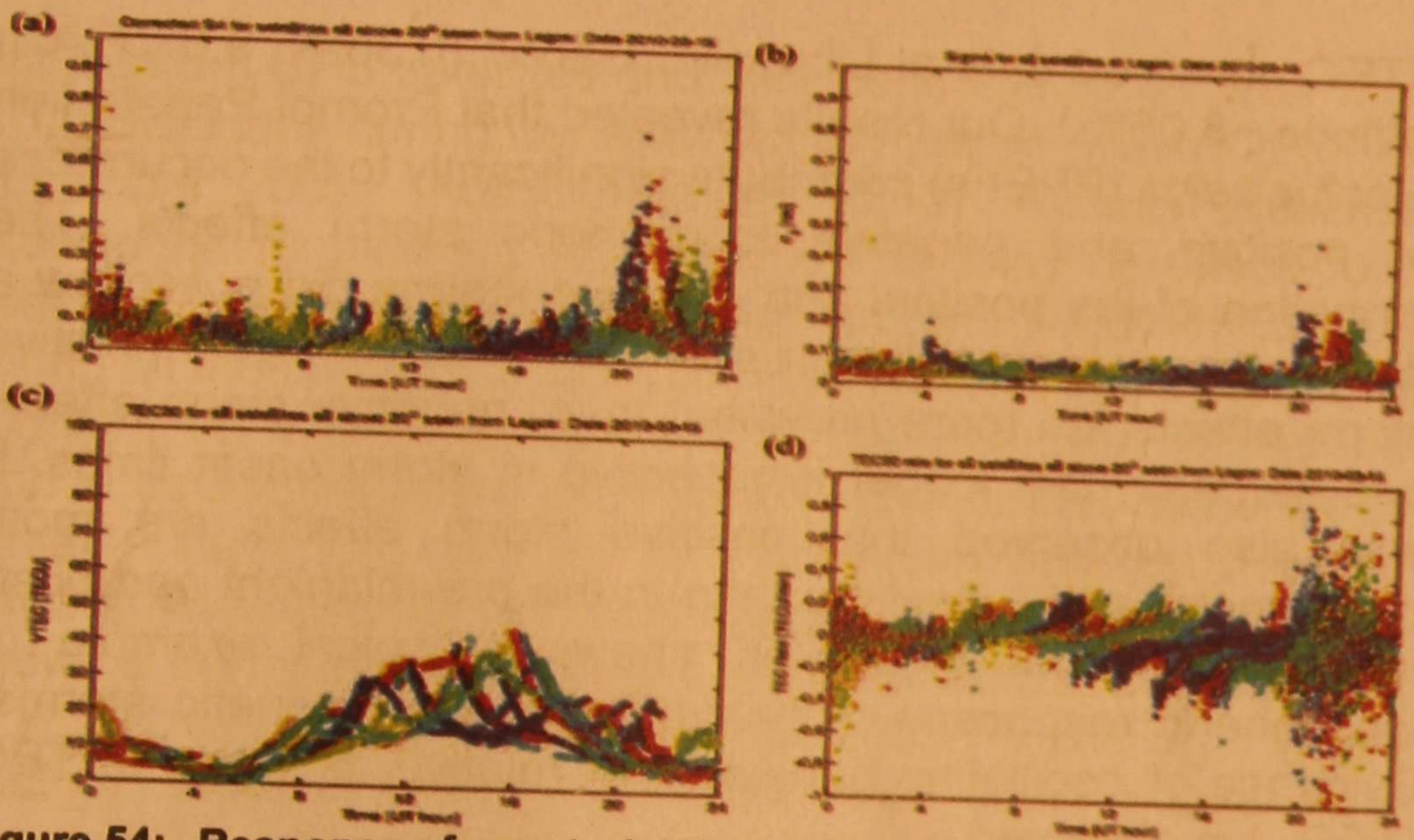

Figure 54: Response of equatorial F-region to geomagnetic storm of 15 March 2010 observed by GPS in the African sector. (a) S4, (b) sigma, (c) VTEC, and (d) TEC rate (LT = UT + 1 h)

Source: *Adewale et al., 2012*

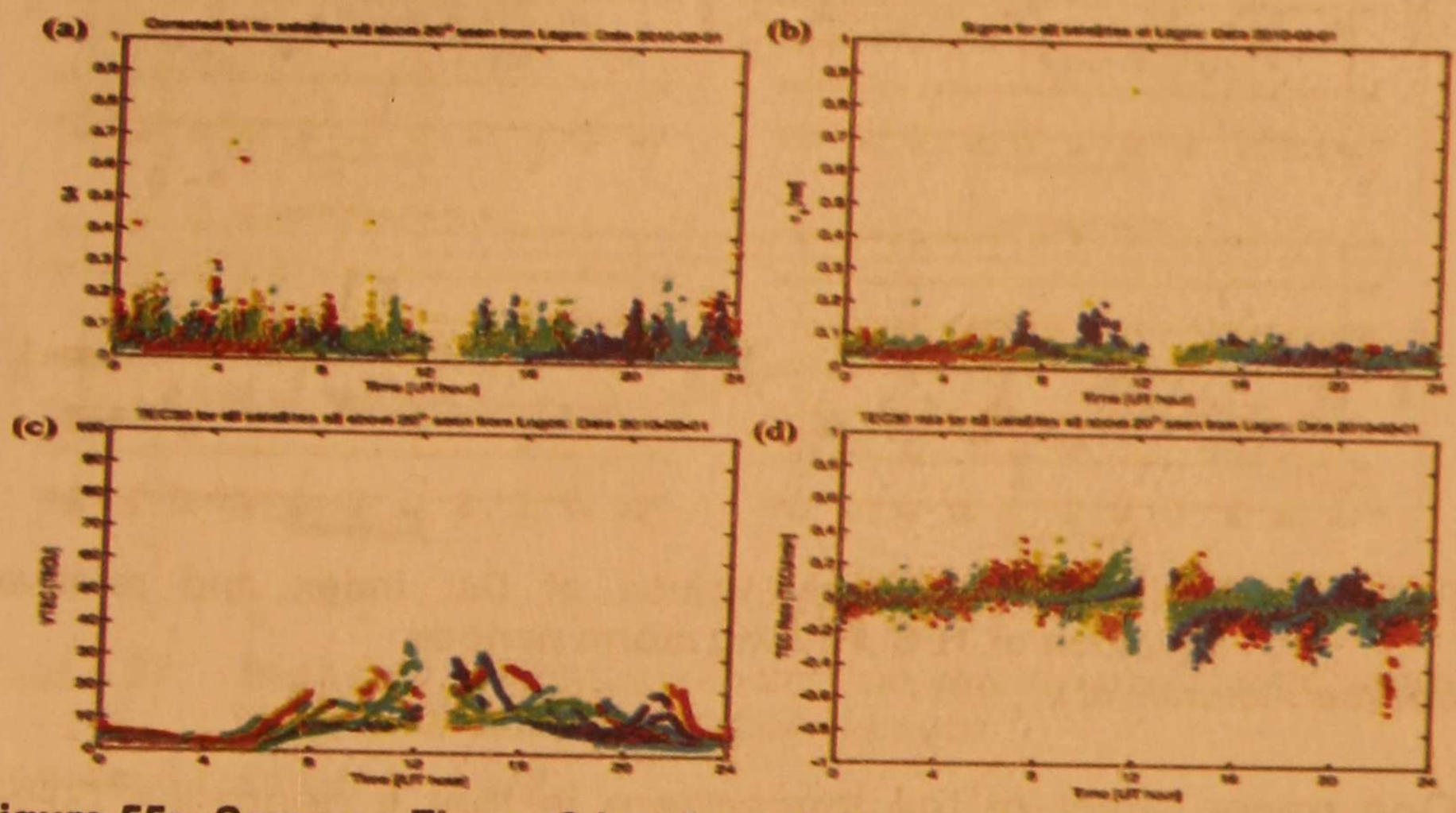

Figure 55: Same as Figure 2 but for 1 February 2010 (non-scintillation day) (gap around 12:00 UT is due to a power outage)

Source: *Adewale et al., 2012*

In Adewale et al. (2011), we presented the first results on the investigation of the response of the equatorial ionospheric region in the African sector during geomagnetic storm periods between April 2000 and November 2007 using GPS-derived

VTEC observed data at Libreville, Gabon (0.35°N, 9.67°E, dip latitude −8.05°S). Our results revealed that Prompt Penetration Electric fields (PPEFs) contribute significantly to the occurrence of positive and negative ionospheric storm effects. The formation of the positive and negative storms did not follow a definite trend, irrespective of storm onset times. Again positive storm effects are more prevalent than negative storm effects and generally last longer irrespective of storm onset times. It was also observed that positive storm effects are most pronounced in the daytime than in the pre-midnight and post-midnight periods. Figure 56 shows a typical example of ionospheric responses to four different geomagnetic storms. Evidence of oscillating behaviour of relative deviation of TEC (TEC_{rel}) is observed.

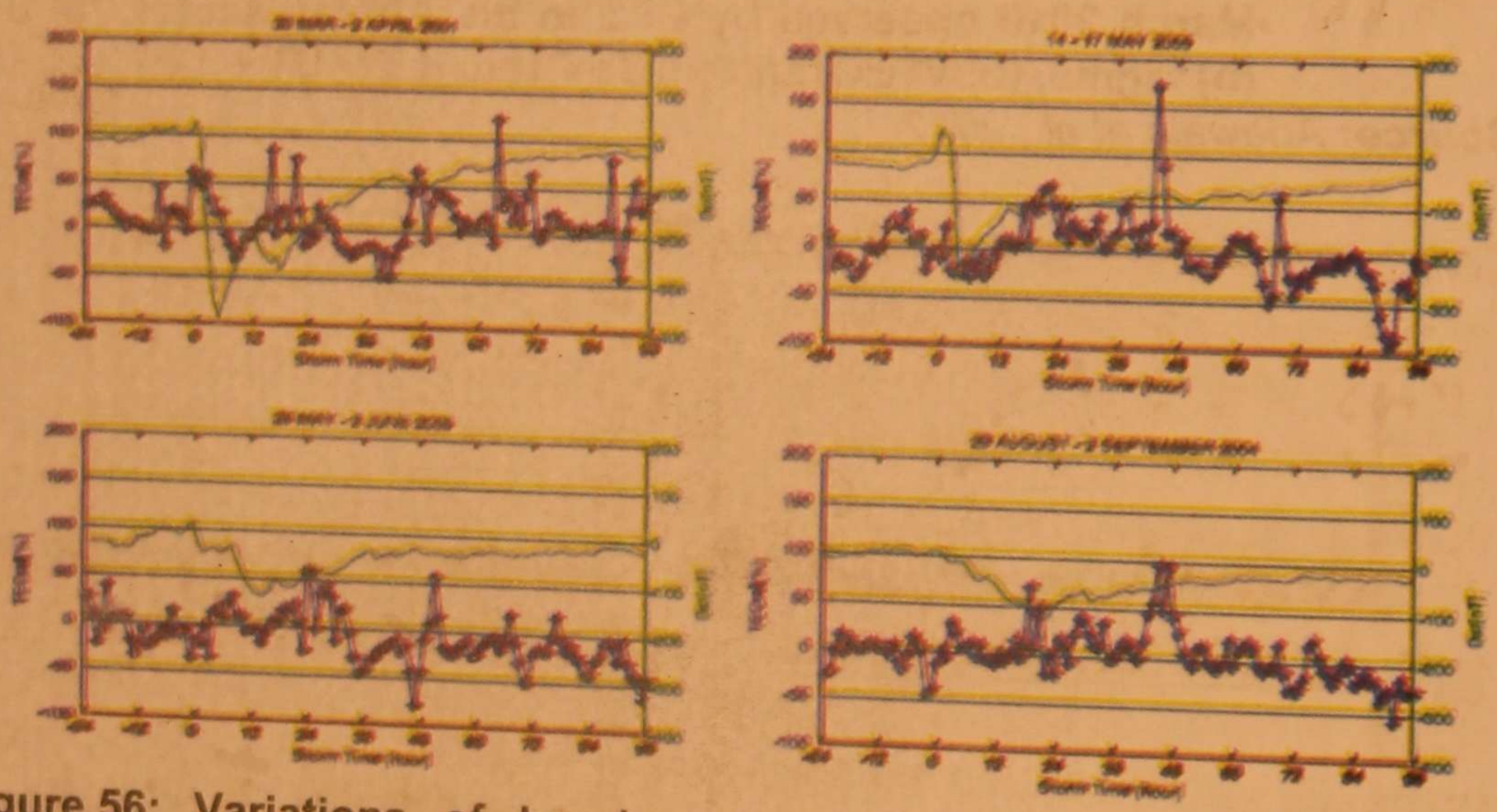

Figure 56: Variations of hourly values of Dst index and relative deviation of TEC_{rel} during storm periods

Source: *Adewale et al., 2011*

One major effect of the ionosphere is that it degrades GPS signals as they propagate through it. This causes range delays leading to error in position estimate and precise time transfer of GPS signals. Therefore, to improve the accuracy of GPS position fixing, it is important to have a good understanding of ionospheric time delay on radio signals. GPS data from an equatorial station, University of Lagos, Nigeria (6.5°N, 3.4°E; magnetic latitude 3.03°S) was used to investigate diurnal and seasonal variations of the ionospheric time delay of radio

signals from GPS satellites and their dependence on solar flux (10.7 cm) index during low solar activity period (March 2008 to December 2009) (Adewale et al., 2013). Results obtained showed that (i) generally, ionospheric time delay increases from 06h00 LT with a maximum value around 14h00-16h00 LT during all the months considered, after which it decreases until midnight, (ii) during low solar activity, the time delay values are high in equinox months, least during summer and moderate in winter (Figure 57), and (iii) the correlation between average daytime peak ionospheric time delay and the solar F10.7 flux shows a low positive correlation, with Correlation Coefficient of R = 0.31 for 2008 and R = 0.15 for 2009 (Figure 58). These findings provide useful information that could support the construction of empirical ionospheric time delay correction models (e.g. space weather forecasting).

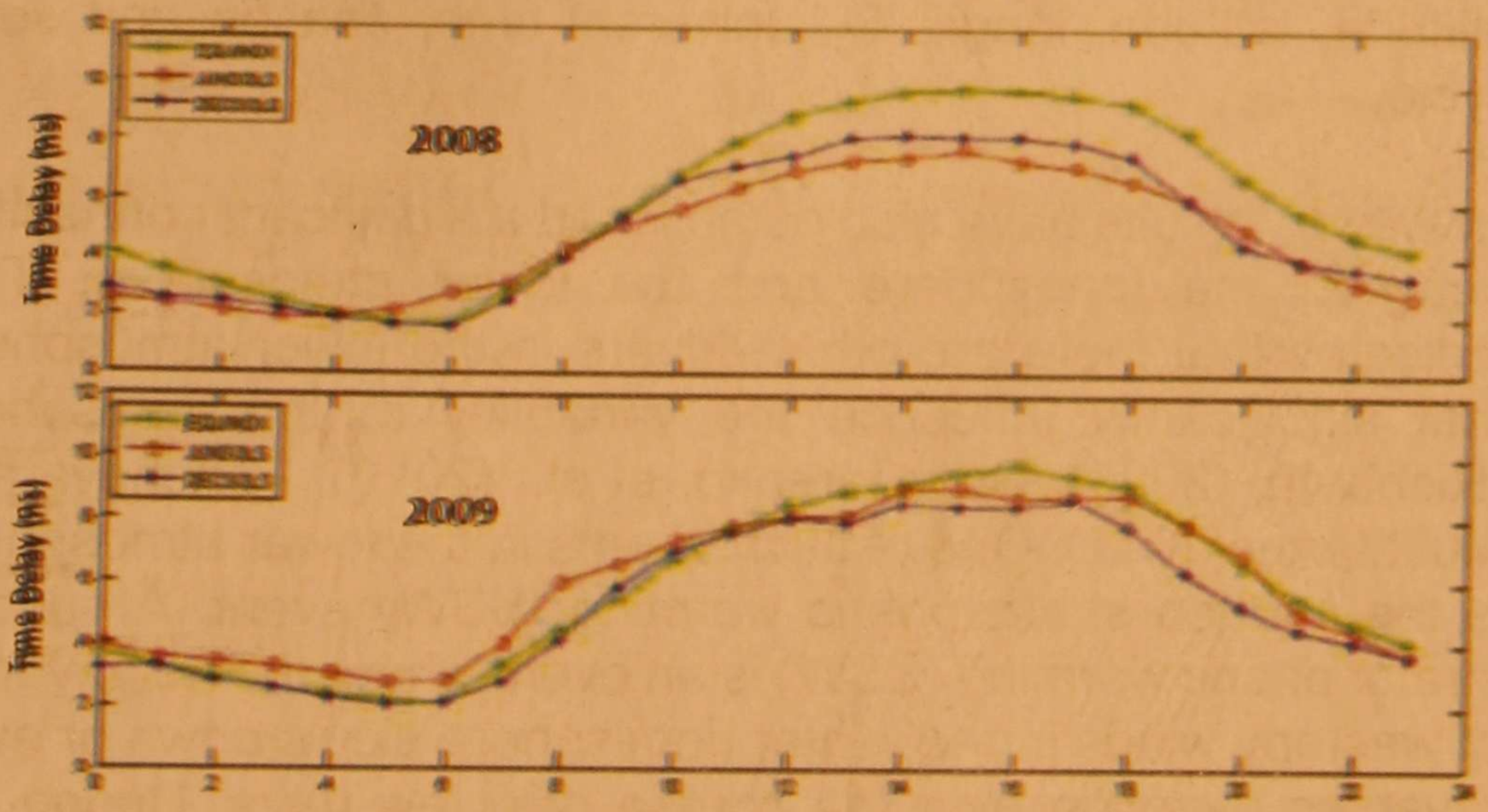

Figure 57: Seasonal mean diurnal variation of ionospheric time delay difference in 2008 and 2009 at Lagos

Source: *Adewale et al., 2013*

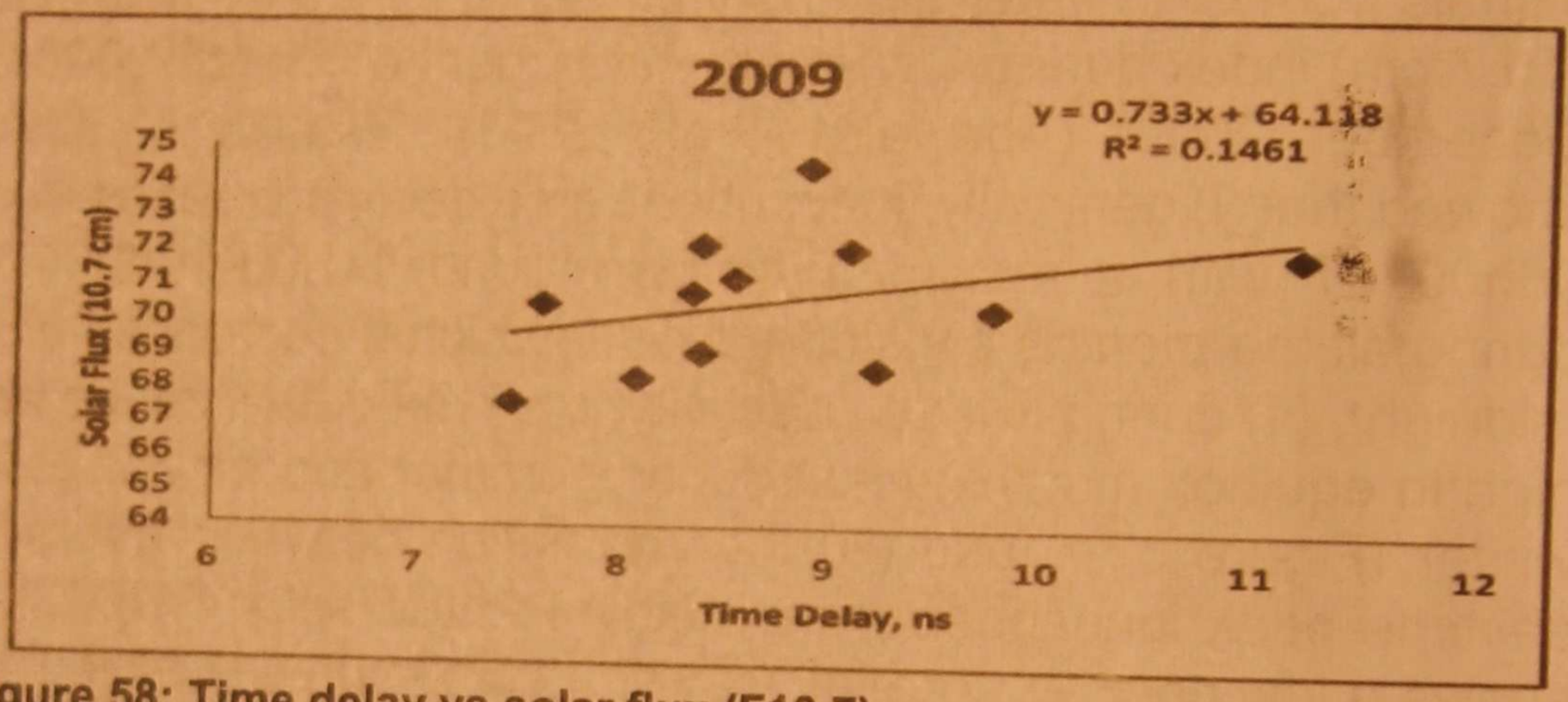

Figure 58: Time delay vs solar flux (F10.7)
Source: *Adewale et al., 2013*

As earlier stated the variability of the Earth's ionosphere is significantly driven by solar ionizing flux, solar wind conditions, altitude, latitude, longitude, universal time, season and solar cycle.

However, results have also established a significant connection between the ionosphere and the lower atmosphere. This indicates that there are other drivers in the lower atmosphere that significantly influence the variability of the ionosphere (Rishbeth, (2006); Goncharenko, et al., (2010); Pancheva and Mukhtarov (2011). One of such events in the lower atmosphere is the sudden stratospheric warming (SSW) event. A sudden stratospheric warming (SSW) is an event where the polar vortex of westerly winds in the winter hemisphere slows down or even reverses direction over the course of a few days. During the SSW, the temperature of the stratosphere increases suddenly, the normal winter polar vortex changes its position and shape, and the zonal winds eventually become weaker or even change direction, Figures 59(a and b).

In Bolaji et al., (2016) we investigated the response of solar quiet (Sq) current in Africa to a 2009 sudden stratospheric warming (SSW) event. This is the first study in Africa that revealed the connection of the lower with the upper atmosphere. One surprising result is the significant increase in the magnitude of Sq that is associated with a counter electrojet

(CEJ) during the descending phase of a SSW. A significant decrease in the magnitude of Sq current was obvious during the peak phase of the SSW in Africa and on world wide scale (Figure 60).

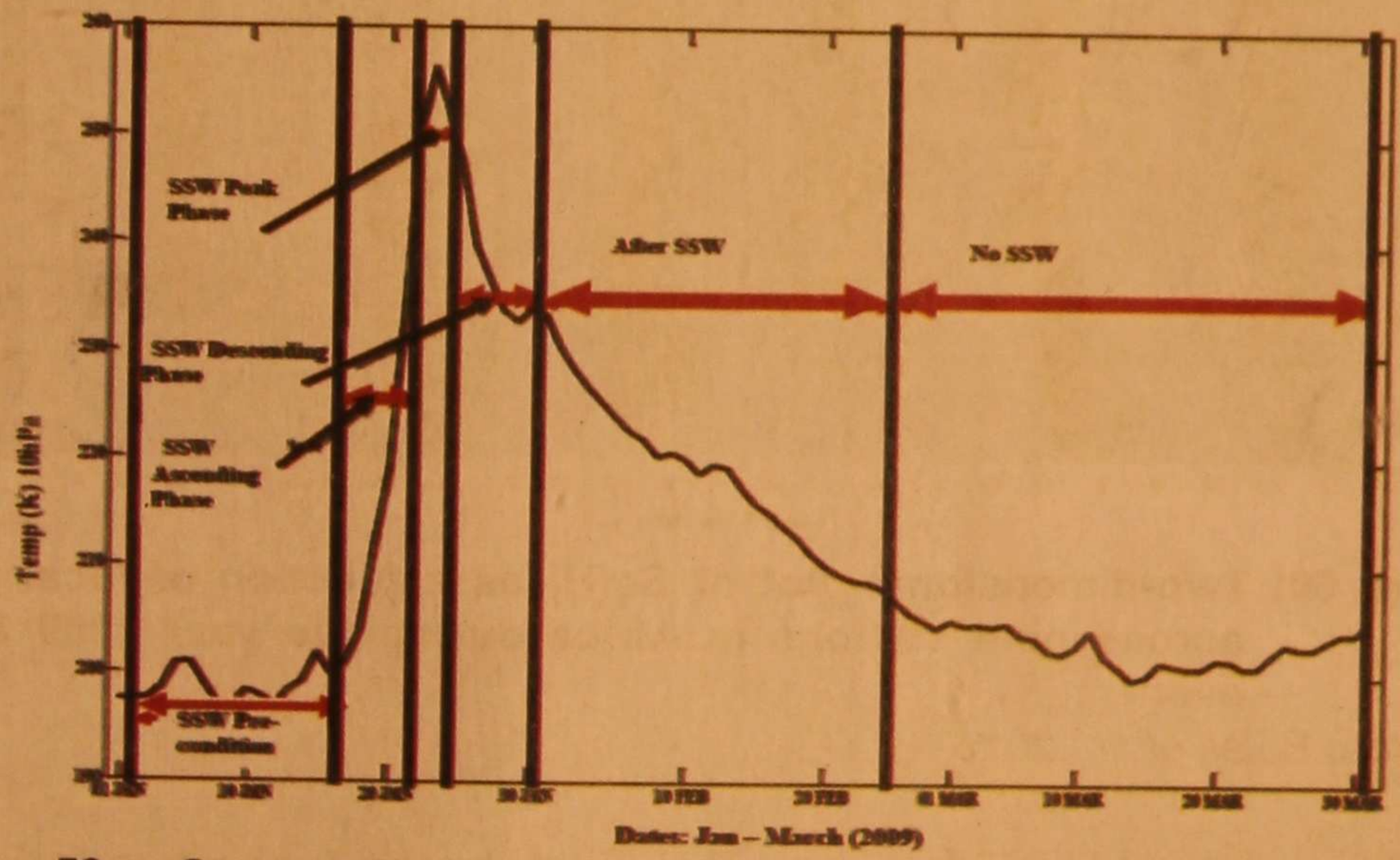

Figure 59a: Stratospheric zonal mean air temperature for January – March 2009 showing the SSW Pre-condition, SSW Ascending, SSW Peak, SSW Descending, after the SSW and No SSW Phase. (Red double arrow indicating period of each phase)

Source: *Bolaji et al., 2016*

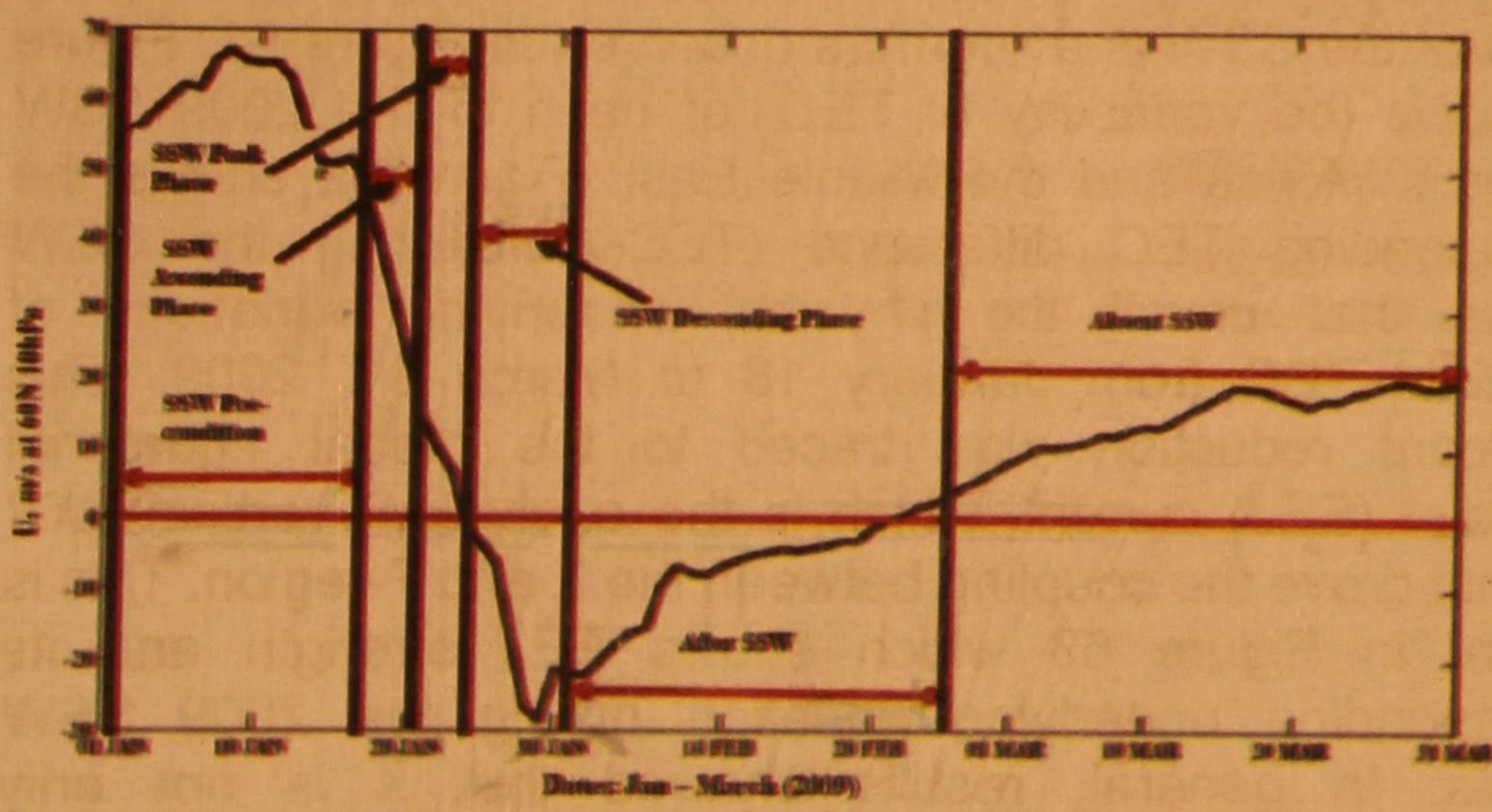

Figure 59b: Stratospheric zonal mean zonal wind for January – March 2009 showing the SSW Pre-condition, SSW Ascending, SSW Peak, SSW Descending, after the SSW and No SSW Phase. (Red double arrow indicating period of each phase)

Source: *Bolaji et al., 2016*

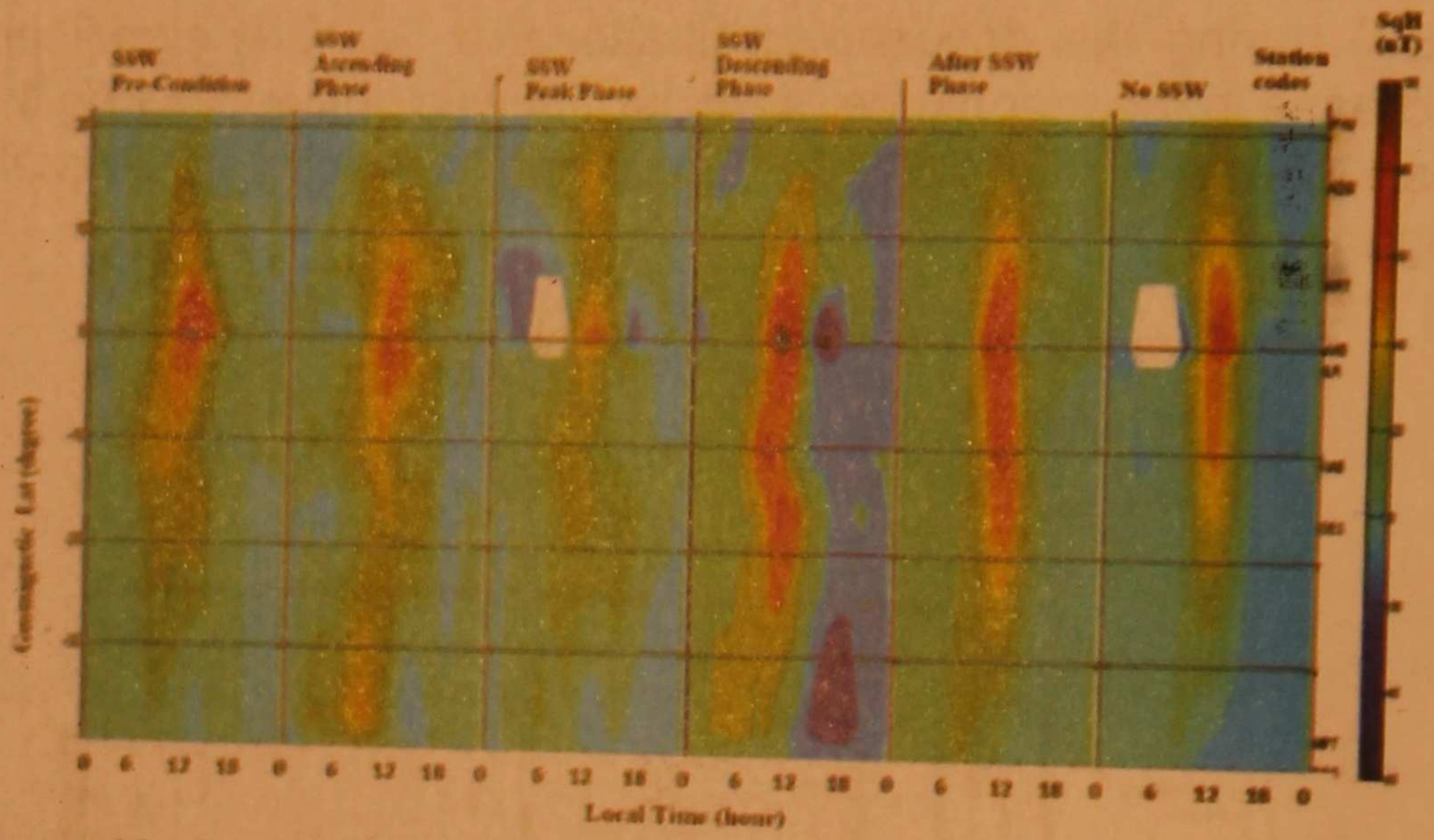

Figure 60: Two-dimensional plot of *Sq*(H) as a function of local time across nine stations in Africa during the year 2009 SSW event

Source: *Bolaji et al., 2016*

In Bolaji et al., (2019), for the first time, we unveiled the morphology of equatorial ionization anomaly (EIA) signatures in Africa and the Middle East during the 2009 sudden stratospheric warming (SSW) event using TEC data deduced from 18 GPS receivers. Results revealed a significant reduction in the magnitude of EIA in all of the latitudes during the peak phase of the SSW is evident as observed in Figure 61. Figure 61 shows the variability of TEC for each of the 2009 SSW phases in Africa and the Middle East. Figure 62 shows the corresponding TEC difference (TEC_{DIFF}) during the SSW phases that unveil the physical underlying variations of latitudinal TEC from January 18 to March 31, 2009. This significant reduction was traced to the global equatorial electrojet (EEJ) current, which is the equivalent vertical EXB drift that drove the coupling between the E and F-region. This is evident in Figure 63 which shows EEJ strength and its corresponding underlying variation during the 2009 SSW phases. In general, results showed that it is not only geomagnetic storms that can create disturbances in the ionosphere, which is the medium of propagating radio waves. The SSW can also modulate the ionosphere.

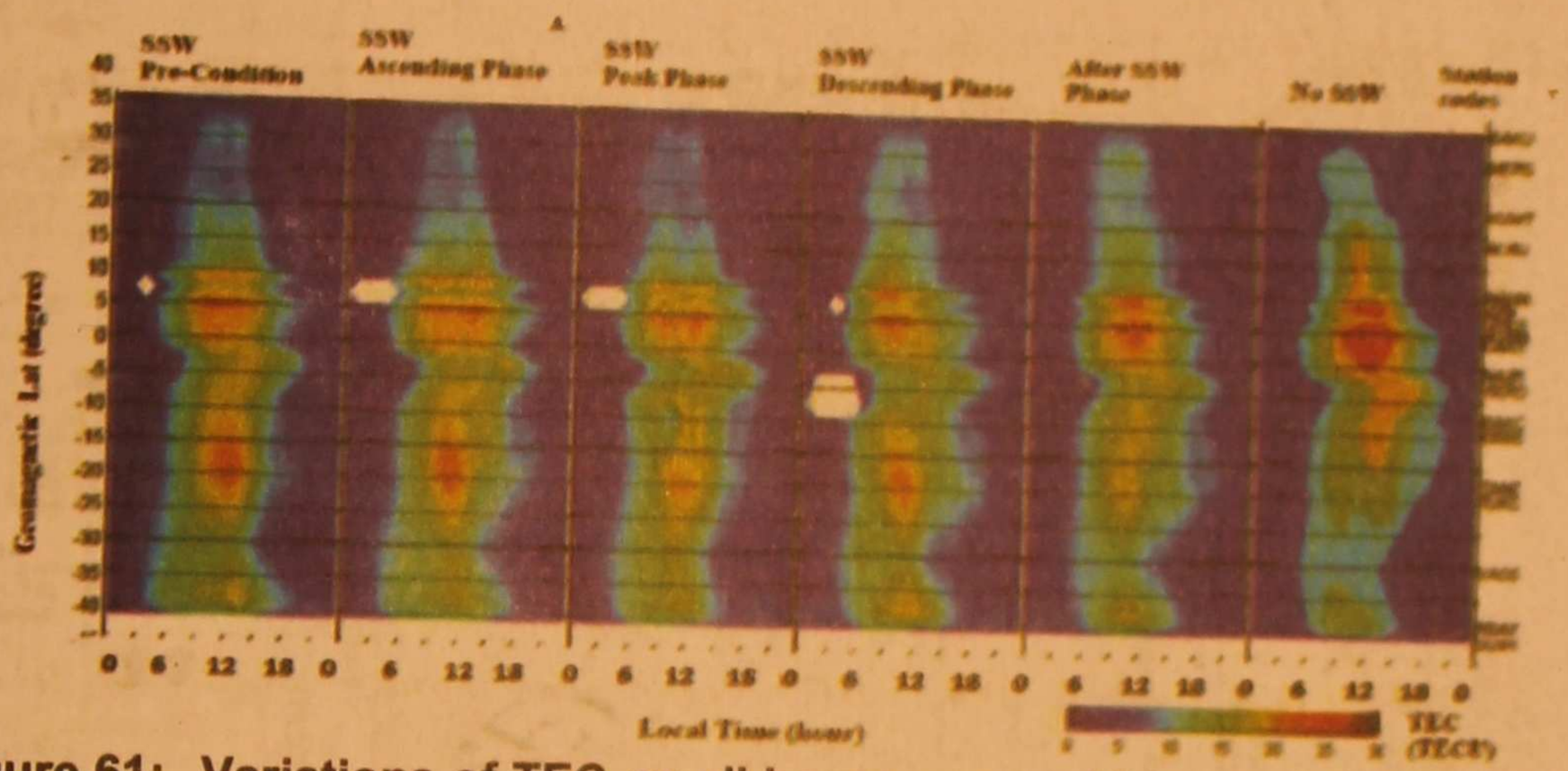

Figure 61: Variations of TEC on all hours across Africa and the Middle East latitudes prior to, during and after the SSW event in 2009

Source: *Bolaji et al., 2019*

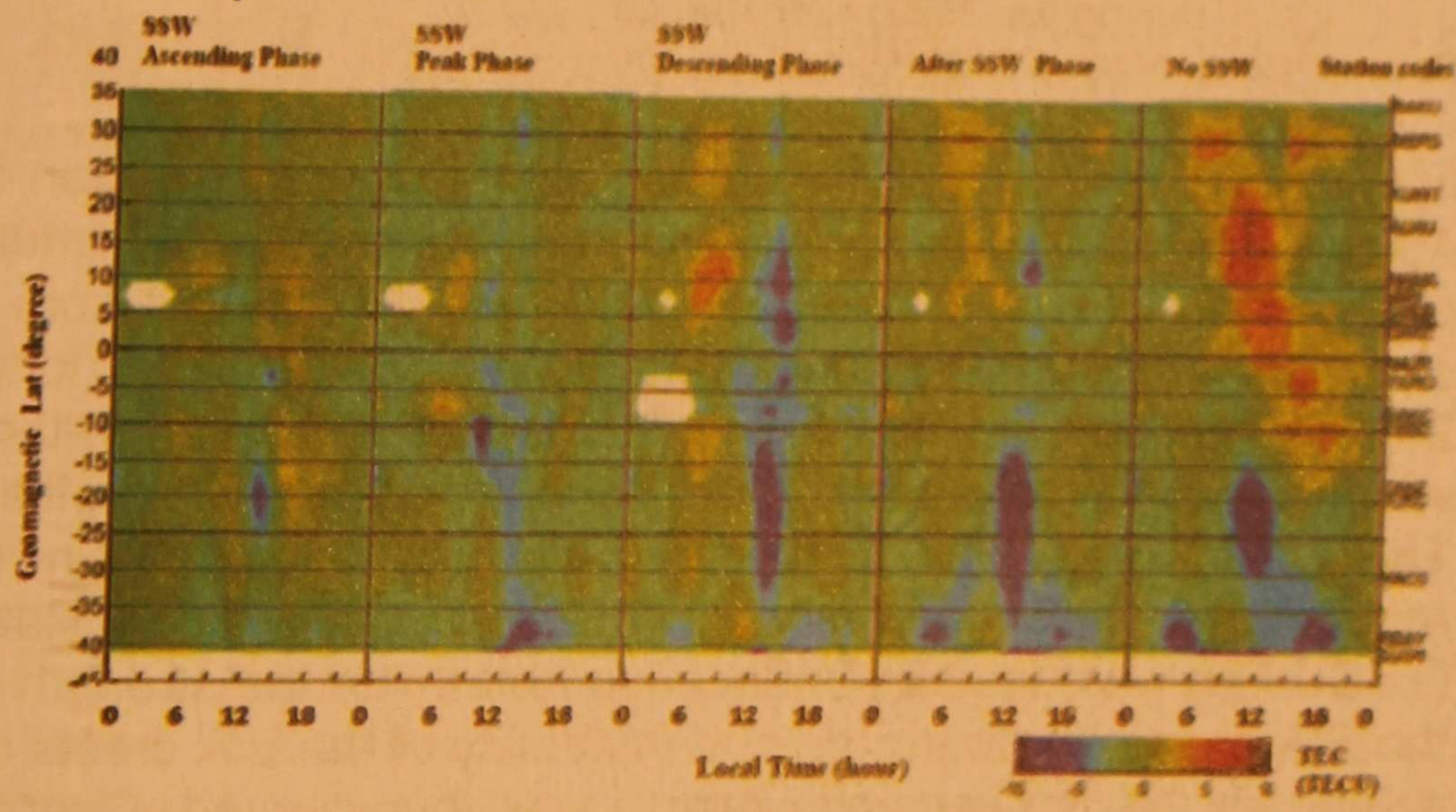

Figure 62: Difference in TEC on all hours across Africa and the Middle East latitudes prior to, during and after the SSW event in 2009

Source: *Bolaji et al., 2019*

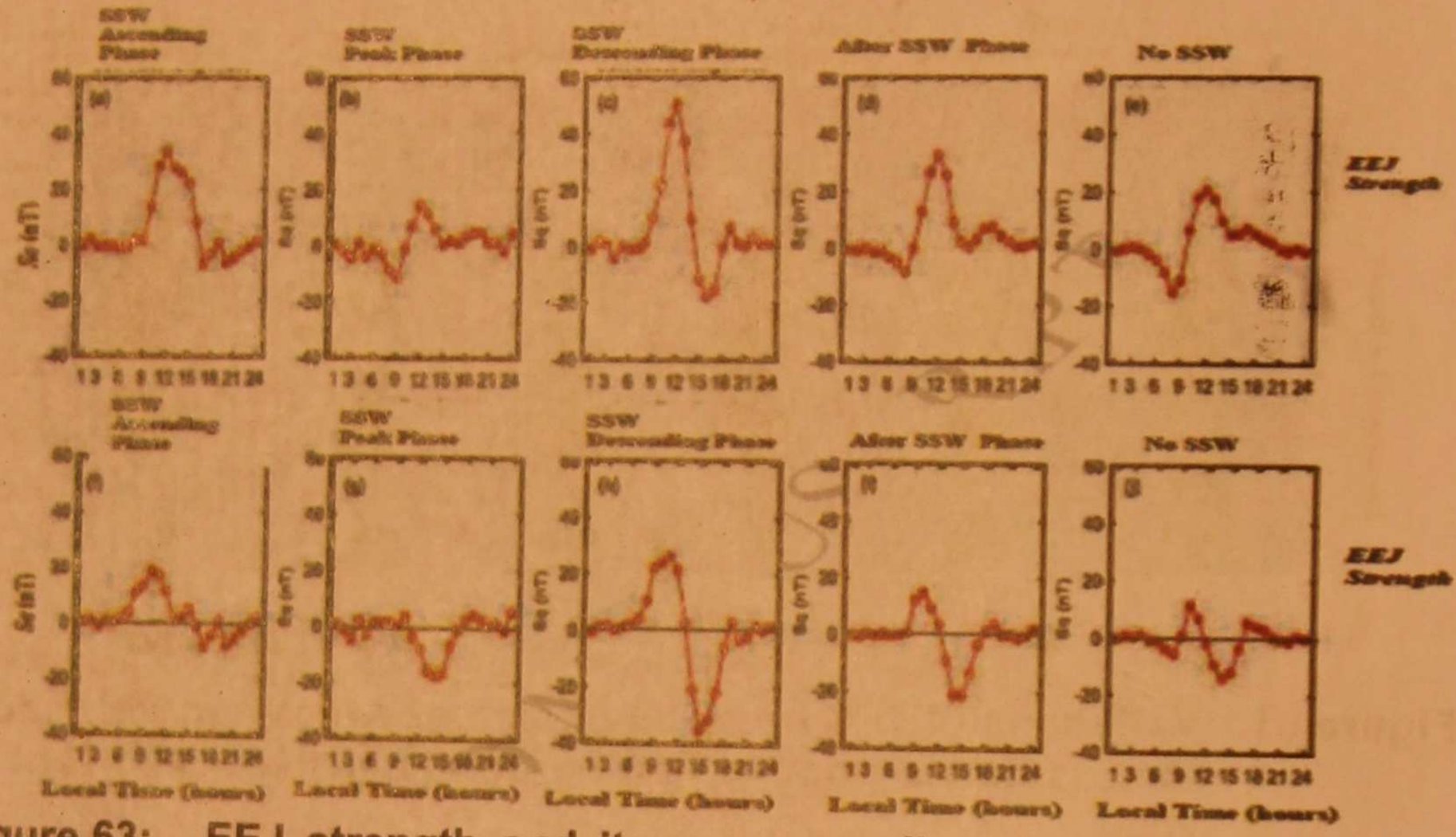

Figure 63: EEJ strength and its corresponding underlying variation during the 2009 SSW phases

Source: *Bolaji et al., (2019)*

In Oyedoku et al. (2020), we carried out the characterisation of African equatorial ionization anomaly (EIA) during the maximum phase of solar cycle 24 (2012 – 2015) using TEC data from a chain of 13 African GNSS receivers (within 36–42°E geo. long; 29°N–10°S geo. lat; ± 20°N mag. lat) to study quiet-time variations of TEC, and thereafter constructed the EIA profiles. The correlations of TEC for pairs of conjugate stations within the African EIA were determined. TEC Station-to-Trough Ratio (TEC-STR) was used as an index to determine the strength of the EIA crests. Furthermore, the variability of the EIA crests on a 3-hourly basis over each month was investigated. Overall, equinoxes recorded the highest values of TEC, with the widest latitudinal location of the EIA crests, and June solstice recorded the least, with the characteristic equatorward collapse of the EIA crests. TEC and the location of the crests of the EIA also increased with solar activity. Results showed that TEC has good correlations for conjugate pairs of stations, especially for stations closer to the trough. The African EIA morphology showed asymmetry in the locations of the Northern Hemisphere (NH) and Southern Hemisphere (SH) crests. One major contribution to knowledge from this research is that the formation of the African EIA starts around 0600–0800 LT and

decays around 2100–2300 LT as observed in Figure 64. Generally, the SH crest forms first before the NH crest and also decays first, we attributed this to the effects of the meridional neutral winds.

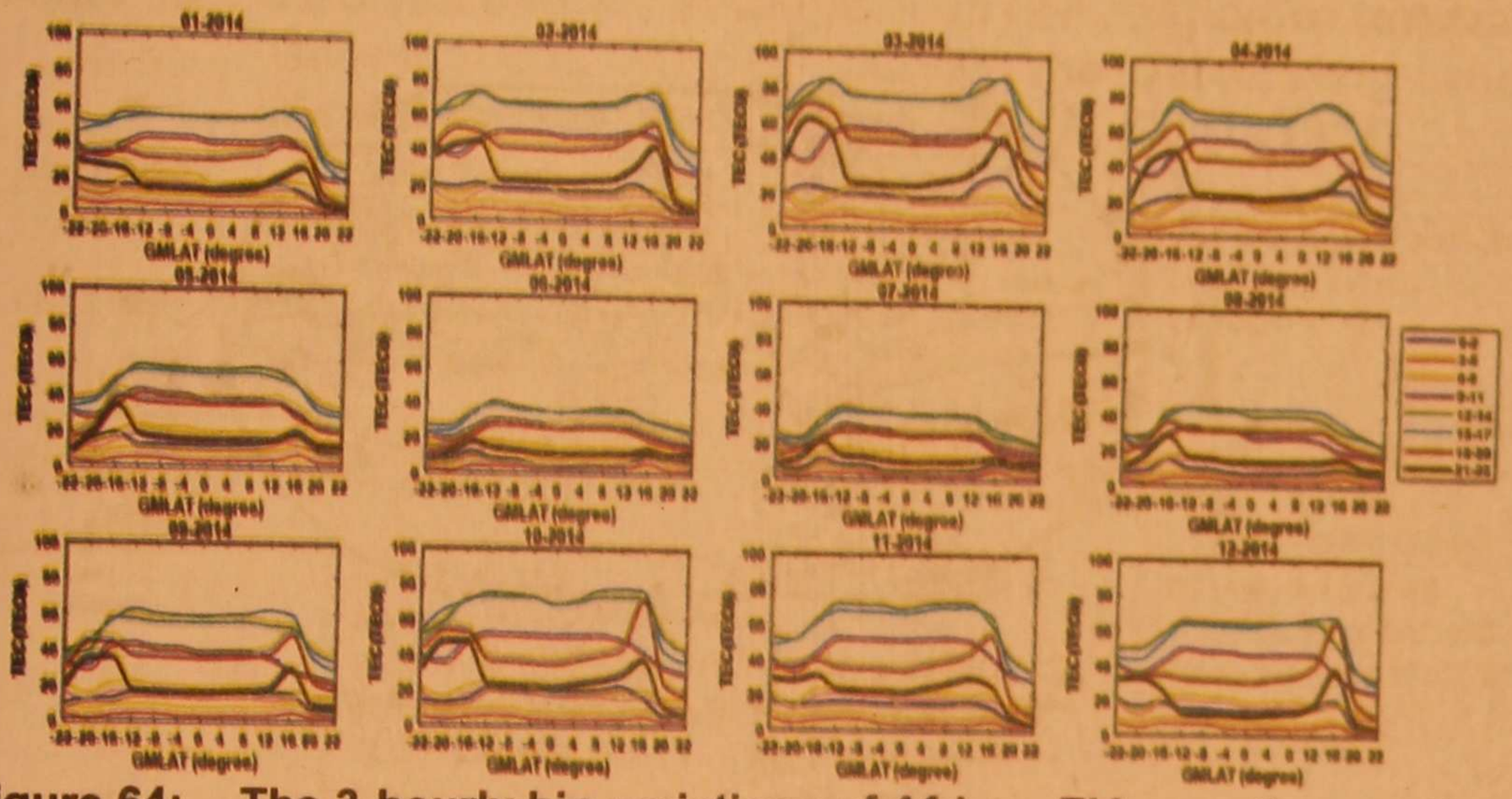

Figure 64: The 3-hourly bin variations of African EIA over the months of the year 2014

Source: *Oyedoku et al., 2020*

Recently, in Akala et al. (2020), we studied the longitudinal dependence of responses of the equatorial and low-latitude ionosphere over the oceanic regions to geomagnetic storms of 28th May and 8th September 2017. We investigated the interplanetary origins of the storms. The Rate of change of TEC Index (ROTI) was used as a proxy for ionospheric irregularities. We used ionospheric disturbance currents, polar cap and aurora electrojet indices to monitor the storm-time electric fields. The May 2017 storm was driven by sheath and magnetic cloud fields, while the September 2017 storm was driven by sheath fields. We observed a comparative dominance of TEC intensities over the Oceans than over the landlocked areas. Our results showed the existence of a dynamic ocean-ionosphere coupling. Prompt Penetration Electric Fields (PPEF) was observed to be a key factor that controls TEC responses to storms. PPEFs caused TEC enhancements, mainly over the Pacific Ocean longitudes during the May 2017 storm and enhanced TEC over the Atlantic Ocean and the Pacific Oceans longitudes during the September 2017 storm. These PPEFs

triggered irregularities over the Pacific Ocean longitudes, particularly during the main phase of the May 2017 storm. Irregularities were generally inhibited by the September 2017 storm.

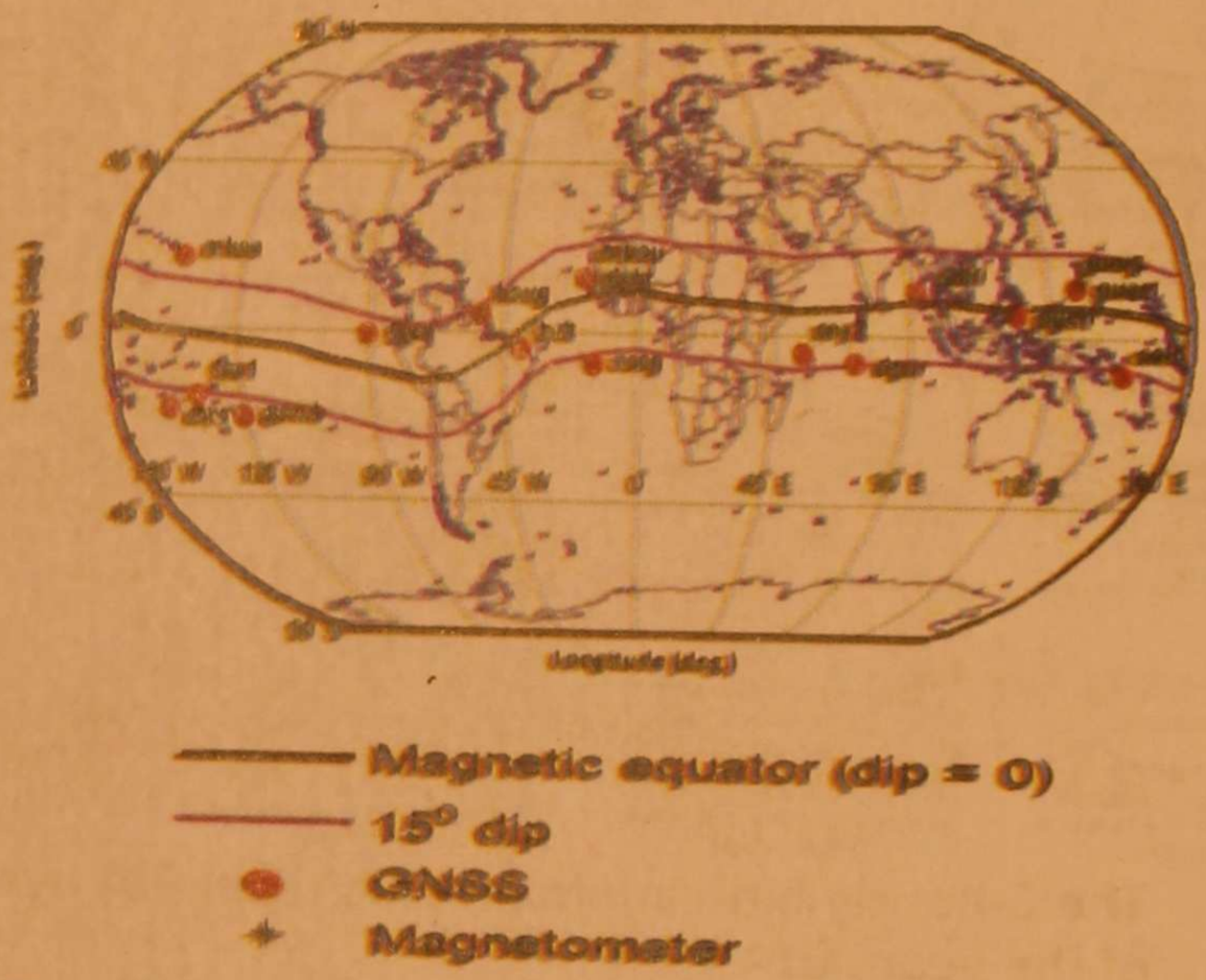

Figure 65: Geographic locations of the GNSS and magnetometer stations

Source: *Akala et al., 2020*

In Oyedoku et al. (2021), we investigated the morphology of the GPS TEC responses in the African EIA region to intense geomagnetic storms during the ascending and maximum phases of solar cycle 24 (2012–2014) within 36–42°E geographic longitude; 29°N–10°S geographic latitude; ± 20°N magnetic latitude. The result obtained revealed that storm-time behaviour of TEC shows clear positive and negative phases relative to the non-storm (median) behaviour, with amplitudes being dependent on the time of sudden commencement of the storm and location. The major contribution to knowledge of this work is that when a storm starts in the morning period, TEC increases for all stations considered while a decrease in TEC is manifested for a storm that had its sudden commencement in the afternoon period. The TEC and the EIA crest during the main phase of the storm are significantly impacted by the geomagnetic storm, which experiences an increase in the intensity of TEC while the location and spread of the crest usually manifest a poleward expansion.

The summary of the results for the period under investigation is as shown in Table 13.

Table 13: TEC Responses in the African EIA Region to Intense Geomagnetic Storms during the Ascending and Maximum Phases of Solar Cycle 24 (2012–2014)

Storm Event	Initial Phase	Main Phase	Recovery Phase
08-12 March 2012	SSC: Afternoon Negative Variation of TEC and equatorward compression of EIA.	Minimum Dst at 0800UT. Poleward expansion of the EIA crest and increase in TEC	The equatorward shrinking of the crest with a decrease in TEC.
22-27 April 2012	SSC: Morning Positive Variation of TEC	Minimum DST in the daytime. Expansion of the EIA crest.	Increase in TEC and greater latitudinal expansion of the crests
13 – 18 July 2012	SSC: Nighttime Negative Variation of TEC at the inner flank of the EIA while a Positive variation of TEC at the outer flank of the EIA.	Minimum DST in the daytime. Increase in TEC but no developed EIA	Increase in TEC and latitudinal expansion of the EIA crests a day after the event.
29 September – 04 October 2012	SSC: Afternoon Negative Variation of TEC after the SSC. Poleward expansion of crest	Minimum Dst was reached in the morning period. Increase in TEC with a little shrinkage in the EIA crest as compared to the day before the event.	A decrease in TEC and compression of the EIA crests.
12 – 17 November 2012	SSC: Nighttime Negative Variation of TEC	Minimum Dst in the daytime. TEC intensity diminished and the collapse of the EIA crest.	Increase in TEC and Poleward expansion of the EIA crests.
15 – 20 March 2013	SSC: Morning Positive Variation of TEC	Minimum Dst at night time. Increase in TEC with equatorward compression of the EIA.	Reduction in TEC, Poleward expansion of the EIA
30 May – 04 June 2013	SSC: Midnight Negative Variation of TEC and reduction of TEC before SSC. Increase in TEC variation at SSC	Minimum DST in the daytime. Increase in TEC but no developed EIA	Increase in TEC and latitudinal expansion of the crests a day after the event.
17 – 22 February 2014	SSC: Afternoon Negative Variation of TEC	Minimum Dst in the daytime. Increase in TEC and EIA crest not properly formed.	A decrease in TEC and compression of the EIA crests.

Source: *Oyedoku et al., 2021*

SUMMARY

Mr. Vice Chancellor Sir, I hereby summarise my contributions to knowledge as follows:The success of HF communications depends on the ability to understand and predict ionospheric conditions and requires up-to-date information on the state of the ionosphere. The key characteristics of particular concern for radio propagation conditions via the ionosphere are the maximum plasma frequency, foF2, maximum height (hmF2) and propagation factor M(3000)F2 for a distance of 3000 km.

The ionosphere, acting as a dispersive medium, has a great influence on the ground and space-based communication and navigation systems, and the effect is directly proportional to the free electron density, which could change the phase and strength of electromagnetic radio frequency wave. The most vulnerable region of the ionosphere to variability both on ***temporal and spatial scales*** is the F2 region due to the effect of the vertical and horizontal winds associated with global thermospheric circulation and non-linear solar cycle dependence of the F2 peak electron density (NmF2). Unpredictable variability of the ionospheric parameters, most especially F2 peak electron density (NmF2), due to the complicated non-linear dynamical processes arising from temporal and geographical variabilities in the upper atmospheric chemistry, ionization, production and loss mechanisms, particle diffusion and electrodynamical phenomena limits the efficiency of communications, radar, and navigation systems. Because the ionosphere varies from hour to hour and from day to day, etc., it is necessary to have good knowledge of this variability in order to select the optimum frequency, required transmitter power, and antenna configuration for effective communication systems.

It is most desirable to drive mathematical ionospheric forecasting and mapping models based on physics and incorporate them in ionospheric services and activities. However, this is a very complex and prohibitively difficult task. In view of these considerations, my research has been focused on the study of the dynamics of the ionosphere and the

development of global models for the prediction of ionospheric parameters (foF2 and M(3000)F2), based on the applications of Neural Networks (NNs). NN exploits its ability to deal with non-linear behaviour thereby establishing and modelling the non-linear dynamical processes (***both in space and time***) associated with F2 region electron density on a global scale. Also investigated are parameters other than geographical coordinates on which the ionosphere is known to depend, and which are more evenly spread over the available data grid points. Unlike the classical methods, the NN technique provides an empirical model that can describe non-linear phenomena and requires no artificial data points in order to be able to generalise. Four different models were developed. These are the foF2 NN model, M(3000)F2 NN model, short-term foF2 NN model up to 5 hours in advance, and a near-real time foF2 NN model.

The results of the foF2 NN model and M(3000)F2 NN model presented compare favourably with the IRI (International Reference Ionosphere) model (i.e. International Union of Radio Science, URSI, and International Radio Consultative Committee, CCIR). This demonstrates the potential of NNs for ***spatial* and *temporal*** modelling of the ionospheric parameters (i.e. foF2 and M(3000)F2) globally. The results obtained from the short-term foF2 NN model and near-real time foF2 NN model revealed that in addition to the ***temporal* and *spatial*** input variables of foF2 and M(3000)F2 NN models, short-term forecasting of foF2 are much improved by including past observations of foF2 itself. Results obtained by the near-real time foF2 NN model also revealed that there is a correlation between experimental electron density (NmF2) at different locations across the globe. Overall, results showed that the NN technique can successfully be employed to model the complex irregularities associated with the equatorial/low and high latitude regions of the ionosphere.

The equatorial ionosphere is a densely populated region characterised by the Equatorial Ionization Anomaly (EIA) and the associated enhancement in ionization at about ±15° of the

magnetic equator. During disturbed geophysical conditions, the electrodynamics of the ionosphere over the equatorial region can vary drastically, with significant implications on the operational capability of the Global Navigation Satellite System (GNSS), which have extensive applications in our day-to-day activities. Several studies on the ionospheric irregularities have been carried out over the equatorial region of the Asian and American sectors with few studies over the equatorial region of the African sector due to paucity of GPS data in this region. The effect of this is that our understanding of the electrodynamics of this region is limited with respect to HF communication.

We have been able to carry out studies on the electrodynamics of the ***equatorial ionosphere*** over the African sector because of the deployment of GPS receivers by various organisations in the last one or two decades. For example:

(i) Our study revealed that ionospheric irregularities vary differently over the eastern and western sectors of Africa and that, irregularities occurred predominantly over all stations in the post sunset to midnight period and they are associated with total electron content (TEC) depletions/fluctuations which are a manifestation of equatorial plasma bubbles (EPB) with characteristic longitudinal dependence, more over the oceanic region than over landlocked regions. Implication of this is that critical GNSS technologies operating in both sectors will be impacted differently during geomagnetic storm periods.

(ii) The contribution of the equatorial electrojet (EEJ) in controlling the formation of the EIA and the latitudinal extent of the crests' position was established.

(iii) Our investigation on the response of African equatorial/low-latitude ionosphere to geomagnetic storm confirmed that prompt penetration electric field (PPEF) was responsible for TEC enhancement as well as the expansion of the northern crest to 22°N.

(iv) Ionospheric imaging technique was employed to assess the accuracy of three-dimensional ionospheric images over African region using differential Global Positioning System (GPS), slant total electron content observations

and a time-dependent tomography algorithm. We concluded that the inclusion of observations from the African Geodetic Reference Frame (AFREF) archive significantly reduces ionospheric specification errors across the African sector, especially in regions that are poorly served by the permanent network of GPS receivers.

(v) Studies of observation data obtained from the GSV4004B GPS Ionospheric Scintillation and TEC Monitor (GISTM) installed in the Department of Physics, University of Lagos show that the presence of some large-scale depletions of TEC or plasma bubbles may be noted during the evening hours and that TEC depletions correspond to an increased rate of change of TEC (ROT). This confirms that plasma bubbles are associated with large scale irregularities.

(vi) Study of response of solar quiet (Sq) current in African sector to sudden stratospheric warming (SSW) event of 2009 established a connection of the lower atmosphere with the upper atmosphere. There is a significant increase in the magnitude of Sq that is associated with a counter electrojet (CEJ) during the descending phase of an SSW. The result showed that not only geomagnetic storms create disturbances in the ionosphere, which is the medium of propagating radio waves, but SSW can also modulate the ionosphere.

(vii) Further study on the African equatorial ionization anomaly (EIA) during the maximum phase of the solar cycle showed that TEC has good correlations for conjugate pairs of stations, especially for stations closer to the trough. The African EIA morphology showed asymmetry in the locations of the Northern Hemisphere (NH) and Southern Hemisphere (SH) crests. One major contribution to knowledge from this research is that the formation of the African EIA starts around 0600–0800 LT and decays around 2100–2300 LT and generally, SH crest forms first before NH crest and also decays first. This can be attributed to the effects of the meridional neutral winds.

Mr Vice Chancellor Sir, indeed, the ionosphere is a **natural mirror and a gift of nature** that readily supports technological advancement for the betterment of humanity.

Mr Vice Chancellor Sir, apart from my contributions to the University, both national and international as earlier stated, I have successfully supervised four PhD students. Three of them are colleagues in the Department of Physics, as Senior Lecturer and Lecturer I. Three are also due for their APC and three are ongoing. Also, through my collaborations with researchers in Nigeria, UK, Italy, Ukraine and South Africa, I have attracted various research equipment used by my students for their research works. I can also say authoritatively that all my PhD students had the opportunity to travel out before they finished their PhD works. The most recent collaboration is the MoU between the South African National Space Agency (SANSA) which brought research equipment worth about ₦16million to the Department of Physics.

RECOMMENDATIONS

Because of the importance of telecommunications to the development of this nation, I humbly make the following recommendations:

(i) First, I recommend the introduction of **Basic Space Science** into the curriculum of Primary and Secondary Schools. This will enable early understanding and benefits of Space Science Education.

(ii) The federal government should establish a research organisation like **Advanced Telecommunications Research Agency** to rejuvenate fundamental and applied Telecommunications research in Nigeria and to stimulate and coordinate activities across industry and academia.

(iii) The nation's Telecommunications Research capacity can be improved by building up research groups, centres, and institutions with sufficient scale and breadth of expertise to tackle real-world problems and strengthen connections between the academic communities and the industry, especially among the Telecommunications and computer segments of the IT industry.

The following can be achieved through University-Industry connections:

(a) Opportunities to provide future work for undergraduate and graduate students can be enhanced.

(b) Companies' internal research and development programmes can be stimulated (University Researchers in the university can help industrial scientists identify current research that might be useful for the design and development of innovative processes and potential products).

(c) Partnership with industries will bring financial rewards of patents and licenses that come from the commercialisation of academic research. (**External funding sources demand up-to-date relevant research topics, which through close collaboration between the Academia and Industry can be realised**).

(iv) Most of the equipment and research facilities available for space research in Nigeria are donated by developed nations. Therefore Nigerian government needs to provide enough funds for the acquisition of space research equipment for institutions and universities.

(v) I recommend that the process of duty fee-waivers on scientific equipment being ordered by academic and research institutions be relaxed. The current process is extremely difficult for researchers to bring research equipment to the country.

(vi) I recommend that all research institutes should be affiliated with universities. This will brings strong synergy between research institutes and universities, and increase productivity in research activities in Nigeria.

ACKNOWLEDGEMENTS

Mr. Vice-Chancellor Sir, I give all glory and thanks to Almighty God who has spared my life till this date and has given me the opportunity to attain this level in academia. In the course of my acknowledgements please do not be offended if your name is not mentioned (most especially from my faculty, Faculty of Science and the university at large) because many people have made great impacts in my life that are too numerous to list.

First, I want to thank Professor Rahamon Bello, under whose tenure as Vice-Chancellor I was appointed an Associate Professor and a Professor, as well as Professor Mathew Ilori, *FAS* who was the Dean of Faculty of Science then. I appreciate you, Prof. Ilori, for always being there for me.

I sincerely thank the University of Lagos for all the supports I received for making me realise my dreams. I can say that I am extremely lucky because the University provided a conducive atmosphere for me to have opportunities to travel around the globe for research.

I wish to acknowledge my PhD supervisor, Prof Allon Pool, for his encouragement and for inspiring and supporting my interest in the field of Ionospheric Physics, and all members of staff of the Department of Physics and Electronics, Rhodes University, Grahamstown, South Africa for all the support during and after my PhD programme.

I acknowledge with deep gratitude, the roles played by the sitting Vice Chancellor, Professor Oluwatoyin Ogundipe, *FAS* and former Vice Chancellor, Prof. A.B. Sofoluwe, *FAS* (late) in my academic career. Professor Ogundipe assisted me to secure PhD admission outside the shores of Nigeria when things were not going on well with my PhD programme in Nigeria. I will ever be grateful to you Sir! I am grateful to Prof. O.B. Familoni *FAS* (past Dean of Faculty of Science and current DVC, Academics & Research) and Prof. L.O. Chukwu (former Dean, School of Postgraduate Studies and current DVC,

Management Services), Prof. Ayodele Victoria Atesenuwa for all their encouragement and advice over the years. I also thank the immediate past DVCs, Prof. Ben Oghojafor, DVC, Management Services, and Prof. F. Ogunsola, DVC, Development Services. My sincere appreciation also go to The Registrar Oladejo Azeez Esq., Bursar Dr. Lekan Lawal and Librarian Dr. (Mrs) Yetunde Zaid.

Many thanks to Dr. Lee-Ann McKinnell, Manager of South African National Space Agency (SANSA), for her untiring assistance at all times during my PhD programme and for the opportunities to do my Postdoctoral Fellowship at SANSA as well as a visiting scholar to SANSA till date since I finished my PhD. She facilitated virtually all my attendances at international workshops/conferences with supports. I appreciate all members of staff of the South African National Space Agency for all the supports through our research collaborations since 2005 till date. My sincere appreciations to both the Hartebeesthoek Radio Observatory (HartRAO), a national facility of the National Research Foundation (NRF) of South Africa, and GrinTek Ewation (GEW) for their scholarship supports during my PhD programme.

I deeply appreciate the opportunities and privileges of working with Professor Sandro Radicella and Bruno Nava of the International Centre for Theoretical Physics (ICTP), Trieste, Italy. Through Professor Radicella I was able to secure Simon Associate Fellowship for six years (2014 to 2019), (the first Nigerian to have the opportunity), and attended several workshops/conferences on GNSS applications at ICTP. Again, I thank Professor Radicella and Dr. Anthon (a visiting researcher at ICTP from Ukraine who has now relocated to Canada) for the research equipment donated to me in 2014 for the training of Masters and PhD students.

I appreciate all my colleagues in the Department of Physics, Prof. A.N. Njah, Prof. A.B. Adeloye, Dr. O.O. Oyebola, Dr. O.I. Olusola, Dr. V.C. Ozebo, Dr. A.O. Akala, Dr. O.S. Bolaji, Dr. O.B. Olatinsu, Dr. A.O. Adewale, Dr. N.E. Erisiafe, Dr.M.A.

Olopade, Dr. U.I. Oduah, Dr. N.I. Obot, Dr. K.S. Ojo, Dr. O.L. Ojo, Dr. O.O. Odeyemi, Dr. I. Humphrey, Dr. B. Olugbon, Dr. (Mrs) M.B. Adedokun, Mr. O.G. Ilori, Mr. Adedeji, M.A, Miss. I.U. Chukwubueze and Mr. Folarin, S.T. I thank you all for the good relationship as a family that exists in the Department. I appreciate Prof. E. Olatunji, Prof. C. Oluwafemi, Prof. M.A.C. Chendo, Dr. J. Akinrimisi (late), Dr. L.L.N. Amaeshi, Dr. D. Olorode and Dr. H. Boyo for the mentorships roles they played while in the system. Words alone cannot express my sincere appreciation. To all Technical and Administrative staff, I appreciate you all. My friend and brother, Mr. Deji Ashaolu, I cannot thank you enough for all you have done in my life and family.

Special acknowledgement to my undergraduate and postgraduate students (present and past). To my PhD students, Dr. A.O. Adewale (late), my first academic child), Dr. Obot and Dr. Olugbon, who are now colleagues in the Department and Dr. Paul Amaechi of Department of Physical Sciences, Chrisland University, Owode, Abeokuta, I thank you all.

To my friends like brothers, Mr. Isaac Folorunso (Deputy Director, Federal Ministry of Education), Mr. C. Owolabi (Assistant Director, Ministry of Education), Prof. Tunde Owolabi (Dean, Faculty of Education, LASU), Mr. Idowu Adekunle, Mr. Abiodun Olowe, Mr. Kehinde Ajadi, Mr Joel Olaniyi, Mr. Sanjo Amole, Mr. Isaac Oladiran and others that are too numerous to mention, I am grateful for all your supports. I thank all my cousins and nephews, Mr. Yomi Oyedeji and family, Mr. Michael Oyeyemi, and others for all your supports.

I am deeply grateful to all my international collaborators, Dr. D. Bilitza, Prof. C.N. Mitchell, Dr. R. Julian, Dr. P. Cilliers, Dr. John Bosco Habarunema, Dr. Stevan, Dr. Patrick Sibanda, Dr. Daliar and others that are too numerous to mention from various Institutes and Universities across the globe for all the ideas and thoughts we have shared. Special thanks to Prof. Babatunde Rabiu (Centre for Atmospheric Research, National Space Research and Development Agency, Anyigba) for all his

supports for me and many of our postgraduate students in the Department of Physics.

My special thanks go to (Distinguish Professors Jide Alo, J.D. Olowokudejo, Olukayode Amund), Professors A.A. Adekunle (Immediate past Dean, Faculty of Science), J.K. Saliu, C.E. Umebeze, I.A. Adeleye, C. O. Uwadia, E.O. Ugoji, Bola Oboh, K.O. Olayinka, W. O. Okiei, O.T. Asekun, L. Adams, O. O. Aiyejuyo, Joy Okpuzor, M.O. Akinola, W.A. Makanjuola, R.I. Egonmwan, A.A. Otitoloju, K.F. Oyedele, S.B. Olobaniyi, E.A. Ayolabi, S.A. Okunuga, J.O. Olaleru and all past and present Heads of Department.

To all other colleagues (academic and non-academic) in the Faculty of Science, you are too numerous to list. Please forgive me if I have not mentioned your name. I appreciate all of you.

I specially thank Comrade Dele Ashiru (Chairman, ASUU Unilag Chapter), Comrade Adelaja Odukoya (IPC Unilag Chapter), Comrade Moses Karo Ogbinaka (past Chairman ASUU Unilag Chapter), all past and present ASUU Executives, Unilag Chapter, Zonal Coordinator (ASUU Lagos Zone), Zonal Coordinator (ASUU Ibadan Zone), all past and present Chairmen from ASUU Lagos and Ibadan Zones. Solidarity forever!

To the House of Commons of Senior Staff Club, University of Lagos, headed by our Governor Prof. Ropo Akinsoji and other members including, Prof. Ademola Adeleke, Prof. Abiola Sanni, Dr. Kayode Adebayo, Dr. Bola Dixon-Ogbechi, Architect Savage, Dr Oladeji Kehinde, Prof Ajiboye, Mr Medubi, Prof. Iyiola Oni, Prof. Olatunde Makanju, Prof. Orimogunje, Prof. Oyatoye, Dr Ayo Yusuff, Dr. Yemi Oke, Prof. Omololu Soyombo, Dr Ladan, Dr. Brai Marlik, Dr. I. Akiije, Dr. Shadare, Dr. Oluwafemi, Dr Adediji, Dr. Akaayar I say thank you to you all.

Special thanks to Prof. Duro Oni (Former DVC, Management Services). You are so wonderful and God will continue to be

with you. I also thank Prof. H.O.D. Longe for his fatherly advice always. You will live long in good health.

I wish to appreciate my great Science Boys and friends for their supports, Prof A. Otitoloju, Prof. K.F. Oyedele (KOB), Dr. M. Kuton, Dr. C. Isanbor, Prof. Akinleye, Dr. S. Adebusoye, Dr. Adenusi, Dr. Akingbeyin, Prof Abiola Sanni, Dr. Ogunyebi, Dr. Dr. Aderonke Lawal-are (QOB), Dr. Shola Adekanbi, Dr. J.C. Anikwe, Prof. Soneye, Dr. A. Abayomi, Mr. Bayo Adegbiji, Dr. A.B. Onadeko, Dr. R. O. Shaibu, Dr. J. U. Izunobi , Dr. Owoeye, Dr. Bankole, Dr. Charles Onyema, Dr. V. Odjegba, Dr. N.H. Amaeze, Dr. Oloruntola, Dr. Abiala, Dr Osilagun, Dr. Oloyede, Dr. Oloruntola, Dr. Shadare, Dr. T. Omeru, Prof. Folarin Oguntoyinbo.

To my teachers, Prof. J. Adeniyi, Prof. Akomolafe (late), Prof. Akosile, Prof. Adimula, Prof. Oyinloye (late), Prof. Bamgboye (late), Prof. Aro. Prof. E. Olatunji, Dr. A. Willoughby, Prof. M.A.C. Chendo, late Prof. J Akinrimisi, Prof. Aina, Mr. Odelade, Mr. G. Bamkole (late). I thank you for the knowledge I received from you.

To my church, RCCG Amazing Graze Parish, I thank all the pastors and ministers (present and past), Pastor Ifeoluwa Akindayomi, Pastor Olitan, Pastor Ojo and Pastor Ajayi for your love and prayers. To all other members of the church. God bless you all.

To my great Rhodeans from Rhodes University: Dr. Bola Ogunsipe, Dr. R. O. Shaibu, Dr. (Mrs.) O.E Ade-Ademilua, Dr Saheed Adekilekun, I thank you for the great time we had together.

To a dear brother, friend and academic colleague, Dr. Adekola Olajide Adewale, (my first academic child), I never thought that this is the way I would appreciate you. I can no longer see you with my eyes or touch you with my hands, but I will ever feel you in my heart forever. SLEEP WELL.

My sincere and unreserved appreciation to my late parents Pa Moses Oyeyemi and Mrs. Ruth Oyeyemi for the care I received from them. You were wonderful. May your souls continue to rest in perfect peace! To my brother, Mr. Gabriel Oyeyemi and his wife Mrs. Mary Oyeyemi, words alone cannot express my sincere appreciation. You stood by me throughout my educational career, even when things were difficult. I thank you.

I sincerely appreciate the prayers and support of my mother-in-law, Mrs Alice Akintonde (A.K.A Jesu Babami). Words are not enough to appreciate your spiritual support. Also, to my brother and sister in-laws, Mr. Akintonde, Mr Akintayo Akintonde, Dr. Wole Akintonde, Temilade Tunwagun (Nee Akintonde), Funmilade Aliu (Nee Akintonde) to mention a few. God bless you all abundantly.

My special thanks and appreciation go to my family. I thank my children, Oluwatimilehin, Ifeoluwa, Florence, Oyebola and Oyedola for their endurance. Most especially Oluwatimilehin, Ifeoluwa, Florence for all you went through when I was away for my PhD programme. To my dear wife Mrs. Olufunke Julianah Oyeyemi, I sincerely appreciate you. I know you went through a lot of stress taking care of the children alone whenever I am not around. I thank you for your prayers. Words alone cannot express my appreciation. God bless you.

REFERENCES

Adewale, A. O., **E. O. Oyeyemi**, A. B. Adeloye, C. M. Ngwira, and R. Athieno. (2011). Responses of equatorial F region to different geomagnetic storms observed by GPS in the African sector, *J. Geophys. Res.*, 116, A12319, doi:10.1029/2011JA016998.

Adewale, A.O., **Oyeyemi, E.O.,** Adeloye, A.B., Mitchell, C.N., Julian, R., Cilliers, P. (2012). A study of L-band scintillations and total electron content at Lagos, Nigeria. *Radio Science*, **47**, RS2011, doi:10.1029/2011RS004846,

Adewale, A.O., **E.O. Oyeyemi,** J. Olwendo. (2012). Solar activity dependence of total electron content derived from GPS observations over Mbarara *Advances in Space Research* 50 415–426

Adewale, A.O., **Oyeyemi, E.O.**, and Akala, A.O. (2010). Comparison of neural network technique with IRI-2001 model ionospheric predictions during great geomagnetic storms for a mid-latitude station. *J. Sci. Res. Dev.*, 12; 75-92.

Adewale, A. O., **Oyeyemi E. O.,** Ofuase U.D. (2010b). Comparison between observed ionospheric foF2 and IRI-2001 predictions over periods of severe geomagnetic activities at Grahamstown, South Africa, *Advances in Space Research* 45 368–373

Adewale, A. O., **E. O. Oyeyemi,** A. B Adeloye, A.O. Akala, O.O. Oyebola. (2013). Ionospheric Time Delay Variations at an Equatorial Station during Low Solar Activity, *Journal of Sci. Res. Dev. 2013, Vol. 14, 85 – 94*

Akala, A. O., **E. O. Oyeyemi,** P. O. Amaechi, S. M. Radicella, B. Nava, C. Amory-Mazaudier. (2020). Longitudinal Responses of the Equatorial/Low-Latitude Ionosphere Over the Oceanic Regions to Geomagnetic Storms of May and September 2017, *Journal of Geophysical Research*

Alex T. Chartier, Joe Kinrade, Cathryn N. Mitchell, Julian A. R. Rose, David R. Jackson et al., , et al., (2014).

Ionospheric imaging in Africa. *Radio Science*, **49**, 19–27, doi:10.1002/2013RS005238.

Altinay, O., Tulunay E., Tulunay Y. (1997). Forecasting of ionospheric critical frequency using neural networks, *Geophys. Res. Lett.* 24, 1467-1470.

Anderson, D., Fuller-Rowell, T.J. (1999). Space Environment Topics, Space Environment Center (SEC) at URL http:/www.sel.noaa.gov/Info/Iono.pdf.

Appleton, E.V., 1946. Two anomalies in the ionosphere. Nature 157, 691.

Araujo-Pradere, E.A., Fuller-Rowell, T.J. (2003). Validation of the STORM response in IRI2000. J. Geophys. Res. 108, 1120, http://dx.doi.org/n10.1029/2002JA009720.

Amaechi, P. O., **E. O. Oyeyemi**, A. O. Akala. (2018a). Geomagnetic storm effects on the occurrences of ionospheric irregularities over the African equatorial/low-latitude region, *Adv. Space Res., 61, 2074 – 2090.*

Amaechi, P. O., **E. O. Oyeyemi**, A. O. Akala. (2018b). The Response of African equatorial/low-latitude ionosphere to 2015 St. Patrick's Day geomagnetic storm, *Space Weather* doi: 10.1029/2017SW001751

Amaechi, P. O., **E. O. Oyeyemi**, A. O. Akala. (2019). Variability of African Ionization anomaly (EIA) crest during year 2013, *Canadian Journal of Physics*, 97(2): 155-165, https://doi.org/10.1139/cjp-2017-0985.

Amaechi, P.O., **E.O. Oyeyemi**, A.O Akala, C. Amory-Mazaudier. (2020). Geomagnetic activity Control of irregularities occurences oer the crests of the African EIA, *Earth and Space Science* 7 (7), e2020EA001183

Amaechi, P.O., **Elijah, O. Oyeyemi**, Andrew, O. Akala, Elijah, O. Falayi, Mohammed Kaab, Zouhair Benkhaldoun, Christine-Amory Mazaudier. (2020). Quiet Time Ionopheric Irregularities over the African Equatorial Ionization Anomaly Region. *Radio Science*, https://doi.org/10.1029/2020RS007077.

Barghausen, A.F., Finney, J.W., Proctor, L.L., Schultz L.D. (1969). Predicting long-term operational parameters of

high-frequency sky-wave telecommunications systems, ESSA Tech. Rep., ERL-110-ITS-78.

Basu, S., Kudeki, E., Valadares, C., & Espinoza, J. (1996). Scintillations, plasma drifts, and neutral winds in the equatorial ionosphere after sunset. Journal of Geophysical Research, 101(A12), 26,795–26,810. https://doi.org/10.1029/96JA00760

Bilitza, D., Sheikh, N.N., & Eyfrig, R. (1979). A global model for the height of the F-2peak using M3000 values from the CCIR numerical maps. *Telecommun. J.* 46, 549-553.

Bilitza, D. (2001). International Reference Ionosphere 2000. *Radio Sci.* 36, 261 – 275,

Bilitza, D. (1990). Internatjonal Reference Ionosphere 1990, *National Science Data Center, Report* 90-22, Greenbelt, Maryland, USA,

Bilitza, D., D. Altadill, V., Truhlik, V., Shubin, I., Galkin, B., Reinisch, & X., Huang. (2017). International Reference Ionosphere 2016: From ionospheric climate to real-time weather predictions, Space Weather 15 (2), 418-429.

Bent, R.B., Lepofsky, J.R., Llewellyn, S.K., & Schmid, P.G. (1978). Ionospheric range-rate effect in satellite-to-satellite tracking, in: Soicher, H. (Ed.), Operational Modelling of the Aerospace Propagation Environment, *Vol. I. AGARD conference Prodeedings,* Vol. 230, 9-1 – 9-15

Blanc, M., & Richmond, A. D. (1980). The ionospheric disturbance dynamo. Journal of Geophysical Research, 85(A4), 1669–1686. https://doi. org/10.1029/JA085iA04p01669

Bolaji, O.S., Rabiu, A.B., **Oyeyemi, E.O.** and Yumoto, K. (2012). Climatology of the inter-hemispheric field-aligned currents system over the Nigeria ionosphere, J. Atmos. Sol. Terr. Phys., Vol. 89, 144-153.

Bolaji, O.S., **E.O. Oyeyemi**, O.E. Jimoh, A. Fujimoto, P.H. Doherty, O.P. Owolabi, J.O. Adeniyi, E.O. Falayi, E. Abe, A. Kotoye. (2019). Morphology of the equatorial ionization anomaly in Africa and Middle East due to a sudden stratospheric warming event, J. Atmos. Sol. Terr. Phys., 10.1016/j.jastp.2019.01.006.

Bolaji, O.S., **Oyeyemi, E.O.,** Owolabi, O.P., Yamazaki, Y., Rabiu, A.B., Okoh, D., Fujimoto, A., Amory-Mazaudier, C., Seemala, G.K., Yoshikawa, A. (2016). Solar quiet current response in the African sector due to a 2009 sudden stratospheric warming event: SSW connects lower with upper atmosphere, J. Geophys. Res., Vol. 121, pp. 8055-8065, doi: 10.1002/2016JA022857.

Bradley P.A., Dudeney J.R. (1973). A simple model of the vertical distribution of electron concentration in the ionosphere, *J. Atmosph. Terr. Phys*. 35, 2131-2146.

Bradley, P.A., (1999). PRIME, Prediction and retrospective ionospheric modelling over Europe Final Reports to project COST238, Rutherford Appleton Laboratory, Chilton, Didcot, UK.

Buonsanto, M. J. (1999). Ionospheric storms—A review. Space Science Reviews, 88(3/4), 563–601.

Cander, L.R., Lamming, X. (1997). Neural networks in ionospheric prediction and short-term forecasting, *10th International Conference on Antennas and Propagation, 14-17 April 1997, Edinburgh, IEEE Conference Publication,* 496. 2.27-2.30

Carrano, C., & Groves, K. (2007). TEC gradients and fluctuations at low latitudes measured with high data rate GPS receivers. Proceedings of the Institute of Navigation, 63rd Annual Meeting, Cambridge, MA, April 23–25.

Challinor, R.A., Eccles D. (1971). Longitudinal variations of the mid-latitude ionosphere produced by neutral–air winds – I, Neutral-air winds and the ionosphere drifts in the northern and southern hemispheres, J. *Atmosph. Terr. Phys.* 33, 363-369.

Chen, Y., Liu, L., Le, H. (2008). Solar activity variations of nighttime ionospheric peak electron density. J. Geophys. Res. 113, A11306, http://dx.doi.org/10.1029/2008JA013114.

Dandekar, B. S., and K. M. Groves. (2004). Using ionospheric scintillation observations for studying the morphology of equatorial ionospheric bubbles, Radio Sci., 39, RS3010, doi:10.1029/2003RS003020.

Fausett, L. (1994). Fundamentals of Neural Networks, Prentice-Hall International Inc.

Field, P.R., Rishbeth H. (1997). The response of the ionospheric F2-layer to geomagnetic activity: an analysis of worldwide data, *J. Atmosph. Solar-Terr. Phys.* 59, 163-180,

Forbes, J.M., Scott E.P., Xiaoli Z. (2000). Variability of the ionosphere, J. *Atmosph. Solar- Terr. Phys.* 62, 685-693.

Fox, M.W., McNamara L.F. (1988). Improved World-Wide Maps of Monthly Median of foF2, *J. Atmosph. Terr. Phys.*, 50, 1077-1086.

Fuller-Rowell, T.J., Araujo-Pradere E., Codrescu M.V. (2000). An empirical ionospheric storm-time correction model, *Adv. Space Res.* 25, 139-146.

Fuller-Rowell, T.J., Araujo-Pradere E., Codrescu M.V. (2000). An empirical ionospheric storm-time correction model, *Adv. Space Res.* 25, 139-146,

Friedrich, M, M. Fankhauser, **E.O. Oyeyemi** and L.A. (2008). McKinnell. A neural network-based ionospheric model for Arecibo, *Adv. Space Res.*, 42; 776-781.

Goncharenko, L. P, J.L Chau, H-L lui and A.J Costa. (2010). Unexpected connections between the stratosphere and the ionosphere, Geophys. Res, Lett, 37, L10101,doi;10.1029/2010GL043125

Gupta, J.K., Lakha S. (2001). Long term ionospheric electron content variations over Delhi, *Ann. Geophysica.* 18, 1636-1644.

Hanbaba, (1999). Improved quality of service in ionospheric telecommunication systems planning and operation, Final Report to Project COST251, Space Research Centre, Warsaw, Poland.

Hargreaves, J.K. (1979). The upper Atmospheric and Solar-Terrestrial Relations, an introduction to the aerospace environment, *Van Nostrand Reinhold Company*, New York,

Haykin, S. (1994). Neural Networks: A Comprehensive Foundation, Macmillan, Indianapolis, Indiana.

Huang, Y., Cheng, K. (1995). Solar cycle variation of the total electron content around equatorial anomaly region in East Asia. J. Atmos. Terr. Phys. 57 (12), 1503–1511.

Jiuhou, L., Liu L., Luan X., Wan W. (2003). Model study of neutral winds in the ionopheric F- region and comparison with the equivalent winds derived from the Wuhan ionosonde data. *TAO*, 14, 1-12

Kumluca, A., Tulunay E., Topalli I. (1999). Temporal and spatial forecasting of ionospheric critical frequency using nueral networks. Radio Sci., 34, 1497-1506.

Lamming, X., Cander LjR. (1999). Monthly median foF2 modelling COST 251 Area by neural networks. *Phys. Chem. Earth (c)*. 24, 349-354,

Liu, J.Y., Chen Y.I., Lin J.S. (2003). Statistical investigation of the saturation effect in the ionospheric foF2 versus sunspot, solar radio noise, and solar EUV radiation. *J. Geophys. Res.*, 108(A2), 1067, doi: 10.1029/2001JA007543.

Liu L., Wan W., Ning B. (2004). Statistical modeling of ionospheric foF2 over Wuhan. *Radio Sci.*, 39, RS2013, doi:10.1029/2003RS003005

Liu, H., C. Stolle, M. Forster, and S.J. Watanabe. (2007). Solar activity dependence of the electron density in the equatorial anomaly regions observed by CHAMP, *J. Geophys. Res.: Space Phys.* 112, A11311. doi:10.1029/2007JA012616.

Lin, C. H., Richmond, A. D., Liu, J. Y., Yeh, H. C., Paxton, L. J., Lu, G., et al. (2005). Large-scale variations of the low-latitude ionosphere during the October–November 2003 superstorm: Observational results. Journal of Geophysical Research, 110, A09S28. https://doi.org/10.1029/2004JA010900

McKinnell L.A. (1996). A new empirical model for the peak ionospheric electron density using neural networks. *MSc. Thesis, Rhodes University*, Grahamstown South Africa.

McKinnell L.A. (2002). A neural network based ionospheric model for the bottomside electron density frofile over

DONATED BOOK

Grahamstown, South Africa, *PhD Thesis, Rhodes University, Grahamstown, South Africa,*

McKinnell, L.A., **Oyeyemi, E.O**. (2009). Progress towards a new global foF2 model for the International Reference Ionosphere (IRI). Adv. Space Res., doi: 10.1016/j.asr.2008.09.035.

McKinnell, L.A., **Oyeyemi, E.O.** (2010). Equatorial predictions from a new neural network based global foF2 model, Advances in Space Research 46 1016–1023

McNamara L.F. (1994). *Radio amateurs guide to the ionosphere*, Krieger Publishing Company.

Nisbet J.S. (1971). On the construction and use of a simple ionospheric model, *Radio Sci.,* 6, 437 – 464.

Opio, P., F.M. D'ujanga, and T. Ssenyonga. (2015). Latitudinal variation of the ionosphere in the African sector using GPS TEC data. *Adv. Space. Phys.* 55, 1640. doi:10.1016/j.asr.2014.12.036.

Oyedokun, O. J., Akala, A. O., & **Oyeyemi, E. O.** (2020). Characterization of African equatorial ionization anomaly during the maximum phase of Solar Cycle 24. Journal of Geophysical Research: Space Physics, 125, e2019JA027066. https://doi.org/ 10.1029/2019JA027066

Oyedokun, O. J., Akala, A. O., & **Oyeyemi, E. O.** (2021). Responses of the African equatorial ionization anomaly (EIA) to some selected intense geomagnetic storms during the maximum phase of solar cycle 24, *Adv. In Space Res.*, 67, 4, 1222-1243.

Oyeyemi, E.O. and Poole, A.W.V. (2004). Towards the development of a new global foF2 empirical model using neural networks, *Adv. Space Res.*, 34; 1966-1972

Oyeyemi, E.O., Poole, A.W.V. and McKinnell, L.A. (2005a). On the global model for foF2 using neural networks, *Radio Sci.*, 40; RS6011, doi:10.1029/2004RS003223, 1 – 15.

Oyeyemi, E.O., Poole A.W.V.and McKinnell, L.A. (2005b). On the global short-term forecasting of the ionospheric critical frequency foF2 up to five hours in advance using neural networks, *Radio Sci.*, 40; RS6012, doi:10.1029/2004RS003239, 1 – 12.

DONATED BOOK

Oyeyemi, E.O., McKinnell, L.A. and Poole, A.W.V. (2006). Near-real time foF2 predictions using neural networks, *J. Atmos. Solar-Terr. Phys*, 68; 1807-1818.

Oyeyemi, E.O., McKinnell, L.A. and Poole, A.W.V. (2007). Neural network-based prediction techniques for global modelling of M(3000)F2 ionospheric parameter, *Adv. Space Res.*, 39; 643 – 650.

Oyeyemi, E.O. and L.A. McKinnell. (2008). A new global F2 peak electron density model for the International Reference Ionosphere (IRI), *Adv. Space Res.*, 42; 645-658.

Oyeyemi, E.O., McKinnell, L.A. (2008). A new global F2 peak electron density model for the International Reference Ionosphere (IRI). *Adv. Space Res.* 42 (4), 645–658, doi:10.1016/j.asr.2007.10.031.

Oyeyemi, E.O. and O.A. Adewale. (2009). Predictions using a Neural Network compared with the IRI-2001 predictions of ionospheric critical frequency observed at Madimbo, South Africa. *J, Sci. Res. Dev.*, 11; 110 – 121.

Oyeyemi, E.O., Adewale, A.O.and Akala, A.O. (2010). Back-propagation neural network: Basic outline and application to ionospheric predictions. *J. Sci. Res. Dev.*, 12; 128-142.

Oyeyemi, E.O., *A.O. Adewale and Adeloye, A.B. (2011). A singel station short-term forecasting of propagation factor M(3000)F2: a technique using neural networks.* Nigerian Journal of Space Research, *10; 243 – 252.*

Pancheva, D and P. Mukhtarov. (2011). Stratospheric warming; the atmosphere-ionosphere coupling paradigm. J.Atmos.Sol.Terr.Phys.73. doi ;10,1016/j,jastp.2011.03.066

Poole A.W.V., McKinnell L.A. (2000). On the predictability of foF2 using neural networks. *Radio Sci.*, 35, 225-234.

Richard S., Belehaki A., Burešovă D., Cander Lj., Kutiev I., Pietrella M., Stanisławska I., Stankov S., Tsagouri I., Tulunay Y., Zolesi B. (2004). Nowcasting, forecasting and warning for ionospheric propagation: tools and methods. *Ann. Geophys.*, 47, 957-983.

Rishbeth H., Garriott O.K. (1969). Introduction to ionospheric physics, *Academic press,* New York and London

Rishbeth H., Mendillo M. (2001). Patterns of F2-layer variability, J. *Atmosph. Solar- Terr. Phys.* 63, 1661-1680.

Rishbeth, H and C.S.G.K. Setty. The *F*-layer at sunrise. (1961). *J. Atmos. Terr. Phys.* 20, 263 doi:10. 1016/0021-9169(61)90205-7.

Rishbeth, H. (2006). F region links with the lower atmosphere? J. Atmos. Sol. Terr. Phys., 68, 469–478, doi:10.1016/j.jastp.2005.03.017.

Ross, W.J. Measurement of electron content at the magnetic equator (1966). J. Geophys. Res. 71, 3671 doi: 10.1029/JZ071i015p03671.

Rush C.M., Pokempner M., Anderson D.N., Stewart, F.G., Perry J. (1984). Maps of foF2 derived from observations and theoretical data, *Radio Sci.*, 19, 1083-1097.

Rush C.M., Fox M., Bilitza D., Davies K., McNamara L., Stewart F., PoKempner M. (1989). Ionospheric Mapping: An Update of foF2 Coefficients, *Telecomm. J.*, 56, 179,

Russell C.T., Mulligan T. (1995). The 22-year variation of geomagnetic activity: Implications for the polar magnetic field of the sun, *Geophys. Res. Lett.* 22, 3287-3288,

Russell C.T. (1974). On the heliographic latitude dependence of the interplanetary magnetic field as deduced from the 22-year cycle of geomagnetic activity, *Geophys. Res. Lett.* 1, 11-12.

Scherliess, L., and B.G. Fejer. (1999). Radar and satellite global equatorial *F* region vertical drift model *J. Geophys. Res.: Space Phys.* 104, 6829 doi: 10.1029/1999JA900025.

Sethi N.K., Goel M.K., Mahajan K.K. (2002). Solar cycle variations of foF2 from IGY to 1990. *Ann. Geophysicae,* 20, 1677-1685.

Tulunay E, Özkaptan C., Tulunay Y. (2000). Temporal and spatial forecasting of the foF2 values up to twenty four hours in advance, *Phys. Chem. Earth(c).* 25, 281-285,

Venkatesh, K., Tulasi Ram, S., Fagundes, P. R., Seemala, G. K., & Batista, I. S. (2017). Electrodynamic disturbances in the Brazilian equatorial and low-latitude ionosphere on St. Patrick's Day storm of 17 March 2015. Journal of

Geophysical Research: Space Physics, 122, 4553–4570. https://doi.org/10.1002/2017JA024009

Walker, G.O. and J.H.K. Ma. (1972). Influence of solar flux and the equatorial electrojet on the diurnal development of the latitude distribution of total electron content in the 'equatorial anomaly' *J. Atmos. Terr. Phys.* 34, 1419 doi:10.1016/0021-9169(72)90199-7.

Wanninger L. (1994). *In* Proceedings of CRCM 93: The Eighth International Symposium on Recent Custal Movements, Kobe, Japan, 6–11 December 1993. pp. 175–179.

Williscroft L.A., Poole A.W.V. (1996). Neural networks, foF2, sunspot and magnetic activity, *Geophys. Res. Lett.,* 23, 3659-3662.

Wintoft P., Cander LjR. (1999). Short-term prediction of foF2 using time delay neural networks, *Phys. Chem. Earth (c).* 24, 343-347,

Wintoft P., Cander LjR. (2000). Ionospheric foF2 storm forecasting using neural networks. *Phys. Chem. Earth (c).* 25, 267-273.

Wintoft P. (2000). Twenty-four hour predictions of foF2 using neural networks, *Radio Sci.,* 35, 395-408,

Wu, C.-C., C.D. Fry, J.-Y. Liu, K. Liou, and C.-L. Tseng. (2004). Annual TEC variation in the equatorial anomaly region during the solar minimum: September 1996–August 1997, *J. Atmos. Sol.-Terr. Phys.* 66, 199 doi:10.1016/j.jastp.2003.09.017.

Xenos T.D. (2002). Neural-network-based prediction techniques for single station modelling and regional mapping of the foF2 M(3000)F2 ionospheric characteristics, *Nonlinear Proc. Geophys.*, 9, 477-486.

Zou, L., H. Rishbeth, I.C.F. Muller-Wodarg, A.D. Aylward, G.H. Millward, T.J. Fuller-Rowell, D.W. Idenden, and R.J. Moffett. (2000). Annual and semiannual variations in the ionospheric F2-layer. I. Modelling, *Ann. Geophys.* 18, 927. doi:10.1007/s00585-000-0927-8.